PART COOLING ANALYSIS BY CONFORMAL COOLING CHANNELS IN INJECTION MOLDING

A THESIS SUBMITTED TO
THE GRADUATE SCHOOL OF NATURAL AND APPLIED SCIENCES
OF
MIDDLE EAST TECHNICAL UNIVERSITY

BY

MEHMET EMIN OZMEN

IN PARTIAL FULFILLMENT OF THE REQUIREMENTS
FOR
THE DEGREE OF MASTER OF SCIENCE
IN
MECHANICAL ENGINEERING

DECEMBER 2007

Approval of the thesis:

PART COOLING ANALYSIS BY CONFORMAL COOLING CHANNELS IN INJECTION MOLDING

submitted by **MEHMET EMİN ÖZMEN** in partial fulfillment of the requirements for the degree of **Master of Science in Mechanical Engineering Department, Middle East Technical University** by,

Prof. Dr. Canan Özgen _____
Dean, Graduate School of **Natural and Applied Sciences**

Prof. Dr. S. Kemal İder _____
Head of Department, **Mechanical Engineering**

Asst. Prof. Dr. Merve Erdal _____
Supervisor, **Mechanical Engineering Dept., METU**

Examining Committee Members:

Asst. Prof. Dr. Serkan Dağ _____
Mechanical Engineering Dept., METU

Asst. Prof. Dr. Merve Erdal _____
Mechanical Engineering Dept., METU

Prof. Dr. S. Engin Kılıç _____
Mechanical Engineering Dept., METU

Asst. Prof. Dr. İlker Tarı _____
Mechanical Engineering Dept., METU

Assoc. Prof. Dr. Göknur Bayram _____
Chemical Engineering Dept., METU

Date:

I hereby declare that all information in this document has been obtained and presented in accordance with academic rules and ethical conduct. I also declare that, as required by these rules and conduct, I have fully cited and referenced all material and results that are not original to this work.

Name, Last name: Mehmet Emin Özmen

Signature:

ABSTRACT

PART COOLING ANALYSIS BY CONFORMAL COOLING CHANNELS IN INJECTION MOLDING

Özmen, Mehmet Emin

M.S. Department of Mechanical Engineering

Supervisor: Asst. Prof. Dr. Merve Erdal

December 2007, 111 pages

Straight cooling channels are the most common method of controlling part temperature in injection molding process. However, straight cooling channels are not enough to manage temperature uniformity of the parts. In this work, a numerical study is conducted to decrease cycle time and cost of the injection molded parts by using conformal cooling channels. For this purpose, the commercial injection molding simulation program Moldflow is used.

The governing physical equations for injection molding were derived and presented. The assumptions of the model were checked for simple geometries by comparing analytical results and numerical results of Moldflow. Then, the effect of conformal cooling channels is investigated for injection molding of a half cylinder shell part. It was seen that conformal cooling channels cools part faster and more uniform than straight cooling channels without corruption on the surface appearance.

Finally, a real life case study was presented. For this purpose, a refrigerator shelf that is manufactured by the Arçelik Company was studied. The process was simulated using actual process parameters and simulation results were compared with production results. Then, the process was simulated using conformal cooling channels

and compared with production results. It is seen that the cycle time of the refrigerator shelf was decreased considerably while preserving surface quality appearance.

Keywords: Injection Molding, Conformal Cooling Channels, Moldflow

ÖZ

PLASTİK ENJEKSİYONDA PARÇA YÜZEYİNİ İZLEYEN SOĞUTMA KANALLARI İLE PARÇA SOĞUMASININ ANALİZİ

Özmen, Mehmet Emin
Yüksek Lisans, Makina Mühendisliği Bölümü
Tez Yöneticisi: Yard. Doç. Dr. Merve Erdal

Aralık 2007, 111 sayfa

Plastik enjeksiyon prosesinde, düz soğutma kanalları parçanın sıcaklığını kontrol etmekte kullanılan en yaygın metoddur. Fakat, düz soğutma kanallarının kompleks parçalarda düzgün bir soğuma sağlaması zordur. Bu çalışmada, parçanın çevrim süresi ve maliyetini düşürmek için parçanın dış kontürünü izleyen kanalları kullanarak sayısal bir çalışma yapıldı. Bunun için Moldflow adlı ticari simülasyon programı kullanıldı.

Plastik enjeksiyon için genel fiziksel denklemler çıkarıldı ve sunuldu. Modelin varsayımları basit geometriler üzerinde analitik sonuçlarla Moldflow'un sayısal çözümleri karşılaştırılarak kontrol edildi. Sonra, parça yüzeyini izleyen soğutma kanallarının etkisi, yarım silindir kabuk parçasının plastik enjeksiyonunda incelendi. Parça yüzeyini izleyen soğutma kanallarının düz soğutma kanallarına göre, parça yüzeyinin görünüşünde bir bozulma olmadan, parçayı daha hızlı ve daha dengeli bir biçimde soğuttuğu gözlendi.

Son olarak gerçek yaşamdan bir örnek sunuldu. Bunun için, Arçelik firması tarafından üretilen buzdolaba kapağı çalışıldı. Proses gerçek üretimden alınan datalar ile simüle edildi ve gerçek üretim sonuçları ile karşılaştırıldı. Proses daha sonra yüzeyi

takip eden soğutma kanalları ile simüle edildi ve gerçek üretim sonuçları ile karşılaştırıldı. Buzdolabı kapağının çevrim süresinin yüzey görünüşünde bir bozulma olmadan önemli ölçüde düştüğü görüldü.

Anahtar Kelimeler: Plastik Enjeksiyon, Parça Yüzeyini İzleyen Soğutma Kanalları, Moldflow

To My Mother and My Sister

for their love and support

ACKNOWLEDGMENTS

I would like to express my gratitude to my supervisor Asst. Prof. Dr. Merve Erdal for her advises, criticisms and especially teaching me being professional.

I would also like to thank Prof. Dr. Engin Kılıç for his advises and helpful conversations.

Barış Kocabaşoğlu, Erhan Özsüer, Hasan Ali Hatipoğlu, Özgür Demir and Gökhan Ertem, thanks for a being great friends and motivating me.

The technical assistance of Mr. Erdinç Uzel for Moldflow is gratefully acknowledged. I also appreciate the support of Mr. Metin Bilgili for helping me injection molding experiments.

TABLE OF CONTENTS

LIST OF TABLES

TABLES

LIST OF FIGURES

FIGURES

CHAPTER 1

INTRODUCTION

In this study, the effect of conformal cooling channels on part cooling and part quality in injection molding process was investigated using the commercial software package "Moldflow Plastic Insight". In this chapter, a background information is presented to the readers for the understanding of the physical events on which injection molding and conformal cooling are based.

1.1 The Injection Molding Process

Injection molding is the process of forcing melted plastic into a mold cavity, that is in the shape of the part to be produced. Upon filling the cavity, the plastic cools and solidifies. The mold is then opened and the plastic part is ejected. This is a process used in mass production of a variety of parts that can have complex shapes as well as a range of surface textures. In fact, for some complex parts, injection molding is the only feasible manufacturing process. Lots of variations of the products can be manufactured by the injection molding process easily. Therefore, injection molding process is the most popular process for manufacturing plastic products. Products of this process are highly repeatable, need little finishing operation and labor costs are very low compared to the part cost [1].

1.1.1 Hardware of Injection Molding

An injection molding machine consists of three basic parts; the injection, the clamping and the mold units, as shown in Fig. 1.1. The injection unit melts the plastic and injects it into the mold as shown in right side of Fig. 1.1. Mold has two halves; one stationary and one movable and it accepts molten plastic material which is injected into

the mold cavity to form a part. Cavity is the hollow section of the mold in the shape of the part. Lastly, during injection of molten polymer, high injection pressure arises inside the mold cavity, therefore clamp system applies high force to keep mold halves closed and prevent leakage, as shown in the left side of Fig. 1.1.

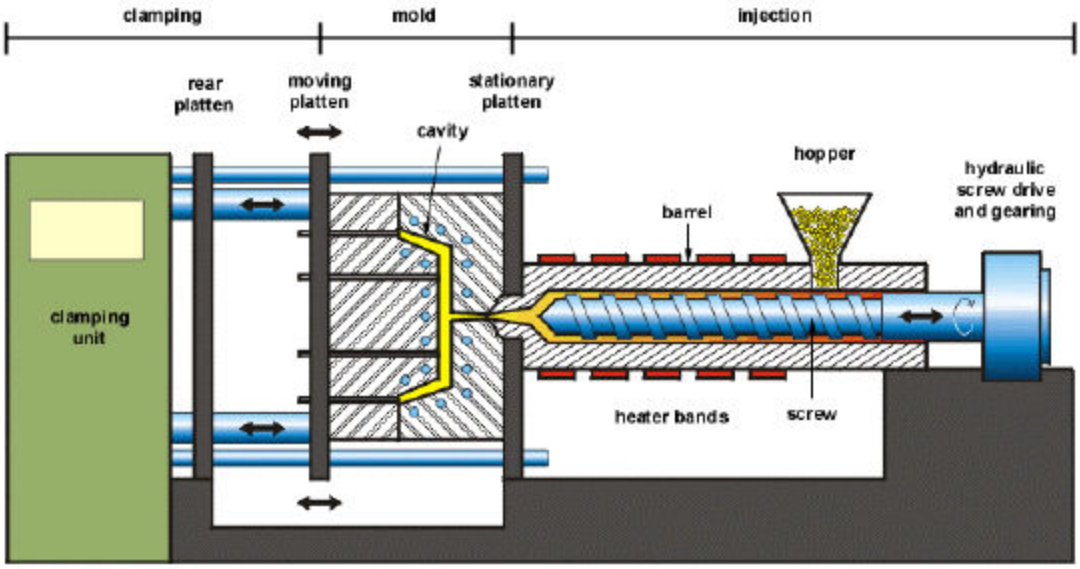

Figure 1.1 Typical injection molding machine: the injection, the mold and clamping unit [2]

There are a few different types of injection molding machines according to ram type; by far the most common are reciprocating screw machines. Reciprocating screw machines comprise more than 95% of machines in use today. The others, single and two-stage plunger machines, and two-stage screw and plunger machines, make up the rest [3]. In a reciprocating screw machine, the injection unit has four functions: heating and melting the plastic material, mixing the melt with additives, homogenizing the melt to a uniform temperature, injecting the melt into the mold cavity. In injection unit, polymer granules are loaded into a hopper on top of the injection unit. Drying units, may be attached to the hopper, heating the pellets to remove moisture. The polymer

granules are fed into the barrel where they are heated until they reached molten form. When screw turns, granules move through the screw channels, towards the injection nozzle, inside the barrel. As molten polymer goes forward, screw retracts. After enough molten polymer is accumulated, screw stops turning. Then the screw goes forward like a plunger and pushes the molten polymer into mold. At this time, the check valves at the end of barrel are closed to prevent leakage of the molten polymer. Screw continues to apply pressure during packing until beginning of the solidification, as shown in Fig. 1.2. After packing, check valves are opened and screw starts to turn again and retract for the next cycle.

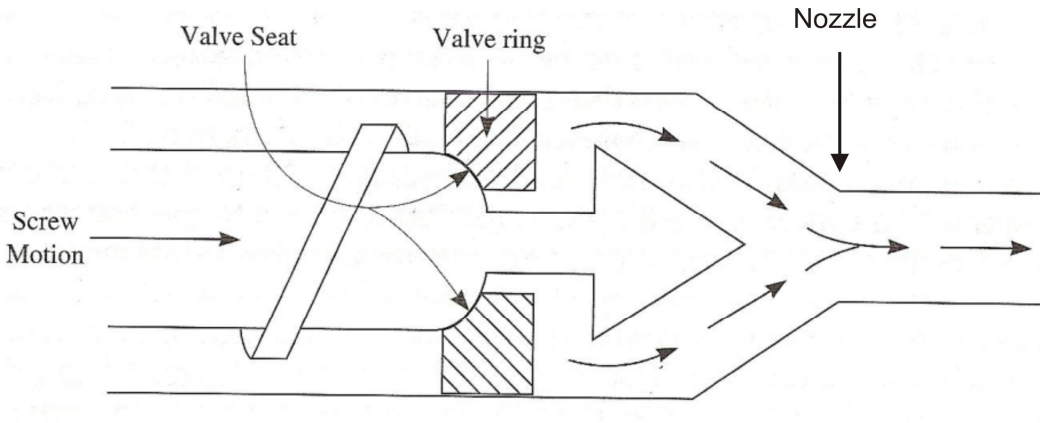

Figure 1.2 Movement of the screw during injection stage of an IM cycle [1]

The mold is one of the main parts of the injection molding process where filling, packing, polymer solidification and safe ejection of the part occur. The simplest mold consists of two plates; a stationary plate into which polymer is injected and a movable plate connected to the clamp system, as shown in Fig 1.3. The line at the meeting of the two plates is called mold open line.

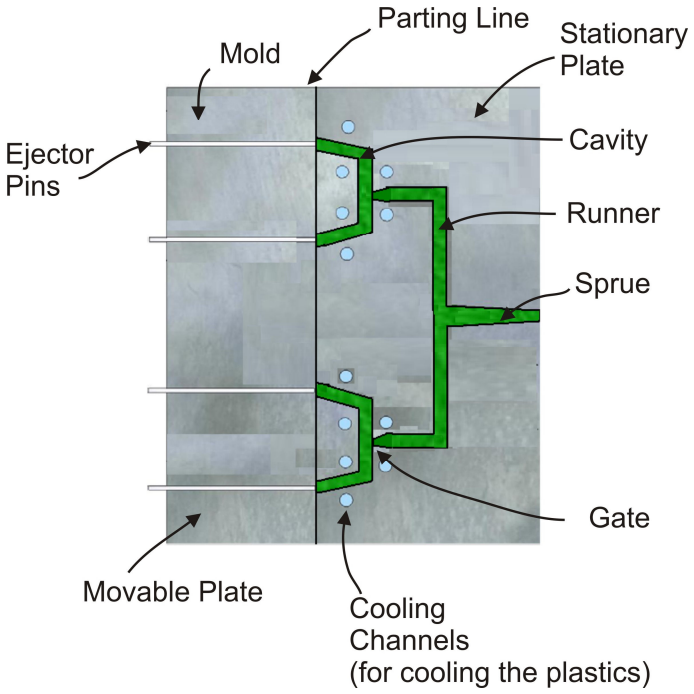

Figure 1.3 A typical mold

The mold is designed with channels called feed systems that direct the molten polymer to the part cavities, as shown in Fig.1.3. The sprue is a tapered channel delivering the molten polymer from the barrel to the relatively cold mold through a nozzle. When the pressure rises in the sprue channel, the plastic melt splits into the runners. Runners only exist in the multi-cavity molds. Especially for small parts in large quantities, several cavities can be included in one mold; such molds are called multicavity molds [1]. The melt moves down the runners until it reaches the gate. Gate holds the melt until the entire runner system is filled. Then, the molten polymer goes through the gate and fills the mold cavity. Gates are very small openings and are usually placed at the thicker portions of the cavity to avoid premature solidification.

Cooling lines drilled through the main body of the mold are used to keep the mold at a constant temperature and to take heat from part in order to cool the part uniformly. Coolant is passed through these lines to cool the part. Cooling time is a key

factor in determining the production rate of injection molded parts and surface quality of the parts. Because of rapid filling of the cavity, a small quantity of compressed air also fills the cavity. Vent channels are drilled into the mold to get rid off the air.

The clamping unit holds the two parts of the mold together while the resin is being injected and the part is cooled. It must withstand injection pressure and keep the mold closed. It also provides the force to open the mold**.** Usually, total clamp force should be 2-2.5 ton per inch square to keep the mold closed properly.

After cooling and solidifying, the part is ejected by ejectors incorporated into the mold. During ejection stage, the mold is opened, the part is ejected, and the mold is then closed again for the next cycle.

1.1.2 An Injection Molding Cycle

One cycle of injection molding process is made up of four steps. These are filling, packing, cooling and ejection, as shown in Fig. 1.4.

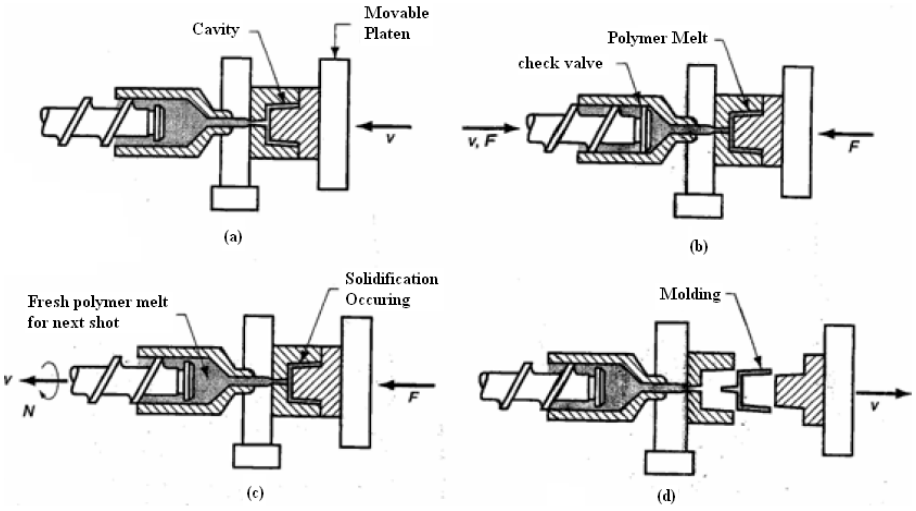

Figure 1.4 Injection cycle for a reciprocating screw injection molding machine a) Filling b) Packing c) Cooling d) Ejecting [4]

The cooling phase starts at the moment the mold cavity is completely filled and goes on until ejection of part as shown in Fig. 1.4.c. The cooling phase of the cycle allows the material to solidify with no packing pressure. When part solidifies, heat is extracted from the part. Most of heat is absorbed by the coolant passed through the cooling channels, some heat stored in the mold and remaining heat leaves the mold by convection with air. During the cooling phase, check valve opens, the screw begins to rotate. By rotating action of screw, plastic begins to melt and to accumulate to front of the screw and forces the screw to retract. The screw continues to rotate and plasticize material until the desired amount of material has accumulated in front of the screw, known as shot size. Cooling time mainly depends on the part thickness, the thicker part is, the longer cooling times takes. In the cooling phase, the thermal and mechanical properties, design of cooling channels dominate the dimensional changes in the material.

After the prescribed cooling period, the part has solidified, the mold is opened and the part is ejected as shown in Fig. 1.4.d. The clamping unit opens, separating the two halves of the mold. An ejecting rod and plate eject the part from the mold. At this time, there is enough material in the barrel for injection to the cavity. After ejection, the mold is closed and ready for next injection stage.

Filling is the forcing of the molten resin into the cavity, as shown in Fig. 1.4.a. The polymer that was melted and accumulated in the previous cooling phase is now injected into the empty cavity. The check valve is opened and the screw moves rapidly without rotation and molten polymer is forced through the nozzle, sprue and runner into the mold cavity. This filling rate can be varied according to injection pressure or screw forward speed.

The packing phase begins after the molten polymer completely fills the cavity, as shown in Fig. 1.4.b. The purpose of the packing phase is to fill empty regions or locations where volumetric shrinkage occurs and to tighten the part, as the material cools and solidifies. At the end of the filling phase, screw movement continues under

pressure control. The pressure applied during this phase is prescribed by the packing profile and injection molding machine parameters can be arranged to get desired packing profiles. The frozen layer thickens according to the convection of material and conduction of heat to the mold. Ultimately, the gate freezes and flow into the part ceases as shown in Fig. 1.4.c. In the packing phase, the significance of the flow properties diminishes. The thermal and volumetric properties determine the ultimate shrinkage of the material.

The whole process is repeated on the next cycle.

1.2 Determination of Thesis Topic

In this study, a production issue related to the injection molding industry in and around Ankara was identified and studied. Specifically the use of conformal cooling channels for increasing production quality and reducing cost has been chosen as the thesis topic. However, arriving at this particular topic required a survey of the major companies in business. Four major injection molding companies (Serdar Plastik, Arçelik Refrigerator Factory, EM-GE, Aygersan) were interviewed and the issues related to their production were investigated for each.

In Arçelik, one of the products produced by injection molding was the refrigerator shelf. During production, cycle time was deemed to be too long. Even when different process parameters were varied to decrease the cycle time, the expected results were not reached. Specifically, a reduction in cooling time was accompanied by reduction in part quality. Therefore, conformal cooling was considered to be a viable solution at this stage. Cooling time makes up the largest portion of the cycle time, as shown in Fig. 1.5. Conformal cooling channels (as opposed to traditional cooling channels) may decrease the cooling time while maintaining part quality by uniform cooling.

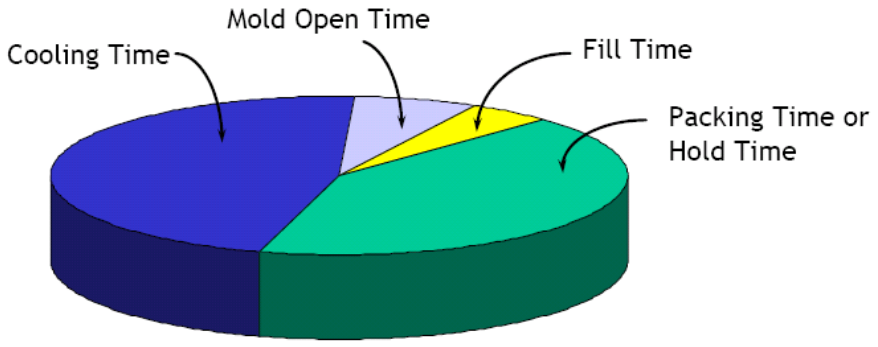

Figure 1.5 Allocation of time in one cycle of the injection molding [2]

Conformal cooling is not a common method in injection molding sector in Turkey. Even though the current study subject arises from a specific case, namely the need to decrease the cycle time of injection molding of a refrigerator shelf, the main purpose is to contribute to the understanding and applicability of conformal cooling technique in general. The study aims to show that conformal cooling can be a viable alternative method to traditional cooling in injection molding sector.

1.3 Conformal Cooling Channels

The efficiency and cost of the injection molding process depends largely on the cooling time spent in the molding cycle. When cooling is not uniform, some regions of the plastic are faster cooled than other regions. This causes uneven part shrinkage and poor part quality. This is usually the case when part geometries are intricate and cooling channels are traditional. Traditional cooling channels are straight channels drilled into the mold cavity, usually on a plane above the cavity. The conformal cooling channels differ from conventional cooling channels such that the conformal channels follow the contours of the cavity (part) (Fig. 1.6). With such a configuration, during solidification of the melted plastic, the cooling rate is expected to be uniform leading to a reduction in the molding cycle time, with fewer part defects due to uneven cooling.

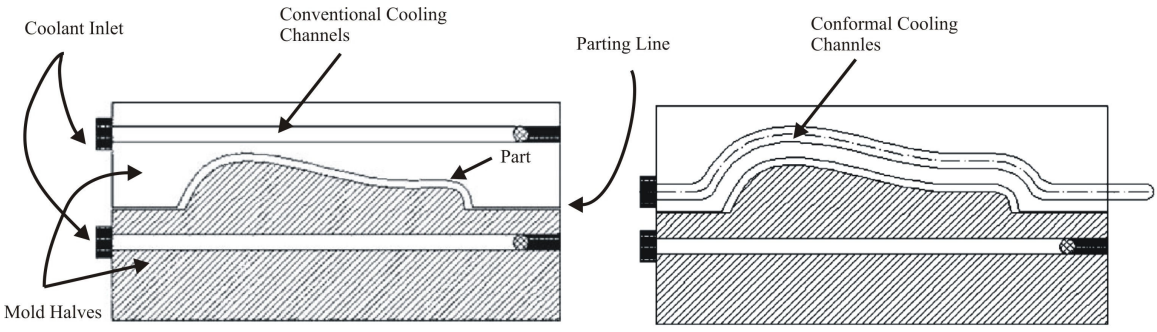

(a) (b)

Figure 1.6 (a) Configuration of conventional cooling channel design (b) Conformal cooling channel design [5]

1.3.1 Background

There have been many methods developed to decrease cycle time of the injection molding and get more uniform cooling. Some approaches involved varying the process parameters to get uniform cooling.

Ji-Zhao Liang [6] has tried to design a conventional cooling system that would absorb the maximum heat by the coolant. For this, he used a simple 1-D heat conduction model and optimized various parameters such as tube diameter, cooling tube spacing and the displacement between the cooling tubes and the cavity wall. Natti et al. [7] have performed a similar study to obtain uniform cavity wall temperature. Mathey et al. [8] have analyzed the cooling of shaped parts (T-shaped and L-shaped) by solving transient heat transfer based on BEM to obtain optimum locations for cooling channels.

Recently molds with cooling channels that follow the complex contours of part geometries have been manufactured. In these molds, the path of the cooling channels follows the cavity surface. Such cooling channel layouts are called conformal cooling channels.

Sun et al. [9] proposed U-shape milled groove cooling channels, manufactured by milling method, for complicated parts. They compared U-shape milled groove

cooling channels with conventional straight ones as shown in Fig. 1.7 and found more uniform temperature distributions with U-shape cooling channels than with straight cooling channels. However, pressure drop in U-shape channels were found to be much higher than pressure drop in straight cooling channels indicating the energy consumed to operate cooling pumps is higher for U-shaped channels.

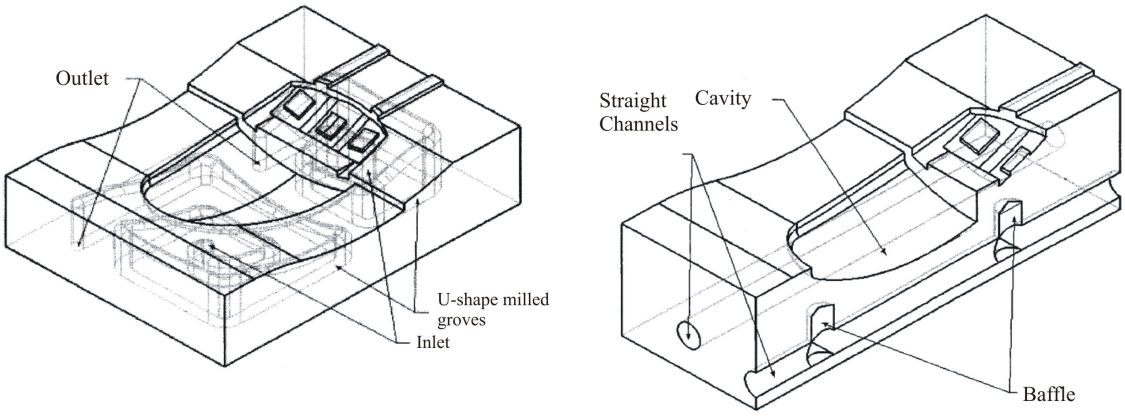

Figure 1.7 Cavity of a mouse cover with U-shape milled grooves and that of a mouse cover with straight cooling channels [9]

Today, some cooling channel layouts are too complex to be produced by traditional machining methods. Therefore, rapid prototyping techniques have been adapted to produce molds with conformal cooling channels. Sachs et al. [10] created a mold by "Three Dimensional Printing Process" spreading layers of stainless steel powder and selectively joining the powder in the layers by ink-jet printing, creating conformal channels layer by layer. They showed that the conformal tool had no period of transient behavior at the start of molding, while the mold with conventional channels took a number of cycles to reach to an equilibrium temperature as shown in Fig. 1.8. At the same time, molds with conformal channels yielded more efficient cooling than conventional channels.

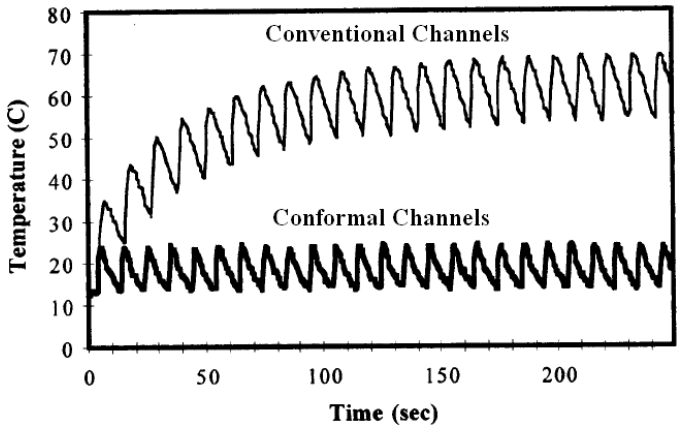

Figure 1.8 Comparison of mold surface temperature for straight cooling channel and conformal cooling channel [10]

1.3.2 Design Issues in Conformal Cooling Channels

Conformal cooling channels have advantages compared to conventional cooling channels in terms of cooling time and surface appearance quality of the part due to uniform cooling. However, it is not a common method in injection molding sector due to some limitations. Molds manufactured by rapid tooling methods have material problems. Mold materials are generally plastic, therefore problems arises from mechanical properties and thermal conductivity and of the mold material.

Thermal conductivity mold material is important in the rapid tooling process. Thermal conductivity of plastics is very low with respect to that of metals, that is, rate of heat transfer is low in rapid tooling molds and heat can not be extracted properly due to low thermal conductivity of the mold material. Therefore, cycle times of molds manufactured by rapid tooling are quite long without additives increasing the thermal conductivity of the part. Different types of mold materials to be used in rapid prototyping process to manufacture molds are being developed by mixing various plastic resins with additives to increase thermal conductivity. For instance, epoxy resin mixed with 40 % aluminum powder by volume was shown to reduce cycle time of the corresponding mold to about 2 min from the 4-5 min [11]. Mold geometries are also

studied to increase heat transfer from the part by installing heat flux channels in the cavity [12]. Except for thermal conductivity, number of cycles in rapid tooling molds is very low compared to traditional molds due to low mechanical property. Especially, molds exhibits wear signs at the high temperature and easily broken down at ejection stages after a few cycles due to excessive ejection forces [13].

1.4 Scope of Thesis

In this study, the effect of conformal cooling channels in injection molding is investigated on the refrigerator shelf, using a commercial molding simulation program, Moldflow Plastic Insight. Various injection and cooling scenarios are modeled and compared for traditional and conformal cooling. The aim is to demonstrate the improvements brought about by conformal cooling as well as its limitations for the feasibility of using them.

In chapter 1, a background on the injection molding process and conformal cooling have been given, along with short description of how the thesis topic was chosen.

Chapter 2 gives an overview of mathematical models used in simulating injection molding process. The simulation program “Moldflow” used in this study is based on these mathematical models.

Chapter 3 gives a detailed description of the software Moldflow, used in this study, as well as comparison with other commercial software codes used in molding simulation in the industry.

Chapter 4 presents the results of this study in which the software Moldflow is used to simulate various processing scenarios. First, 1-D plastic melt flow simulation results are compared with analytical results to assess the approximations used in the mathematical models in Moldflow. Next, the effects of conformal cooling channels are studied in depth by simulating the injection and cooling stages of the process for a

benchmark part geometry. Lastly, the effects of conformal cooling channels are studied on a real life example. For this case, a refrigerator shelf that is injection molded by the company Arçelik is analyzed. The simulation results are compared with experimental data gathered from the company. A simulation of the molding of the part is presented for conformal cooling and the results are discussed.

CHAPTER 2

MODELING OF INJECTION MOLDING

2.1 Background

Most work in injection molding in literature appears in experimental nature. Mathematical models for injection moldings were developed to examine flow velocity, pressure, temperature fields and the position of the flow fronts. Process parameters of the injection molding machine can be selected based on simulation results. Such simulations help with process design, as well as foreseeing design problems that might increase process cost.

Research on injection molding started with the works of Spencer and Gilmore [14] in the early fifties. They were the first to describe the fluid dynamics and the pressure drop of Newtonian fluid in pipe filling and developed a correlation to calculate filling time associated with the molding process.

Broyer et al. [15] have solved the isothermal filling of rectangular cavity with Newtonian fluid to study flow behaviors. Menges and Liebfried [16] have investigated non-Newtonian flow into a rectangular cavity to find the path of the streamlines. White et al. [17] conducted similar studies in cavities having complex geometries. In studies of Menges, Liebfried and White and Dee, it is concluded that heat transfer can be neglected during filling. In addition to planar flow, investigations have been made on cylindrical cavities. Berger et. al [18] have solved the problem of radial filling of a circular cavity with a power–law fluid under non-isothermal conditions. Kamal and Kenig [19] have solved the same flow in a semi-circular cavity. They have studied position and orientation of the flow fronts during filling. Wu [20] further extended the

model of Berger and Gogos to the filling of a circular cavity with a power law fluid, under non-isothermal and transient conditions.

Hieber and Shen [21] developed the Generalized Hele-Shaw Model, also called 2.5D model in simulation programs to simplify complicated 3-D Navier-Stokes equations to model inelastic and non-Newtonian fluids under non-isothermal conditions in filling of thin cavity. The model ignores the velocity and pressure distribution along gapwise direction. This becomes important, as part geometry gets complicated and 3-D effects become prominent. However, today, Hele-Shaw model still remain the most popular models as most injection molded parts have small thickness variations.

Zhou [22] presented a three-dimensional finite element model to perform more accurate simulations of 3-D Newtonian flow by using Cross-type viscosity model to find the weldlines and compare with experimental results. In his model, pressure and velocity distribution along gapwise direction is not neglected. Gao [23] et al. present a 3-D finite element model capable of predicting the velocity, pressure, and temperature fields, as well as the position of the flow fronts. The velocity and pressure fields were governed by the generalized Stokes equations. The fluid behavior was predicted through the Carreau Law and Arrhenius constitutive models.

2.2 Governing Equations for Modeling Injection Molding

Injection molding process can be divided into several stages including filling, packing and cooling. Each of these stages can affect the dimension or precision and the performance of the molded part after the process. In this section, mathematical models will be presented for each injection molding stage. The software package used in this thesis, Moldflow, utilizes these models.

2.2.1 Flow Equations for the Filling Phase

In this section, the most general form of flow equations are presented. The Hele-Shaw approximation which is used in almost all injection molding simulation will

be derived, based on the general form of the conservation equations. These basic laws are derived for Newtonian fluids.

2.2.1.1 Continuity Equation

The basic principle of conservation of mass applied to an infinitesimal control volume within the fluid melt yields the continuity equation. In Cartesian coordinate system,

$$\frac{\partial \rho}{\partial t} + \frac{\partial (\rho u)}{\partial x} + \frac{\partial (\rho u)}{\partial y} + \frac{\partial (\rho w)}{\partial z} = 0 \tag{2.1}$$

or

$$\frac{\partial \rho}{\partial t} + \nabla \bullet \left(\rho \vec{V}\right) = 0 \tag{2.2}$$

2.2.1.2 Momentum Equation

For an infinitesimal fluid control volume, the force balance can be written using Newton's second law. For Newtonian fluids, the momentum eqn. yields the Navier-Stokes equation. In Cartesian coordinates, the equations are

$$\rho\left[\frac{\partial u}{\partial t}+u\frac{\partial u}{\partial x}+v\frac{\partial u}{\partial y}+w\frac{\partial u}{\partial z}\right]=-\frac{\partial P}{\partial x}+\frac{\partial}{\partial x}\left[2\mu\frac{\partial u}{\partial x}-\frac{2}{3}\left(\frac{\partial u}{\partial x}+\frac{\partial v}{\partial y}+\frac{\partial w}{\partial z}\right)\right]$$

$$+\frac{\partial}{\partial y}\left[\mu\left(\frac{\partial v}{\partial x}+\frac{\partial u}{\partial y}\right)\right]+\frac{\partial}{\partial z}\left[\mu\left(\frac{\partial u}{\partial z}+\frac{\partial w}{\partial x}\right)\right]+\rho g_x \tag{2.3.a}$$

$$\rho\left[\frac{\partial v}{\partial t}+u\frac{\partial v}{\partial x}+v\frac{\partial v}{\partial y}+w\frac{\partial v}{\partial z}\right]=-\frac{\partial P}{\partial y}+\frac{\partial}{\partial y}\left[2\mu\frac{\partial v}{\partial y}-\frac{2}{3}\left(\frac{\partial u}{\partial x}+\frac{\partial v}{\partial y}+\frac{\partial w}{\partial z}\right)\right]$$

$$+\frac{\partial}{\partial x}\left[\mu\left(\frac{\partial v}{\partial x}+\frac{\partial u}{\partial y}\right)\right]+\frac{\partial}{\partial z}\left[\mu\left(\frac{\partial w}{\partial y}+\frac{\partial v}{\partial z}\right)\right]+\rho g_y \tag{2.3.b}$$

$$\rho\left[\frac{\partial w}{\partial t}+u\frac{\partial w}{\partial x}+v\frac{\partial w}{\partial y}+w\frac{\partial w}{\partial z}\right]=-\frac{\partial P}{\partial z}+\frac{\partial}{\partial z}\left[2\mu\frac{\partial w}{\partial z}-\frac{2}{3}\left(\frac{\partial u}{\partial x}+\frac{\partial v}{\partial y}+\frac{\partial w}{\partial z}\right)\right]$$

$$+\frac{\partial}{\partial y}\left[\mu\left(\frac{\partial w}{\partial y}+\frac{\partial v}{\partial z}\right)\right]+\frac{\partial}{\partial x}\left[\mu\left(\frac{\partial u}{\partial z}+\frac{\partial w}{\partial x}\right)\right]+\rho g_z \tag{2.3.c}$$

2.2.1.3 Energy Equation

During filling, molten polymer begins to cool as it enters the cavity. Though the temperature change during filling is relatively small compared to filling, it can still affect the flow. Volume expansivity of molten polymer is zero, $\alpha_P = 0$, then energy equation can be expressed as

$$\rho C_P \frac{DT}{Dt} = \nabla\bullet\left(k\nabla T\right)+\Phi \tag{2.4}$$

or in Cartesian coordinate

$$\rho C_P\left(\frac{\partial T}{\partial t}+u\frac{\partial T}{\partial x}+v\frac{\partial T}{\partial y}+w\frac{\partial T}{\partial w}\right)=k\left(\frac{\partial^2 T}{\partial x^2}+\frac{\partial^2 T}{\partial y^2}+\frac{\partial^2 T}{\partial z^2}\right)+\Phi \tag{2.5}$$

In eqn. (2.4), the left hand side represents the rate of change of energy, the first term on the right hand side represents rate of heat diffusion in the molten polymers and the second term on the right hand side represents the rate of viscous dissipation per unit volume. Viscous dissipation is the rate at which the work done against viscous forces is irreversibly converted into heat in a viscous fluid per unit volume. In plastics, viscous dissipation can not be neglected and is expressed as [24];

$$\Phi=2\mu\left[\left(\frac{\partial u}{\partial x}\right)^2+\left(\frac{\partial v}{\partial y}\right)^2+\left(\frac{\partial w}{\partial z}\right)^2+\frac{1}{2}\left(\frac{\partial u}{\partial z}+\frac{\partial w}{\partial x}\right)^2+\frac{1}{2}\left(\frac{\partial v}{\partial x}+\frac{\partial u}{\partial y}\right)^2+\frac{1}{2}\left(\frac{\partial w}{\partial y}+\frac{\partial v}{\partial z}\right)^2 -\frac{1}{3}(\nabla\bullet V)^2\right] \tag{2.6}$$

2.2.2 Hele-Shaw Approximation

Parts produced through injection molding are generally thin parts, thus the mold cavities have thicknesses much smaller than their planar dimensions. Hele-Shaw model is appropriate to represent the flow of a generalized Newtonian fluid in a thin cavity. The small gapwise dimensions allow the use of the Hele-Shaw approximation while analyzing the flow in injection molding [25]. Fig. 2.1 shows flow through a narrow gap into a mold cavity. The Hele-Shaw equation will be derived based on this schematic. No-slip conditions apply at the cavity boundaries. The momentum equations stated earlier will be simplified using the Hele-Shaw approach. For Hele Shaw approximation, the following assumptions are made [26]

- The cavity is thin; b/L << 1, where b is thickness of the cavity and L is the length of the cavity in the flow direction. As the width to thickness ratio increases, the results will be more accurate

- The velocity component in the z direction is neglected and pressure is function of x and y only.
- The velocity gradient in the x and y directions is negligible compared to the z direction gradient
- The inertial terms are negligible in comparison to the viscous terms.
- Surface tension and body forces are negligible
- Heat conduction in the flow direction is neglected
- Thermal convection in the gapwise direction is neglected
- Material is incompressible and viscous with the melt density remaining constant during filling

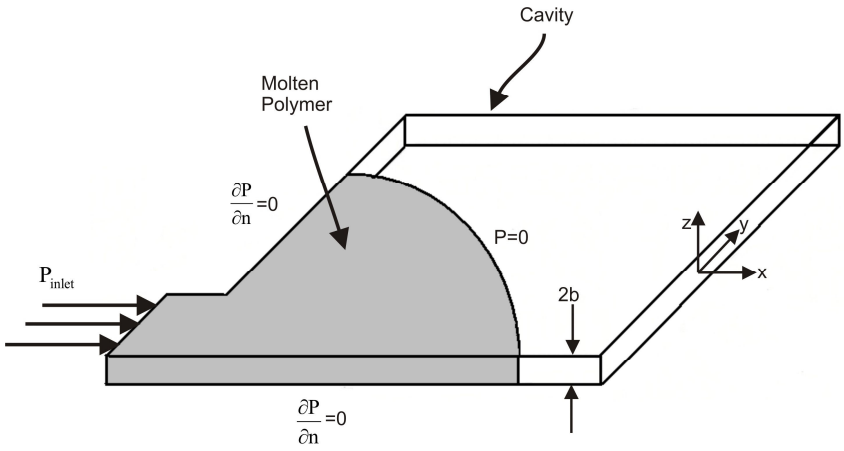

Figure 2.1 A narrow gap cavity used in the Hele-Shaw approximation

(Dantzig and Tucker, 2001, p. 218)

2.2.2.1 Continuity Equation

Applying Hele-Shaw assumptions to the continuity eqn. (2.1) yields eqn. (2.6). Since, the z-component of the velocity is neglected and the fluid is incompressible, eqn. (2.1) becomes

$$\frac{\partial u}{\partial x}+\frac{\partial v}{\partial y}=0 \tag{2.7}$$

2.2.2.2 Momentum Equation

For the x-momentum equation eqn. (2.3.a), neglecting the velocity component in z-direction and body forces yields

$$\rho\left[\frac{\partial u}{\partial t}+u\frac{\partial u}{\partial x}+v\frac{\partial u}{\partial y}\right]=-\frac{\partial P}{\partial x}+\frac{\partial}{\partial x}\left[2\mu\frac{\partial u}{\partial x}-\frac{2}{3}\left(\frac{\partial u}{\partial x}+\frac{\partial v}{\partial y}\right)\right]$$

$$+\frac{\partial}{\partial y}\left[\mu\left(\frac{\partial v}{\partial x}+\frac{\partial u}{\partial y}\right)\right]+\frac{\partial}{\partial z}\left[\mu\frac{\partial u}{\partial z}\right] \tag{2.8}$$

The left hand side of the above equation denotes inertial forces. Since, in the Hele-Shaw approximation, the viscous forces dominate the inertial forces, then the x-momentum equation becomes

$$0=-\frac{\partial P}{\partial x}+\frac{\partial}{\partial x}\left[2\mu\frac{\partial u}{\partial x}-\frac{2}{3}\left(\frac{\partial u}{\partial x}+\frac{\partial v}{\partial y}\right)\right]+\frac{\partial}{\partial y}\left[\mu\left(\frac{\partial v}{\partial x}+\frac{\partial u}{\partial y}\right)\right]+\frac{\partial}{\partial z}\left[\mu\frac{\partial u}{\partial z}\right] \tag{2.9}$$

Using the continuity eqn. (2.7), eqn. (2.9) yields

$$0=-\frac{\partial P}{\partial x}+\frac{\partial}{\partial x}\left[2\mu\frac{\partial u}{\partial x}\right]+\frac{\partial}{\partial y}\left[\mu\left(\frac{\partial v}{\partial x}+\frac{\partial u}{\partial y}\right)\right]+\frac{\partial}{\partial z}\left[\mu\frac{\partial u}{\partial z}\right] \tag{2.10}$$

Due to small gap presence, the velocity gradient along z-direction dominates other velocity gradients, i.e

$$\frac{\partial u}{\partial z},\frac{\partial v}{\partial z}>>\frac{\partial u}{\partial x},\frac{\partial u}{\partial y},\frac{\partial v}{\partial x},\frac{\partial v}{\partial y} \tag{2.11}$$

The final form of the x-momentum equation becomes

$$\frac{\partial P}{\partial x} = \frac{\partial}{\partial z}\left[\mu \frac{\partial u}{\partial z}\right] \tag{2.12}$$

Likewise, the momentum equation in the y-direction is obtained as

$$\frac{\partial P}{\partial y} = \frac{\partial}{\partial z}\left[\mu \frac{\partial v}{\partial z}\right] \tag{2.13}$$

with the momentum equation in the z-direction reducing to

$$\frac{\partial P}{\partial z} = 0 \tag{2.14}$$

Integrating equations (2.12) and (2.13) with respect to z yields

$$\frac{\partial u}{\partial z} = \frac{\partial P}{\partial x}\frac{z}{\mu} + f(x, y) \tag{2.15.a}$$

$$\frac{\partial v}{\partial z} = \frac{\partial P}{\partial y}\frac{z}{\mu} + g(x, y) \tag{2.15.b}$$

where f and g are integration functions

$\frac{\partial P}{\partial x}, \frac{\partial P}{\partial y}$ can only be functions of x, y. Flow is symmetric about the center plane, therefore

$$\left(\frac{\partial u}{\partial z}\right)_{z=0} = \frac{\partial P}{\partial x}\frac{0}{\mu} + f(x, y) = 0 \tag{2.16}$$

leading to f(x, y) = 0. Same argument is applied to eqn. (2.15.b) yielding g(x, y) = 0

Then (2.15.a) and (2.15.b) become

$$\frac{\partial u}{\partial z} = \frac{\partial P}{\partial x}\frac{z}{\mu} \tag{2.17.a}$$

$$\frac{\partial v}{\partial z} = \frac{\partial P}{\partial y}\frac{z}{\mu} \tag{2.17.b}$$

Integrating equations (2.17.a) and (2.17.b) from z to b leads to

$$u(x,y,b)-u(x,y,z)=\frac{\partial P}{\partial x}\int_{z}^{b}\frac{z^{*}}{\mu}dz^{*} \tag{2.18.a}$$

$$v(x,y,b)-v(x,y,z)=\frac{\partial P}{\partial y}\int_{z}^{b}\frac{z^{*}}{\mu}dz^{*} \tag{2.18.b}$$

where z^{*} is a dummy integration variable

Applying no slip condition exists at z = b,

$$u(x,y,z)=-\frac{\partial P}{\partial x}\int_{z}^{b}\frac{z^{*}}{\mu}dz^{*} \tag{2.19.a}$$

$$v(x,y,z)=-\frac{\partial P}{\partial y}\int_{z}^{b}\frac{z^{*}}{\mu}dz^{*} \tag{2.19.b}$$

Equations (2.19.a) and (2.19.b) yield the velocity components in x and y direction based on pressure gradient, fluid viscosity and gap dimensions. These equations are then integrated across the gap to yield average velocities in x and y direction as

$$\bar{u}(x,y)=-\frac{1}{b}\frac{\partial P}{\partial x}\int_{0}^{b}\int_{z}^{b}\frac{z^{*}}{\mu}dz^{*}dz \tag{2.20.a}$$

$$\bar{v}(x,y)=-\frac{1}{b}\frac{\partial P}{\partial y}\int_{0}^{b}\int_{z}^{b}\frac{z^{*}}{\mu}dz^{*}dz \tag{2.20.b}$$

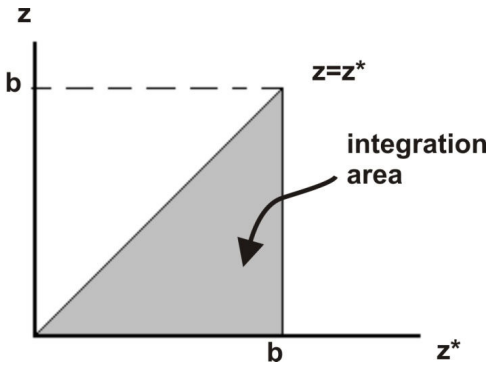

Figure 2.2 Integration region

Equations (2.20.a) and (2.20.b) are double integrals in z-z* domain. Changing the order of integration and adjusting integration limits with respect to Fig. 2.2, eqns. (2.20.a) and (2.20.b) become

$$\bar{u}(x,y) = -\frac{1}{b}\frac{\partial P}{\partial x}\int_0^b\int_0^{z^*}\frac{z}{\mu}dzdz^* = -\frac{1}{b}\frac{\partial P}{\partial x}\int_0^b\frac{z^{*2}}{2\mu}dz \tag{2.21.a}$$

$$\bar{v}(x,y) = -\frac{1}{b}\frac{\partial P}{\partial y}\int_0^b\int_0^{z^*}\frac{z}{\mu}dzdz^* = -\frac{1}{b}\frac{\partial P}{\partial y}\int_0^b\frac{z^{*2}}{2\mu}dz \tag{2.21.b}$$

The dummy variable z^* is dropped and fludity S is defined as

$$S(x,y) = \int_0^b\frac{z^2}{\mu}dz \tag{2.22}$$

The fluidity S represents the sum of the effect of changing temperature and fluid rheology across the gap. S depends on the melt viscosity μ and the half thickness of the mold cavity. This term is constant if the fluid is Newtonian. Physically, the fluidity determines the ease with which the melt can be forced through the mold cavity. A high value of fluidity is associated with easy flowing materials. Conversely, a low value of fluidity indicates that the feedstock melt offers a high resistance to flow [27].

Placing (2.22) into equations (2.21.a) and (2.21.b), the final form of average velocities are obtained as

$$\bar{u}(x,y) = -\frac{S}{2b}\frac{\partial P}{\partial x} \tag{2.23.a}$$

$$\bar{v}(x,y) = -\frac{S}{2b}\frac{\partial P}{\partial y} \tag{2.23.b}$$

Equations (2.23.a) and (2.23.b) indicate that if pressure distribution and melt properties are known, the average flow velocities can be determined. The pressure

equation is obtained by substituting equations (2.19.a) and (2.19.b) in the continuity equation (2.7), integrating along the cavity thickness as

$$\frac{\partial}{\partial x}\left[S\frac{\partial P}{\partial x}\right]+\frac{\partial}{\partial y}\left[S\frac{\partial P}{\partial y}\right]=0 \tag{2.24}$$

Pressure distribution of molten polymer in the cavity can be found by eqn. (2.24) at any instant of the filling. For the solution of eqn. (2.24), the pressure boundary conditions are needed. The boundary conditions are shown in Fig. (2.3). At the melt front, the pressure is constant and it is often set to atmospheric pressure as zero gage [28].

$$P_{\text{flow front}} = 0 \tag{2.25.a}$$

On the side walls, the normal components of the velocity vanish,

$$\left(\frac{\partial P}{\partial n}\right)_{\text{wall}} = 0 \qquad \text{at the side walls} \tag{2.25.b}$$

At the flow inlet (injection gate), the pressure is the injection pressure

$$P_{\text{inlet}} = P_i \tag{2.25.c}$$

Injection molding machines operate either with prescribed injection pressure or prescribed plastic flow rate. In the case of prescribed volumetric flow rate, the pressure boundary condition at inlet would be a Neumann type boundary condition**,** obtained from equation (2.23.a) and (2.23.b).

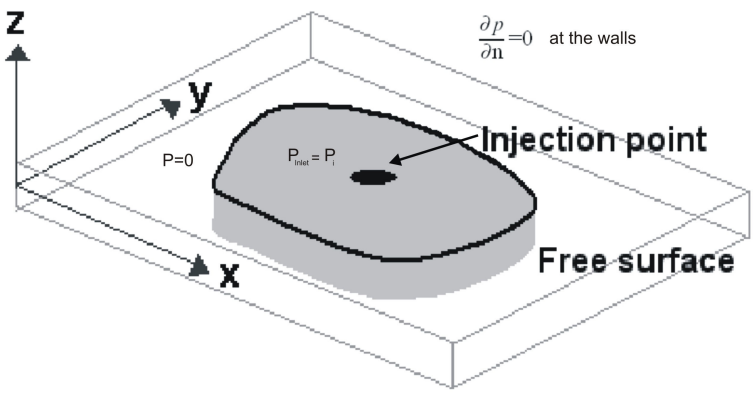

Figure 2.3 Pressure boundary conditions in Hele-Shaw flow [26]

2.2.2.3 Energy Equation

Due to small gap (thin cavity) assumption, temperature gradients along z-direction dominate gradients along x & y-directions. Neglecting velocity component in gapwise direction (w=0), the energy equation (eqn. 2.5) becomes

$$\rho C_P\left(\frac{\partial T}{\partial t}+u\frac{\partial T}{\partial x}+v\frac{\partial T}{\partial y}\right)=k\frac{\partial^2 T}{\partial z^2}+\Phi \tag{2.26}$$

Using continuity eqn. (2.7), neglecting the gapwise component of velocity and the velocity gradients along x & y components, the viscous dissipation terms becomes

$$\Phi=\mu\left[\left(\frac{\partial u}{\partial z}\right)^2+\left(\frac{\partial v}{\partial z}\right)^2\right] \tag{2.27}$$

Final form of the energy equation becomes

$$\rho C_p\left(\frac{\partial T}{\partial t}+u\frac{\partial T}{\partial x}+v\frac{\partial T}{\partial y}\right)=k\frac{\partial^2 T}{\partial z^2}+\mu\left[\left(\frac{\partial u}{\partial z}\right)^2+\left(\frac{\partial v}{\partial z}\right)^2\right] \tag{2.28}$$

with boundary and initial conditions

$$T = T_w \qquad \text{(cavity walls)} \qquad (2.29.a)$$

$$\left(\frac{\partial T}{\partial z}\right)_{z=0} = 0 \qquad \text{(center of cavity)} \qquad (2.29.b)$$

$$T = T_i \qquad t = 0 \qquad (2.29.c)$$

where T_i is the initial melt temperature and T_w is the cavity wall temperature

The Hele-Shaw approximation reduces the three dimensional viscous unsteady melt flow into a two-dimensional problem. The primary variable for melt flow through the narrow gap is the pressure, which varies with x and y. Filling progression of the program is represented in Fig. 2.4. Firstly, fluidity is calculated, then pressure distribution is found from eqn. (2.24) with given boundary conditions. Since viscosity can vary due to rate of shear strain, and thus the flow domain, fluidity is updated until a convergence reached. After that, flow front temperature distribution is calculated from energy equation (2.28). Average velocities are determined from eqns. (2.23.a.) & (2.23.b), and then flow progression is calculated with given time increment. Once the new flow domain is defined based on the new position of the melt flow front, the solution is repeated until cavity is filled [29].

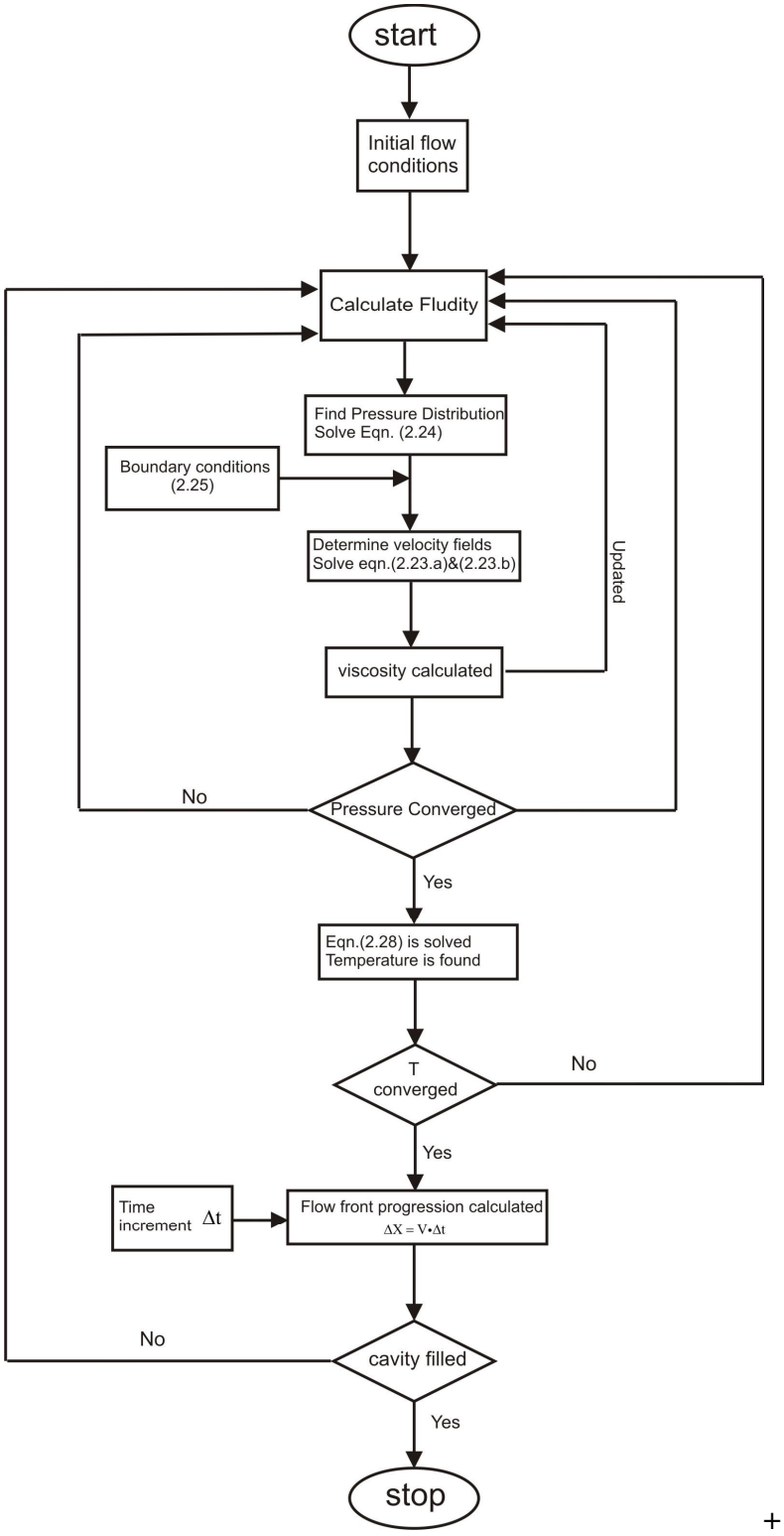

Figure 2.4 Filling progression chart

2.3 Fountain Flow

Hele-Shaw approximation fails when 3-D flow effect become prominent, as in varying thickness cavities or the fountain flow as shown in Fig. 2.5. The flow behavior at the flow front, usually referred as "fountain flow," has to do with the fluid near the center moving faster than the average velocity across the thickness. As plastic flows into the cavity, the plastic in contact with the mold wall quickly freezes. This creates a frozen layer of plastic between the mold and the molten plastic. At the interface between the static frozen layer and the flowing melt, the polymer molecules are stretched out in the direction of flow. This alignment and stretching is called orientation. This phenomenon (high shear rates near the wall and therefore high orientation) causes the fluid elements to be highly distorted. In most injection molding applications, the fountain flow region is the order of magnitude of the gap thickness. As a consequence, the convection effects in the fountain region cannot be represented with only the knowledge of a gapwise averaged velocity (Hele-Shaw approximation). Also, since the details of the fountain region are lost, it is not possible to track the particle trajectories in the newly filled part of the expanding fluid domain. The Hele-Shaw type filling simulations cannot provide accurate details of the flow in the gate or fountain region because the flow remains three dimensional.

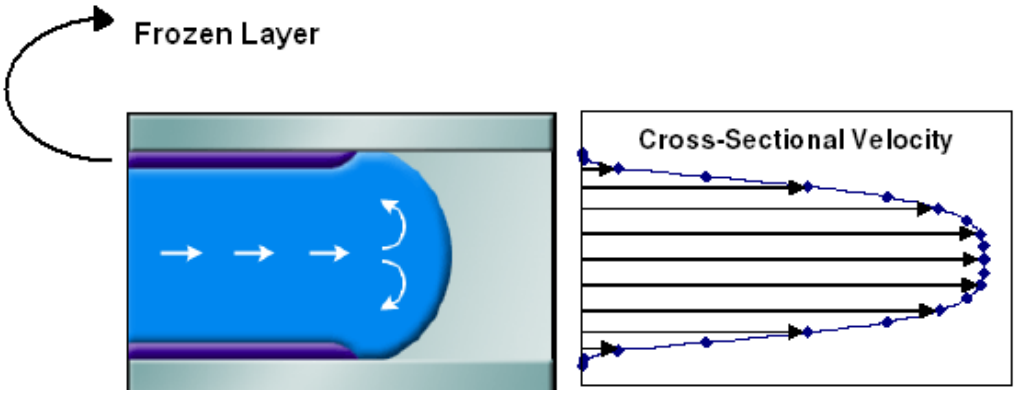

Figure 2.5 Fountain flow and velocity profiles for flow through a channel [2]

2.4 Viscosity Models in Simulation of the Filling Stage of Injection Molding Process

In plastic melt flows, the rheological behavior of the melt can be complicated. Usually, molten polymer will be non-Newtonian. In order to solve for flow pressure, velocity and temperature in the cavity, the fluid behavior must be accurately described with the appropriate constitutive model. Common models such as Carreau and Cross models [31] are included in the fluidity term during solution of flow equations. Such models relate melt viscosity to temperature and shear rate.

2.5 Packing Phase

In injection molding process once the mold is completely filled, the packing phase of the cycle begins. A pre-arranged pressure profile is applied until the gate freezes. During this phase, as the plastic in the mold cools and shrinks, a small amount of plastic flows into the mold to compensate shrinkage. The pressure gradients, $\frac{\partial P}{\partial x}, \frac{\partial P}{\partial y}$ and $\frac{\partial P}{\partial z}$, are relatively low in the packing phase with respect to filling phase, but pressure variation with time, $\frac{\partial P}{\partial t}$, is relatively high.

Unlike filling stage, density is not incompressible in packing stage; therefore a mathematical representation of the specific volume is necessary. A compressible formulation is required for the packing phase. “Two domain Tait Model” [eqn. (2.30)] is used to describe the variation of the specific volume as function of the pressure and temperature during the packing phase by the PVT behavior of the plastic material [32].

$$\nu(P,T) = \nu(0,T)\left[1 - 0{,}894 \ln\left(1 + \frac{P}{B(T)}\right)\right] \tag{2.30}$$

Here $\nu(0,T)$ is specific volume at zero gauge pressure and $B(T)$ is the pressure sensitivity of the material. $\nu(0,T)$ and $B(T)$ are calculated depending on the glass transition temperature of the polymer.

When the temperature is above the glass transition temperature,

$$\nu_0(T) = b_{1m} + b_{2m}(T - T_t) \tag{2.31.a}$$

$$B(T) = b_{3m} e^{(-b_{4m}(T-T_t))} \tag{2.31.b}$$

When the temperature is below the glass transition temperature,

$$\nu_0(T) = b_{1s} + b_{2s}(T - T_t) \tag{2.31.c}$$

$$B(T) = b_{3s} e^{(-b_{4s}(T-T_t))} \tag{2.31.d}$$

Here, T_t is the glass transition temperature. b_{1m}, b_{2m}, b_{3m}, b_{4m}, b_{1s}, b_{2s}, b_{3s} and b_{4s} are experimentally obtained data for the molten polymer.

The PVT relationship suggests using high packing pressure to compensate volumetric change during cooling.

2.6 Cooling Phase

The cooling phase occurs following the end of packing. The cooling lasts until the mold opens and the part is ejected. In a typical mold injection cycle, filling time is very small compared to the cooling time. In modeling part cooling, the contact resistance between the mold cavity and the part interfaces is ignored and a perfect thermal contact between the two is assumed.

Fig. 2.6 presents a schematic view of a mold with cooling channels and a cavity filled with part. A coolant is passed through the cooling channels that remove heat from the mold which is heated by the hot plastic part through the conduction.

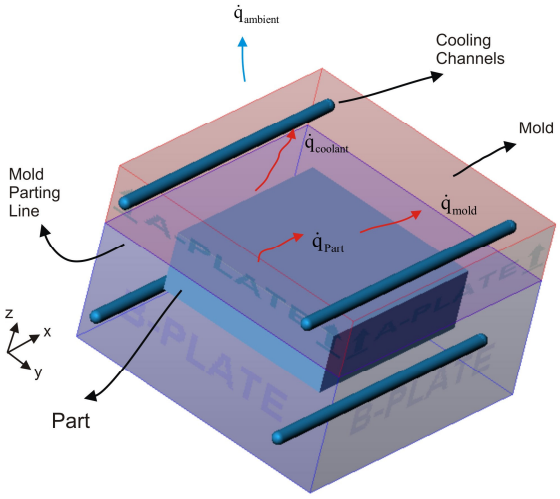

Figure 2.6 Heat transfer configuration within the mold

Heat is transferred from the polymer to the mold, which is then partly transferred to the coolant moving through the cooling channels and the surrounding air with convection. The energy balance can be expressed by

$$\dot{q}_{Part} = \dot{q}_{coolant} + \dot{q}_{mold} + \dot{q}_{ambient} \tag{2.32}$$

where $\dot{q}_{Part}$ is the rate of heat transferred from the polymer, $\dot{q}_{coolant}$ is the rate of heat transferred to the coolant, $\dot{q}_{mold}$ is the rate of change of the energy stored in the mold and $\dot{q}_{ambient}$ is the rate of heat transferred to the surround air.

2.6.1 Part

During cooling, energy equation for the part can be stated as

$$\rho_p \left(C_P\right)_p \frac{\partial T_p}{\partial t} = k_p \nabla^2 T_p \tag{2.33}$$

where subscript p denotes the part

The initial and boundary conditions for part cooling are

$$T_p = T_{pi} \qquad \text{(initial temperature of polymer)} \tag{2.34.a}$$

$$-k_p \frac{\partial T_p}{\partial n_p} = -k_m \frac{\partial T_m}{\partial n_m} \qquad \text{(at part} - \text{mold interface)} \tag{2.34.b}$$

where n_p and n_m are the outward unit vectors of the part and mold at the interface, and subscript m denotes the mold.

2.6.2 Cooling Channels

The flow in the cooling channel is 1-D, steady, turbulent and fully developed. For axisymetric flow with convection dominating conduction in flow direction, the energy equation for the coolant becomes.

$$\rho_c (C_P)_c \left[u \left(\frac{\partial T_c}{\partial x} \right) \right] = k_c \left[\left(\frac{1}{r} \right) \frac{\partial}{\partial r} \left(r \frac{\partial T_c}{\partial r} \right) \right] \tag{2.35}$$

where r is radial direction, x is axial flow direction, subscript c denotes coolant.

The boundary conditions are expressed as

$$T_c (0, r) = T_{ci} \tag{2.36.a}$$

$$\left(\frac{\partial T_c}{\partial r} \right)_{r=0} = 0 \tag{2.36.b}$$

$$h_c (T_m - T_c) = -k_m \left(\frac{\partial T_m}{\partial n_c} \right)_{r=R_0} \tag{2.36.c}$$

where n_c is the outward unit vector of the coolant interface, T_{ci} is the inlet temperature of the coolant, R_0 is the radius of the coolant channel.

The heat transfer coefficient h_c is based on the Dittus-Boetler correlation [33],

$$h_c = 0.023\left(\frac{k_c}{D}\right)(Re)^{0.8}(Pr)^{0.4} \tag{2.37}$$

which is valid for 10000<Re<12000 and 0.7<Pr<12. The Reynolds number is based on coolant channel diameter

2.6.3 Mold

Energy equation for cooling of mold is expressed similar to the part, as

$$\rho_m (C_P)_m \frac{\partial T_m}{\partial t} = k_m \nabla^2 T_m \tag{2.38}$$

The boundary and initial conditions for mold cooling are

$$T_m(x, y, z, 0) = T_{mi} \tag{2.39.a}$$

$$-k_p \frac{\partial T_p}{\partial n_p} = -k_m \frac{\partial T_m}{\partial n_m} \qquad (\text{part} - \text{mold interface}) \tag{2.39.b}$$

$$h_c (T_m - T_c) = -k_m \left(\frac{\partial T_m}{\partial n_c}\right) \qquad (\text{part} - \text{coolant interface}) \tag{2.39.c}$$

$$h_\infty (T_m - T_\infty) = -k_m \left(\frac{\partial T_m}{\partial n_\infty}\right) \qquad (\text{mold-ambient interface}) \tag{2.39.d}$$

where T_{mi} is the initial temperature of the mold, T_∞ is the ambient temperature, n_∞ is the outward unit vectors of mold-ambient interface.

It can be seen that two boundary conditions of mold (2.39.b and 2.39.c) are same as that of part (2.34.b) and that of coolant (2.36.c) due to including same interfaces. Except first cycle, initial mold temperature of every cycle is the ejection mold temperature of the former cycle.

CHAPTER 3

NUMERICAL IMPLEMENTATION: MOLDFLOW

In this study, the commercial injection molding simulation program Moldflow Plastic Insight (MPI) is used to analyze filling, packing and cooling of the injection molding process. The software is versatile and is designed to determine various process and mold parameters such as cooling channel layout, configuration of the feed system, details of the mold, polymer type and optimum parameter values such as coolant flow rate and inlet melt temperature of the molten polymer. The purpose of using such a simulation program is to foresee possible design and processing problems before the molds are produced and production is carried out, so that time and money consumption can be decreased.

In this chapter, the details of the Moldflow program are presented in a sequential manner, based on the order of the processing steps.

3.1 Description of Moldflow Plastic Insight

3.1.1 Creation of Mesh for the Part that will be Injection Molded

At the beginning of molding analysis the solid model of the part that will be produced needs to be input to Moldflow. The solid model must be in .stl (standart triangulator language) format. CAD/CAM software packages convert 3-D models into .stl format in order to be read by another software packages. Before importing the solid model, the mesh type is chosen from task bar (1) as shown in Fig. 3.1. The mesh types are composed of mid-plane (2-D), fusion type (2.5D) and tetra type (3-D). According to mesh type, solution approaches change. A geometry represented by mid-plane mesh is assigned a thickness. All properties are calculated based on this thickness. Fusion type mesh is appropriate for Hele-Shaw model. It simplifies a 3-D model into a 2-D

model reducing the computation time. Outer surfaces of the part are aligned with a boundary shell mesh. It looks like a 3-D model but the solution does not consider variations along thickness. Therefore, this model is not appropriate for thick parts. As parts get thicker, the accuracy of analysis decreases in Hele-Shaw model. In that case, 3-D model is used to perform more accurate simulations of a fully 3-D flow, though this model takes more computational time.

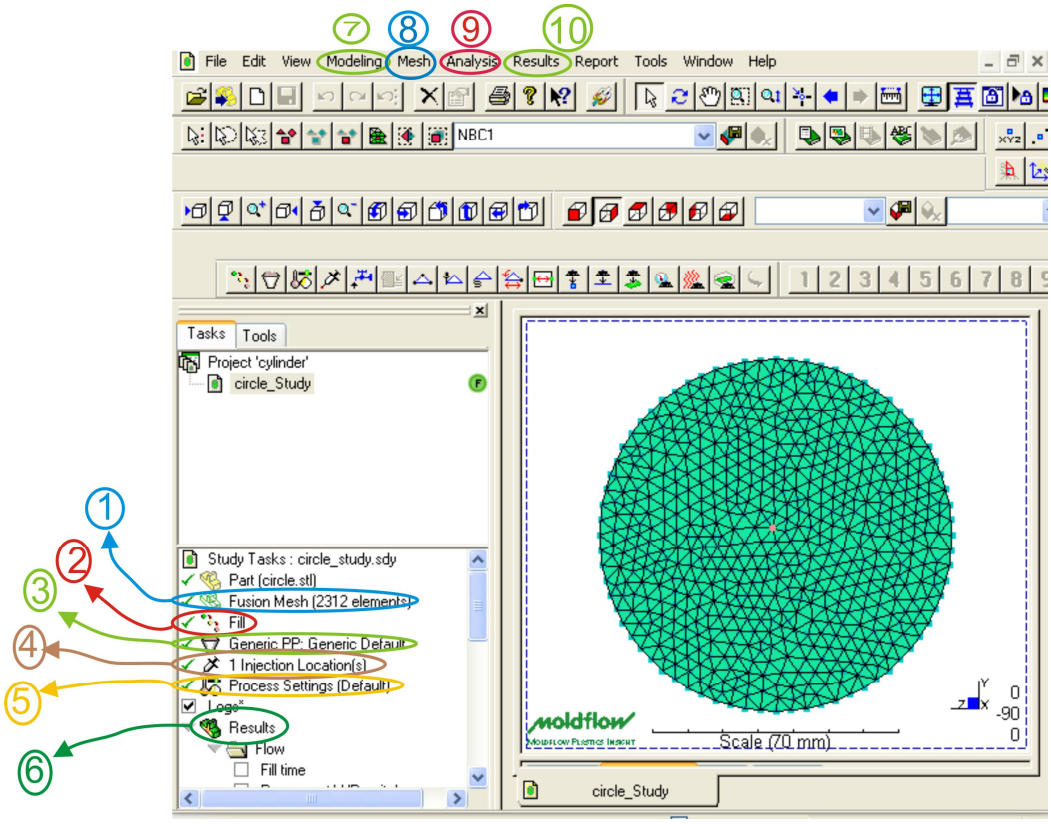

Figure 3.1 The default MPI screen layout

3.1.2 Mesh Analysis

After mesh is generated, mistakes such as unstitched elements, overlapping elements and elements having high aspect ratio in meshes can be corrected by using necessary mesh tools from mesh task bar (8) as shown in Fig.3.1. Quality of mesh is

important because it affects the analysis accuracy. Furthermore, grid adaptation of mesh is also important. Mesh density should be arranged with respect to gradient of properties. For example, mesh density should be large at the inlet of the gate and at regions where thickness changes suddenly. The window shown in Fig. 3.2 presents information about the generated mesh.

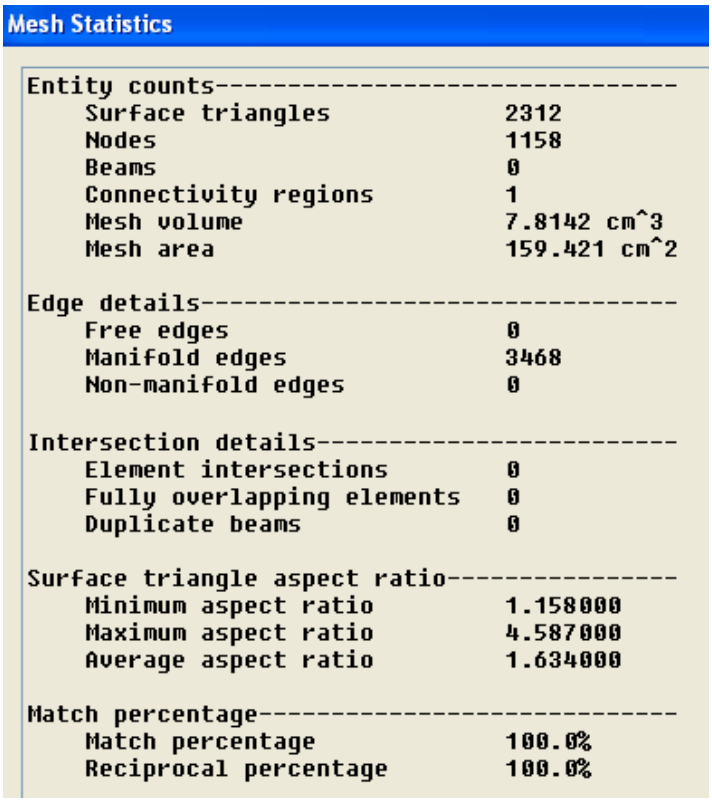

Figure 3.2 Information table about mesh quality (mesh type: fusion)

In entity counts, surface triangles indicate number of meshes and nodes indicate number of nodes in mesh. Beam is the number of mesh used in the cooling channels and the feed system as shown in Fig.3.3. Connectivity regions show the number of pieces the part consists of. Mesh volume and area give the total part volume and surface area.

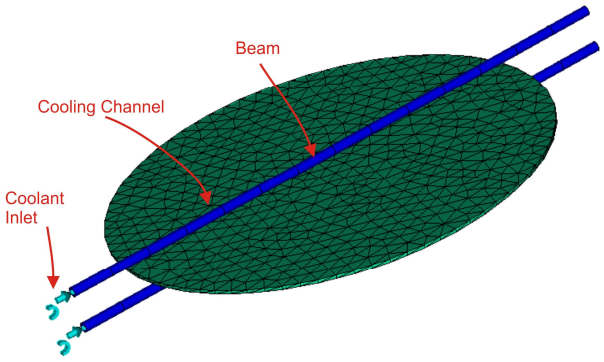

Figure 3.3 Demonstration of beam mesh in cooling channels

In edge details, number of free, manifold and non-manifold edges on the meshes is shown. A free edge is a surface triangle edge that is only belongs to one surface triangle element, not shared by other elements as shown in Fig 3.4.a. A manifold edge is a surface triangle edge shared by two surface triangles attached to it as shown in Fig 3.4.b. Non-manifold edge is shared more than two surface triangle elements as shown in Fig 3.4.b. Non-manifold and free edges must be cleaned among the surface triangles elements, only manifold edges must remain.

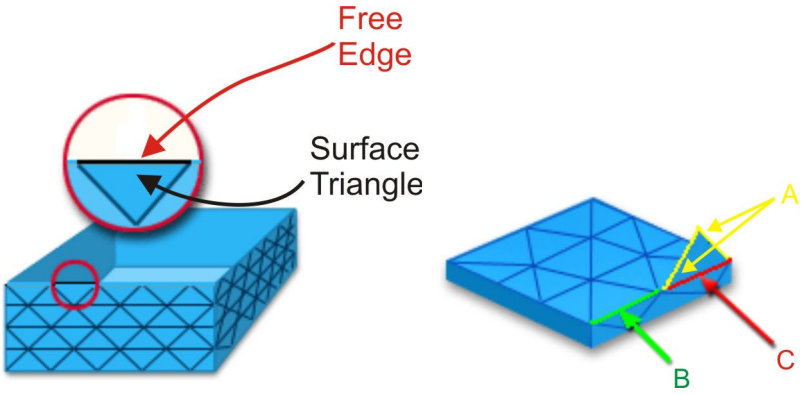

(a) **(b)**

Figure 3.4 (a) Representation of free edge (b) A is free edge, B is a manifold edge, C is non-manifold edge

In intersection details, number of intersecting and overlapping elements is given. Overlapping mesh elements are mesh elements that overlap in the same plane, as shown in right side of Fig. 3.5.a. Intersecting elements are mesh elements that lie on different planes and intersect each other, as shown in right side of Fig. 3.5.b. Overlapping elements must be deleted and elements should be prepeared as shown in left side of Fig. 3.5.a. Intersecting elements are corrected by re-arranging nodes of the surface triangles and represented as shown in left side of Fig. 3.5.b.

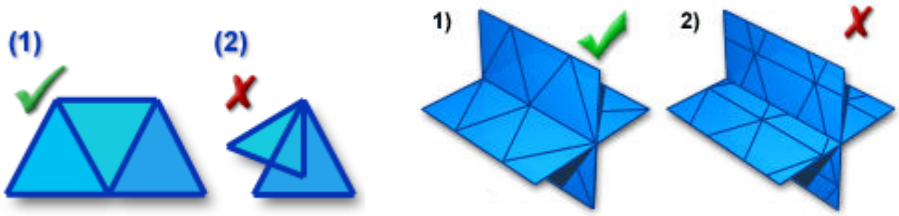

(a) **(b)**

Figure 3.5 (a) 1) Mesh elements not overlapping 2) overlapping mesh elements (b) 1) elements join at their edges 2) intersecting elements which cut through each other

In surface triangle aspect ratio, maximum, minimum and average aspect ratio values of the meshes are represented. Aspect ratio is equal to w/h as shown in Fig. 3.6. Aspect ratios are especially important in sensitive areas such as gates. Meshes having lower aspect ratio usually give more accurate results.

Figure 3.6 Aspect ratio relation of tetra element

From mesh statistics of Fig. 3.2, errors such as unstitched edges, overlapping elements, holes in elements or elements with high aspect ratio can be observed. These mistakes are corrected by mesh tool options “Mesh Repair Wizard” or “Mesh Tools”. Difference between “Mesh Repair Wizard” and “Mesh Tools” is that “Mesh Repair Wizard” finds free edges, holes, overlapping elements and elements with high aspect ratios and fixes them automatically. However, when it fixes the corrupted elements, it could corrupt the smooth elements. “Mesh Tools” can fix corrupted mesh manually, one by one. Fig. 3.7 presents various meshing errors and corrections.

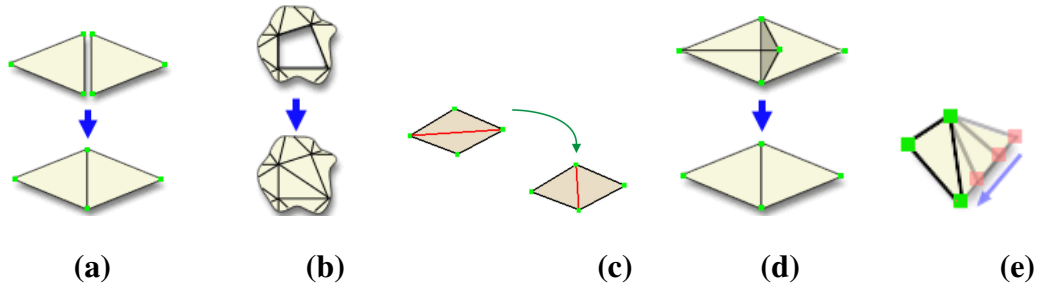

Figure 3.7 (a) Stitch free edges are fixed (b) Holes are closed (c) High aspect ratio is decreased (d) Overlapping elements fixed (e) Location of nodes modified

Elements on opposite skins of a fusion mesh match one another as best as possible. The mesh percentage in Fig. 3.2 represents the percentage of elements that have a direct partner on the other side. A mesh match percentage of 85% or higher is acceptable for a flow (fusion) analysis. A percentage of 50% or lower will cause the flow analysis to fail. Fig. 3.8.a shows an example of good mesh matching: where element 1 matches with element 2, and element 3 matches with element 4. Fig 3.8.b shows a bad matching. Element 1 matches with element 2, but element 2 matches with element 3 also.

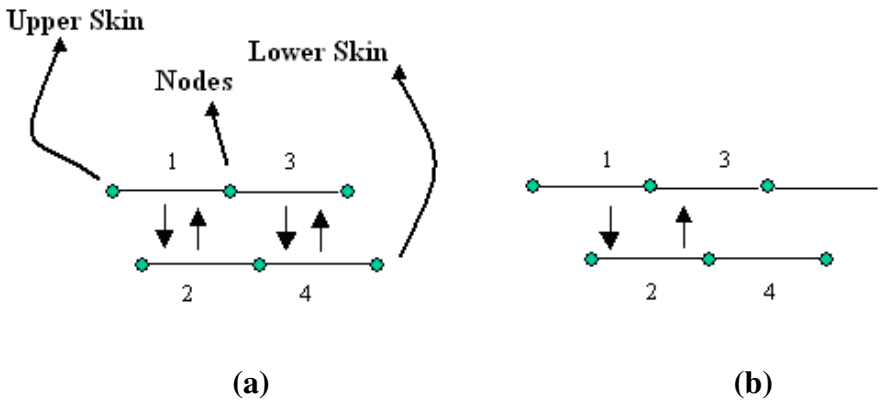

Figure 3.8 Illustration of mesh match

3.1.3 Gate Analysis

Once the solid model is input to the program and the mesh is generated, the location of injection gate or gates need to be determined in the part cavity through which plastic will be injected. For this purpose, the gate location analysis which is accessed under the "analysis" task bar (2) or (9) is used. The analysis presents the suitability for an injection location, from the worst position (red) to the most suitable one (blue) as shown in Fig. 3.9. Then injection location is defined by using task bar (4) in Fig. 3.1. The analysis looks for the best location based on flow resistance, thickness of the gate location and geometry of the part. Molten polymer flow front should reach the cavity walls at the same time evenly without overpacking, therefore program looks for symmetry in geometry. Molten polymer could also freeze before complete filling of the cavity if the gate location is too thin or flow resistance is too high.

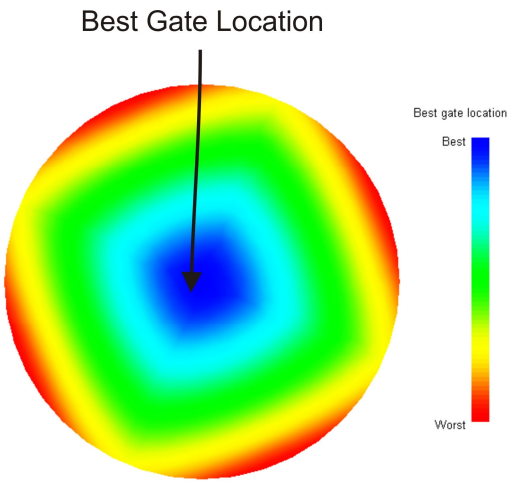

Figure 3.9 Gate location results

3.1.4 Feed System

Structure and location of the feed system (Fig. 3.11) can be set as shown in Fig. 3.10. The size and geometry of the runner, sprue and geometry are defined at this section. It is applicable under “Modeling” task bar (7) in Fig. 3.1.

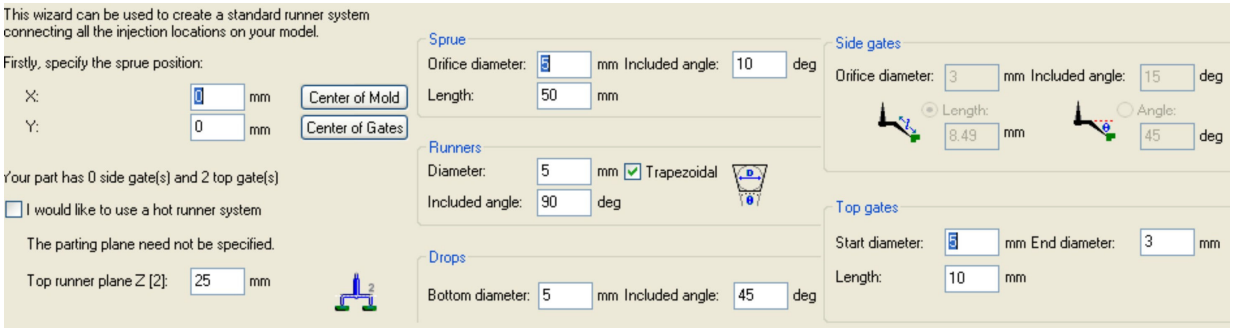

Figure 3.10 Manual of the feed system

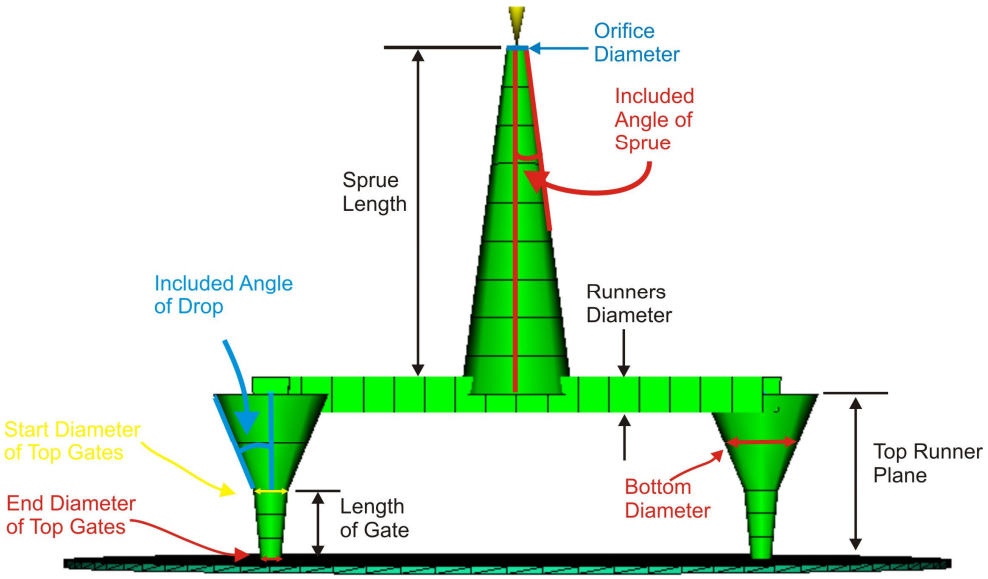

Figure 3.11 Representation of the feed system

3.1.5 Cavity Duplication Wizard

In “Cavity Duplication Wizard”, number of cavities and alignment of cavities for multicavity injection molding is arranged from information about only one part, according to the quantity of the parts to be manufactured as shown in Fig. 3.12. Column and row spacing can be arranged and can be previewed. It is applicable under “Modeling” the task bar (7) in Fig. 3.1.

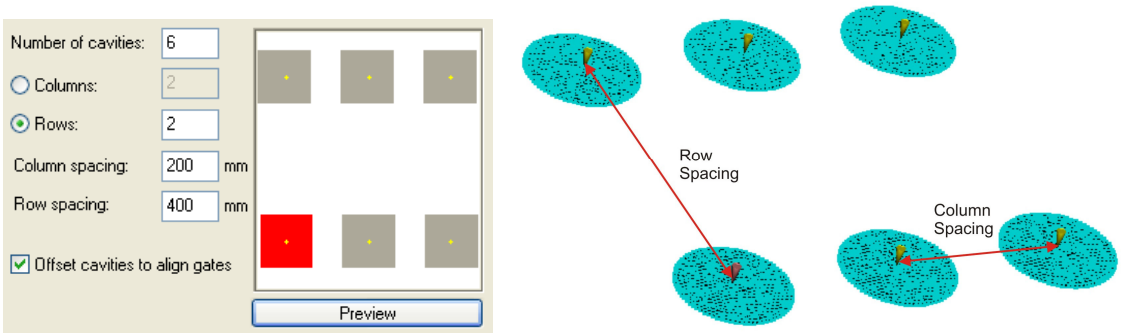

(a) **(b)**

Figure 3.12 (a) "Cavity Duplication Wizard" (b) Representation of the "Cavity Duplication Wizard" in Moldflow monitor

3.1.6 Cooling Circuit Wizard

In "Cooling Circuit Wizard", locations and diameters of cooling channels are set up. Coolant flow rate and inlet temperature of the coolant are defined on the model as shown in Fig. 3.12.b. It is applicable under "Modeling" task bar (7) in Fig. 3.1.

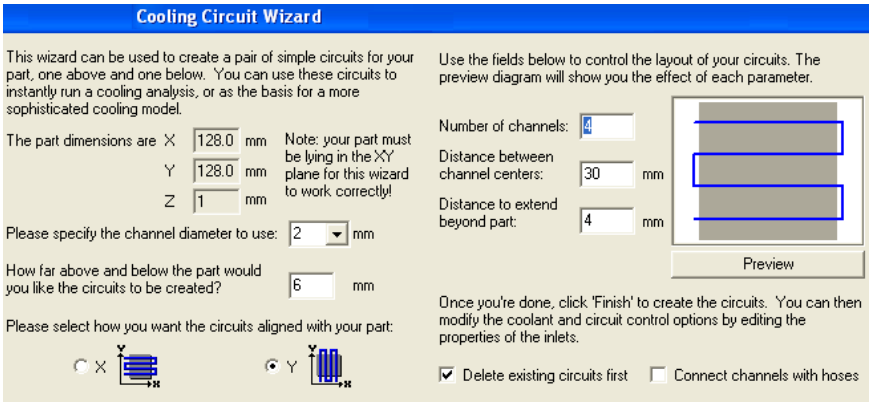

(a)

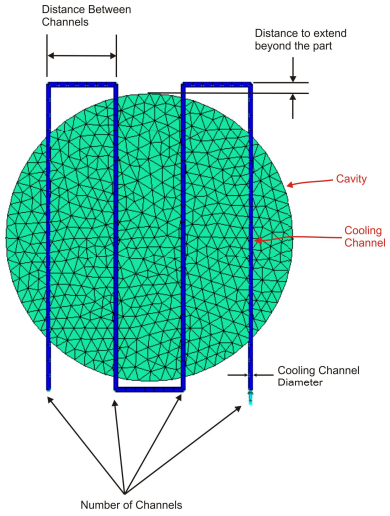

(b)

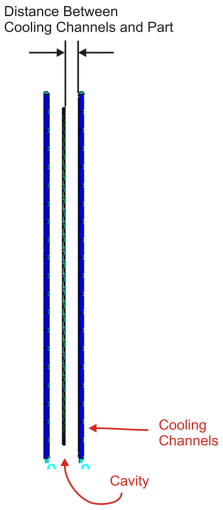

(c)

Figure 3.13 (a) "Cooling Circuit Wizard" (b) Representation of parameters on the model on top view (c) Representation of parameters on the model on right view

3.1.7 Molding Window

"Molding Window" is used to determine the best preliminary process parameters for analysis. The molding window analysis provides recommendations for the injection time, mold temperature and polymer melt temperature values to use as

preliminary inputs for a full flow analysis. It is applicable under the task bar (2) or (9) in Fig. 3.1.

The molding window analysis uses part geometry, the material, and selected injection location and optionally, the specified process ranges and limits such as maximum melt, and mold temperatures. With this input, the molding window analysis runs a series of calculations, varying the process settings each time.

For each of these calculations, the molding window analysis checks whether certain results are achieved. From this data, the analysis determines the injection time and the temperature zones for mold and the melt. These results are compared with "Recommended Process Conditions" for the polymer (molding material) used in the process. After comparison, molding feasibility is determined with respect to colors. The analysis shows the feasible and preferred molding zones by colors (green, yellow and red), as shown in Fig. 3.14. Green represents feasible molding window. Red indicates there is no feasible molding window.

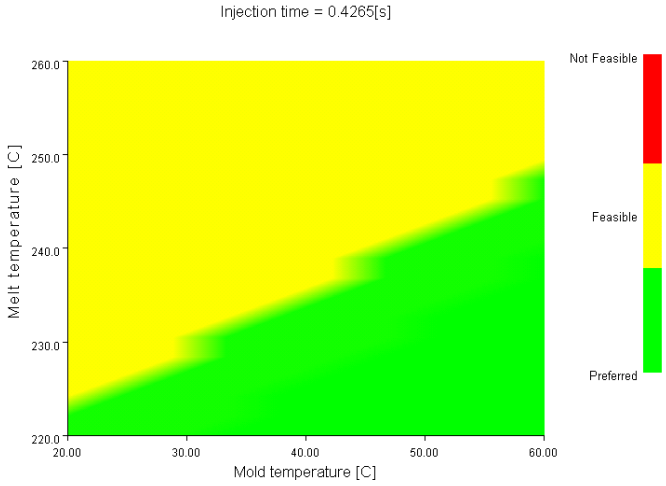

Figure 3.14 Molding window analysis results

If the processing settings represented by green are used, the molding is likely to be successful. Green area in molding match the following conditions:

1) The injection pressure required to fill the part is less than 80% of maximum machine injection pressure capacity,

$P < 0.8 * P_{max}$.

2) The flow front temperature is within 10°C range of the injection (melt) temperature,

$\left|T_{front} - T_{melt}\right| < 10°C$

3) The maximum shear stress in process is less than the maximum shear stress specified for the used polymer in the "Recommended Process Conditions",

$\tau < \tau_{max}$

4) The maximum shear rate in process is less than the maximum shear rate specified for the used polymer in the "Recommended Process Conditions",

$\dot{\gamma} < \dot{\gamma}_{max}$

The yellow zone indicates that the cavity is filled with the chosen process parameters without short shots. However, surface quality of the part is not good. It also indicates that there is no optimum combination of process parameters. The injection pressure required to fill the part is between the 100 % and 80 % of the maximum machine injection pressure capacity,

$0.8 * P_{max} < P < P_{max}$

The red zone shows that cavity is not filled with the chosen process parameters and there is short shot. The injection pressure required to fill the part is not sufficient and still greater than the maximum machine injection pressure capacity,

$P > P_{max}$

3.1.8 Process Parameter Setting

Before beginning the analysis, material properties, mold material, injection molding machine settings and process controller are selected. For this purpose, "Process Setting Wizards" is used (task bar (5) in Fig. 3.1). "Flow Analysis Advanced Options" can be activated from "Advanced Options" in red circle (Fig. 3.14). Mold material, part material, process parameters and machine settings can be arranged in this menu. Fig. 3.15 presents the process settings wizard.

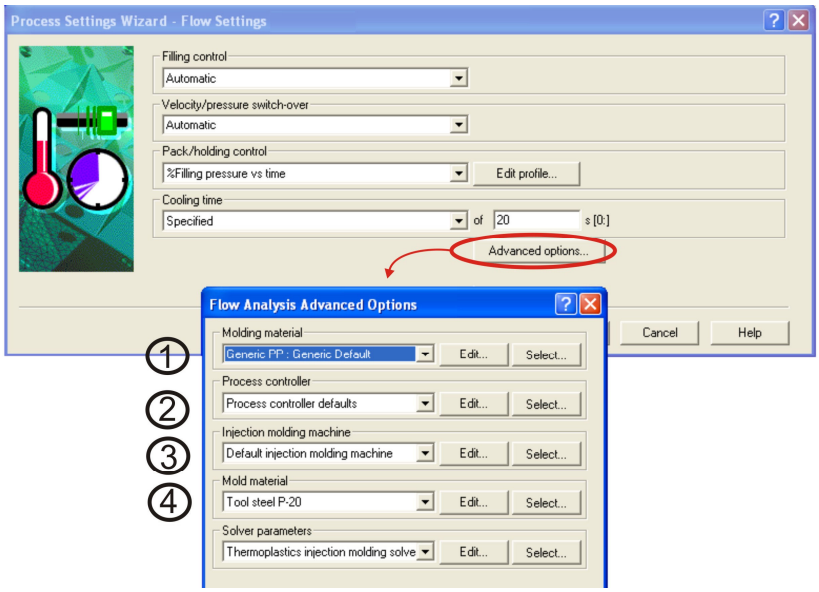

Figure 3.15 Flow analysis menu

3.1.8.1 Molding Material

In this part, part material is chosen. This menu is applicable from task bar (1) in Fig. 3.15 or task bar (3) in Fig. 3.1. Polymer properties of a part can be edited; also new material can be selected manually as shown in Fig. 3.16. Thermal properties, mechanical properties, recommended process conditions, PVT properties of the part can be arranged.

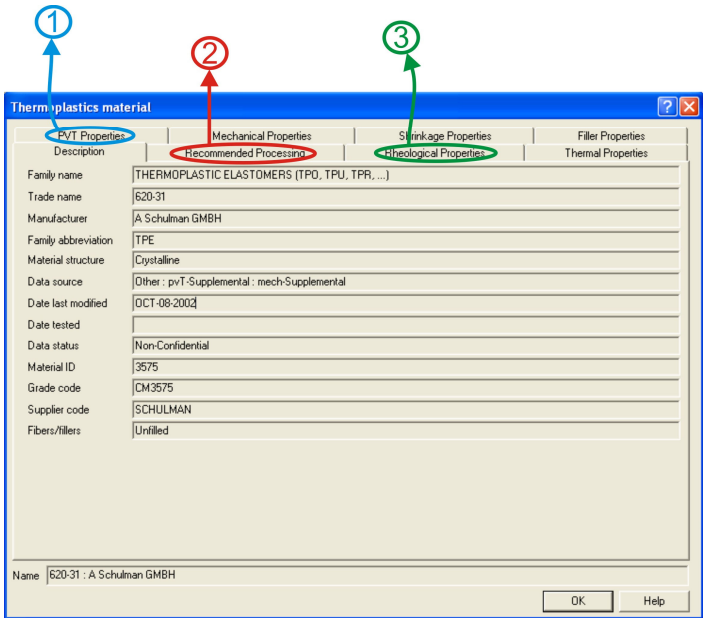

Figure 3.16 Molding material properties

Rheological properties define the viscosity model as shown in Fig. 3.17. Rheological properties are applicable under the task bar (3) in Fig. 3.16. Moldflow uses temperature and shear rate dependent viscosity models. These are labeled as “Second Order Model” and “Cross WFL Model”. These viscous models can be plotted by activating “Plot Viscosity” in Fig.3.17.

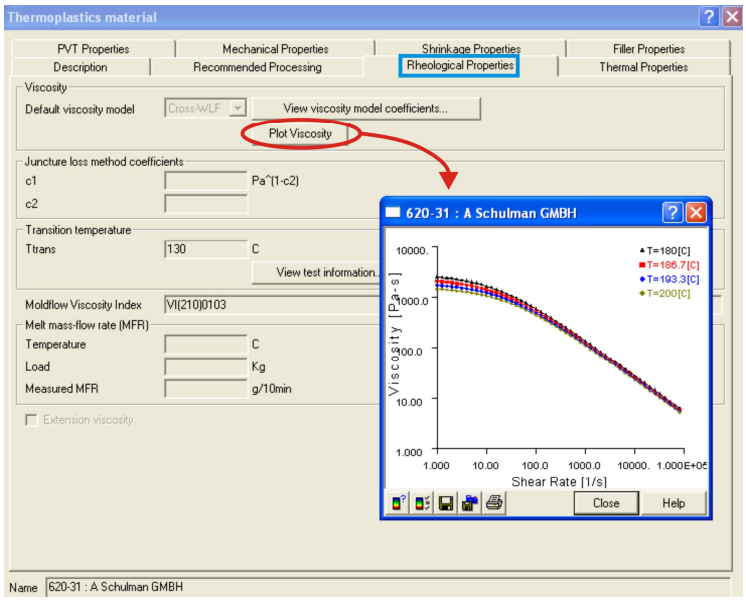

Figure 3.17 Rheological properties of the molding material

PVT properties describe how the plastic contracts and expands with different pressure and temperature profiles during the packing phase. “PVT properties” is accessed under the task bar (1) in Fig. 3.16. The plastic contracts due to increased pressure in both liquid form and solid form. During cooling, the plastic contracts due to temperature decrease. Moldflow uses 2-domain Tait PVT Model. The model presents specific volume-temperature profiles under different pressure values, for the chosen material as shown in Fig. 3.18. PVT models of polymer can be plotted by activating “Plot PVT data” in red circle in Fig. 3.18.

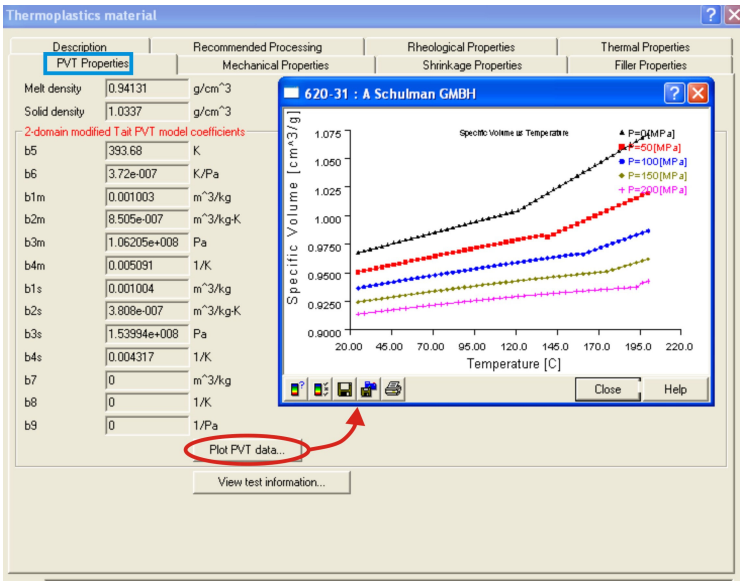

Figure 3.18 PVT properties of molding material

"Recommended Process Conditions" presents the best range of parameters for the process (Fig. 3.19). It is applicable under the task bar (2) in Fig. 3.15. If the process parameters are not changed at the beginning of an analysis, these are the default values. The processing temperatures and maximum injection pressure are set based upon manufacturers' recommendations. "Molding Window" ranks the process conditions from red (not suitable) to green (suitable) based on these recommended process conditions.

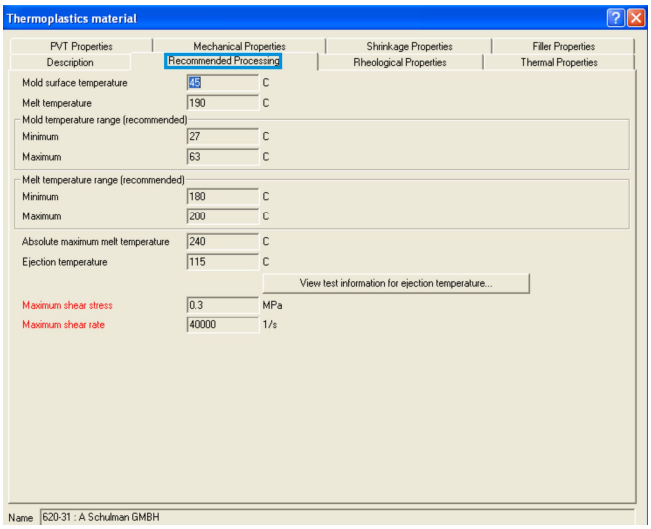

Figure 3.19 Recommended process conditions of molding material

3.1.8.2 Mold Material

In this section, the properties of the mold material are defined (Fig. 3.20). This menu is applicable from task bar (4) in Fig. 3.15.

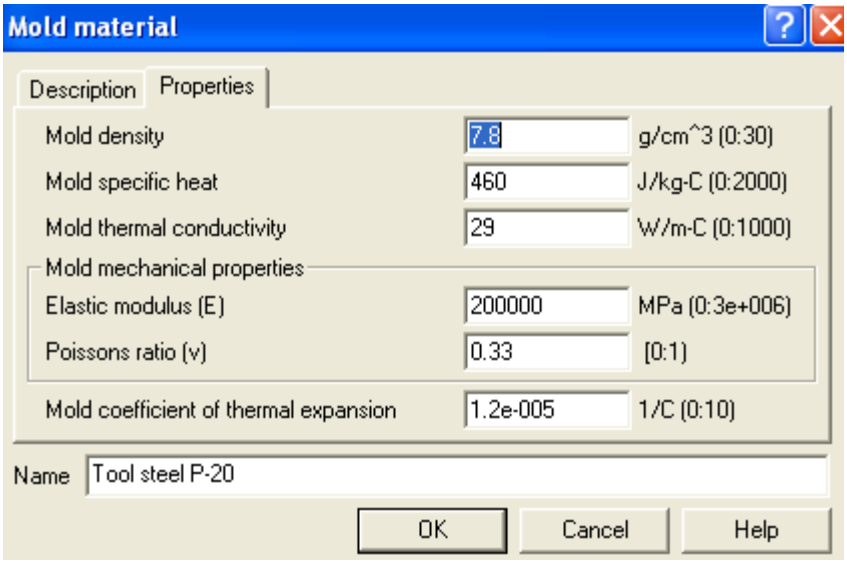

Figure 3.20 Thermal and mechanical properties of mold material

3.1.8.3 Injection Molding Machine Settings

In this section, the machine settings, such as screw diameter, maximum clamp force and filling control are adjusted, as shown in Fig. 3.21. This menu is applicable from task bar (3) in Fig. 3.15.

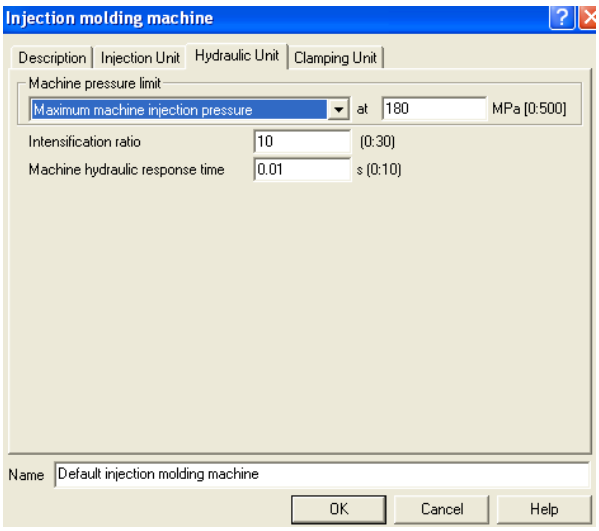

Figure 3.21 Manual of injection molding machine settings

3.1.8.4 Process Controller

In this part, various process control parameters such as filling time, packing time, cooling time, mold open time, mold temperature, melt temperature, velocity/pressure-switch-over and ambient temperature are set before analysis as shown in Fig. 3.22. Process controller is applicable from task bar (2) in Fig. 3.15. Mold open time starts from complete solidification of part and ends at the ejection of the part. During mold open time, heat transfer goes on only between mold and ambient by convection.

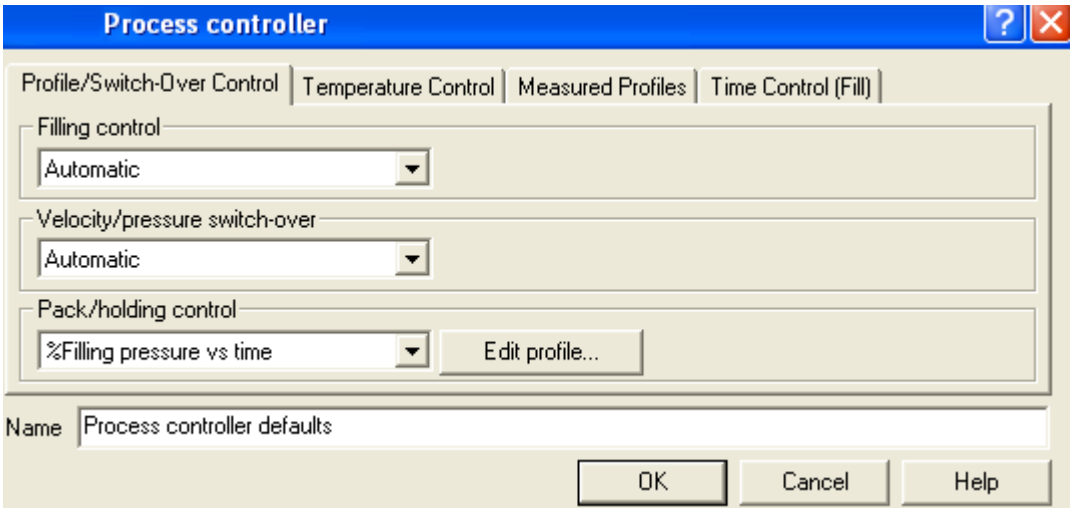

Figure 3.22 Process Control

In process controller section, filling time can be chosen with respect to three different cases: injection time, flow rate or ram speed. Ram speed can also be given as a profile with respect to time.

Near the end of the filling stage before the cavity is completely filled, velocity/pressure (V/P) switch is activated. “Velocity/Pressure Switch Over” controls velocity of polymer and injection pressure. Actually, this parameter controls a transition phase between filling and packing phase. Generally this transition occurs before polymer completely fills the cavity, polymer velocity decreases and pressure remains constant. The reasons for this are to avoid flash of the molten polymer from mold open line and the impact of the ram at the end of filling, which could damage the injection machine and the mold. After filling stage, (V/P) switch-over can be arranged by one of the V/P switch-over conditions: V/P switch-over by percent volume, V/P switch-over by injection pressure or V/P switch-over by ram position.

Up to now, the process parameters are mentioned. After analysis is over, simulation results are viewed and accessed from task bar (6) or (10) in Fig.3.1. The simulation results are presented at chapter 4 “Results and Discussion”.

3.2 Other Commercial Simulation Programs For Injection Molding

Early simulation programs for injection molding were generally developed to compare simple injection molding scenarios with experimental results. Narazaki and Mizukami [34] explain the development of the finite element code MOLDIA-F, where the volume of fluid method is used in tracing the advancing melt front. This program package was especially designed for tracking the formation of weld lines.

Poslinski and Fox [35] developed "1-D FLOW" based on finite element method and Hele-Shaw approximation. The simulation code "1-D FLOW" was developed to predict the location of the polymer flow front. The program calculates the required injection pressure and "Melt Flow Index" of polymer in injection molded plastic parts. In this program, cavity is separated into simpler geometries, where each is represented by a disk (partial and full), a channel (constant width or diverging/converging) or a rod (constant radius or diverging/converging). Long runner systems and sprues are modeled through a combination of rod components. Radial flow within a part is modeled as a disk component. Planar flow is modeled with a strip component of specified width and thickness, including a converging or diverging strip capability.

Fidap was developed [36] by the Fluent Company to simulate highly viscous laminar flows, such as in injection molding. Fidap has a preprocessor (Gambit) that generates the mesh. It includes Bingham, Carreau and power-law shear thinning viscosity models and is cabaple of modeling relatively complex free surface flows. Fidap is not only developed to simulate injection molding likewise Moldflow. It is a general purpose fluid simulations program such as air, water including applications in injection molding.

Moldex3D [37] is another injection molding package program based on finite element method like Moldflow. It also uses Hele-Shaw approximation. Futhermore, it provides information such as melt front advancement, welding lines, air traps, runner balancing, temperature and pressure distributions in injection molding process.

C-COOL was designed by Himasekhar et al. [38] to determine best cooling channels location and simulate uniform cooling with the shortest cooling time before the experiment. It simulates only cooling phase of the injection molding. C-COOL ignores the convection heat transfer to the air. For each material, several mold trials were performed with different coolant inlet temperatures and cooling channel configurations. For each mold trial, the part surface temperature distribution was measured by using infrared thermography; in addition, mold wall temperatures were also measured at specific locations in the cavity. Coolant flow rates, inlet and outlet temperatures, and pressure drops across the inlet and outlet for each trials were recorded. Simulation results were compared with the actual measured data. The best agreement has been obtained between the simulations and measurements to help the engineer to optimize the cooling phase of an injection-molded plastic part.

The traditional numerical simulation of injection molding is the 2.5D technique based on the Hele-Shaw behaviors such as the fountain flow. However, most parts that are constant thickness parts, thus approximation, which cannot predict the filling of thick or nonuniform-thickness parts and some flow Hele-Shaw approximation works for most cases.

Moldflow has many advantages over the CAE software mentioned above. Firstly, it can model very complex shapes. It meshes the parts quickly and it is equipped with “Mesh Tools” and “Mesh Wizard” to improve mesh quality and clean the defects among the mesh. For thin parts, it represents fusion type mesh model to decrease computational time without decreasing assessment of the program. In Fidap, the benchmark studies are not transferred properly from solid modeling program, especially holes having small diameter are transferred as square holes, unlike Moldflow. Furthermore, designing feed system of the mold is very easy by using Moldflow, even it is complex. Moldflow is also very appropriate to model highly viscous model with respect to other commercial software programs.

CHAPTER 4

RESULTS AND DISCUSSION

Introduction

In this chapter, injection molding process is simulated with different scenarios by Moldflow Plastic Insight (MPI). Firstly, analytical solutions are compared with the numerical results of MPI filling mode for simple geometries. Then, a benchmark simulation study is conducted to study and compare conformal cooling channels and conventional cooling channels, in filling and cooling mode of Moldflow Plastic Insight. Finally, a real life case study is presented. For this purpose, a refrigerator shelf that is injection molded by the Arçelik Company is studied. The process is simulated using actual process parameters and simulation results are compared with production results. The process is also simulated using conformal cooling channels and improvements that could be brought about by conformal cooling channels as the plastics are discussed.

4.1 Comparison of 1-D Filling Simulation Results with Analytical Solutions

In this part, Hele-Shaw filling model is solved analytically for thin rectangular prism and thin disc geometries. The injection is at constant injection time of polymer. The same problem is then solved using MPI and the analytical and numeric results are compared. The aim here is to verify the assumption and boundary condition of the Hele-Shaw model used in simulations.

4.1.1 1-D Planar (Linear) Flow Numerical Solution

A simple scenario is prepared for analytic solution of the filling. For 1-D steady, Newtonian flow through the cavity, Hele-Shaw formulation permits an analytical solution. The cavity geometry is shown in Fig. 4.1. A point gate at one end injects the molten polymer. The cavity thickness is taken at least one order of

magnitude smaller than the planar dimensions per Hele-Shaw approaches. In order to obtain linear (1-D) flow, the length of channel is taken one order of magnitude greater than the width of the channel.

For the numerical simulation, in order to keep polymer viscosity constant per Newtonian flow, the mathematical constants in the Cross-WFL viscosity model are adjusted as:

$$D_1 = 2 \text{ Pa.s} \qquad \tau^* = 182140 \text{ Pa} \qquad D_3 = 0 \text{ K/Pa} \qquad A_1 = 10^{-99} \qquad A_2 = 51.6 \text{ K} \qquad n = 1$$

In the model,

$$\mu = \frac{\mu_0}{1 + \left(\frac{\mu_0 \dot{\gamma}}{\tau^*} \right)^{(1-n)}} \tag{5.1}$$

$$\mu_0 = D_1 e^{\left[\frac{-A_1 (T - T^*)}{A_2 + (T - T^*)} \right]} \tag{5.2}$$

$$T^* = D_2 + D_3 P \tag{5.3}$$

leading to a constant viscosity value of

$$\mu = 1 \text{ Pa/s}$$

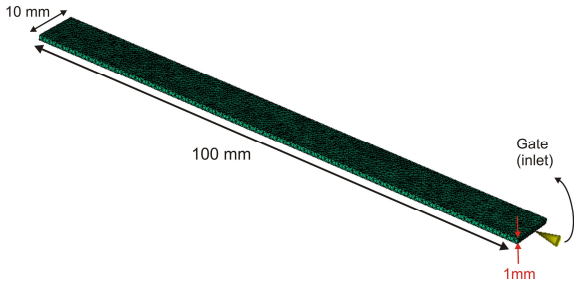

Figure 4.1 Representation of thin rectangular prism

For the numerical simulation of filling in MPI, initial molten polymer temperature is arranged 230°C and mold temperature is 40°C. Injection time is arranged constant ($t_{inj} = 0.11s$) at the beginning of the analysis. Fig. 4.2 presents the injection flow rate during filling. The injection flow rate suddenly decreases at the end of filling as shown in Fig. 4.2. Because, the velocity/pressure switch over takes place right before end of filling. Once the injection pressure in cavity reaches maximum allowable pressure, program begins to decrease the flow rate to keep the maximum pressure below allowable pressure to avoid flash. When the numerical and analytical results are compared, this sudden drop in flow rate and the numerical results beyond t=0.1046 s (when the switch-over takes effect) will not be considered.

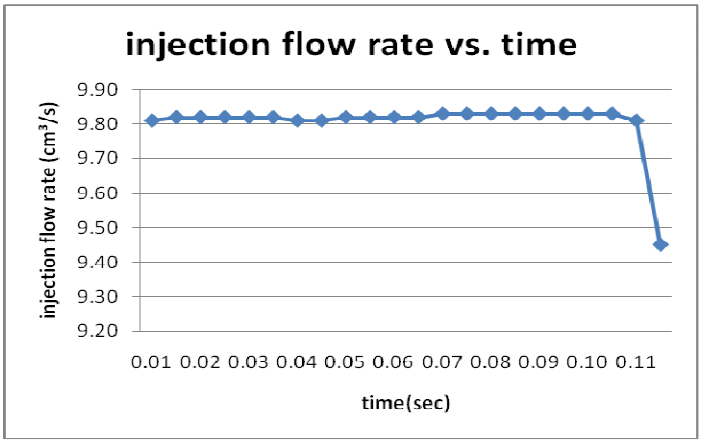

Figure 4.2 Injection flow rate during filling in rectangular prism cavity

The flow at the intermediate vicinity of gate is radially outward as shown in Fig. 4.3.a. Therefore, this portion of injection is 2-D flow. However after about t=0.0276 s the flow front flattens and the flow resembles a 1-D flow. For comparison with analytical results; the results beyond this time instant will be used. Fig. 4.3.b presents the position of the middle of the flow front from the injection gate with time.

The slope of distance vs. time graph seems constant indicating the flow velocity is constant. This indicates that problem is steady state.

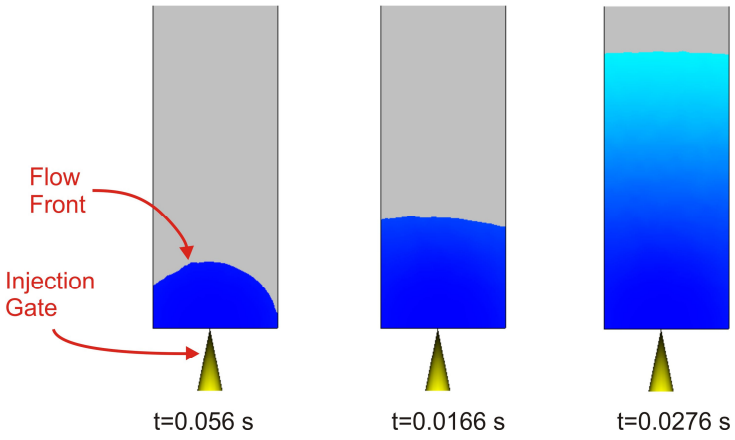

(a)

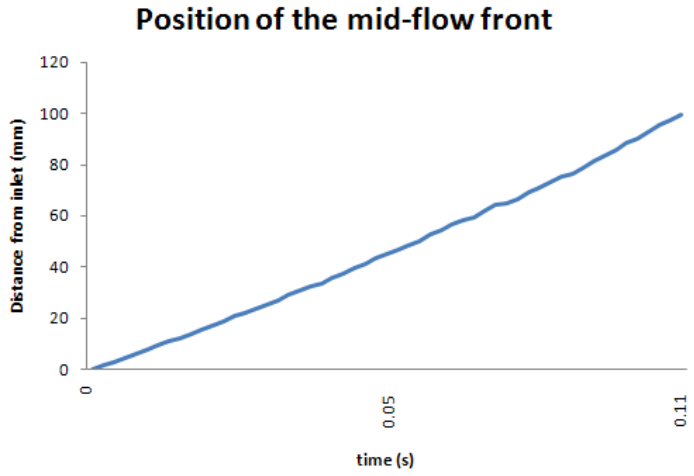

(b)

Figure 4.3 (a) Flow progression near the inlet (b) Flow front location vs. time, in 1-D planar flow in numerical results

For the analytical solution of 1-D filling in the given rectangular domain, Hele-Shaw approximation eqn. (2.24) yields

$$\frac{\partial}{\partial x}\left(S\frac{\partial P}{\partial x}\right)=0 \tag{4.1}$$

Where the fluidity, S, is constant due to constant viscosity of the polymer.

$$S=\int_0^b \frac{z^2}{\mu}dz=\frac{b^3}{3}\approx 0.04167\ \left(mm^3.s/Pa\right)$$

Integrating pressure along the flow path twice leads to

$$P=C_1x+C_2 \tag{4.2}$$

where C_1, C_2 are integration constants. The constants C_1 and C_2 will be determined from the appropriate boundary conditions.

Injection time is given at the beginning of the analysis, also volumetric flow rate ($\dot{Q}$) is known, therefore average velocity is found from eqn. (4.3)

$$\bar{u}=\frac{\dot{Q}}{A} \tag{4.3}$$

where A (=10 mm²) is the cross sectional area that the polymer flows through.

Due to 1-D, steady state flow, eqn. (4.3) gives the average flow velocity throughout the flow domain.

The average flow velocity is related to the pressure gradients per eqn. (2.23.a) as

$$\bar{u}=-\frac{S}{2b}\frac{\partial P}{\partial x} \tag{4.4}$$

where b(=0.5 mm) is the half of the thickness of the cavity

Combining eqn. (4.3) and eqn. (4.4) yields the constant pressure gradient along the flow path as

$$\frac{\partial P}{\partial x} = -\frac{2b}{S}\frac{\dot{Q}}{A} \tag{4.5}$$

Pressure gradient along flow path can be also found from eqn. (4.2) as

$$\frac{\partial P}{\partial x} = C_1 \tag{4.6}$$

Then, the integration constants (C_1) can be found from eqns. (4.5) & (4.6) as

$$C_1 = -\frac{2b}{S}\frac{\dot{Q}}{A} \tag{4.7}$$

The pressure is zero gage (atmospheric), x_{ff} , i.e.

$x = x_{ff}$, $P = 0$

Using eqn. (2.25.a), coefficient C_2 in eqn. (4.2) is found as

$$C_2 = \left(\frac{2b}{S}\frac{\dot{Q}}{A}\right) x_{ff} \tag{4.8}$$

where x_{ff} is the position of flow front

$$x_{ff} = \bar{u} \cdot t \tag{4.9}$$

where t is time elapsed since the beginning of injection.

Finally replacing (4.7) & (4.8) & (4.9) into eqn. (4.2) gives the pressure distribution within the flow domain as

$$P(x) = \left(\frac{2b}{S} \frac{\dot{Q}}{A} \right) (\bar{u} \cdot t - x) \tag{4.10}$$

where x is the position within the flow domain. Fluidity S is calculated based on the constant viscosity (1 Pa.s). The other process parameters in eqn. (4.10) are the same as those for the numerical solution.

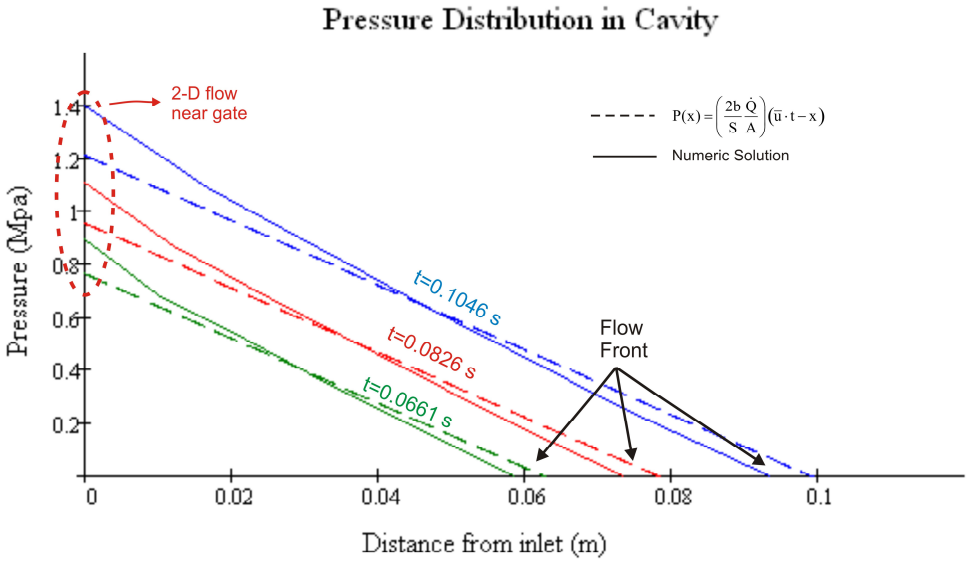

Figure 4.4 Pressure variation in 1-D flow in rectangular thin cavity

Fig. 4.4 presents pressure distributions of midplane of the cavity. Except the flow near the inlet and flow after t=0.1046 s, pressure distributions solved by Moldflow is nearly same as the analytical solution with acceptable errors. Therefore, 1-D Hele-Shaw assumption is valid. Errors near the inlet shown in dashed circle is very big with respect to other regions. Because, flow is radially progress at the inlet, so it does not obey 1-D Hele–Shaw assumption and so inlet region is neglected. Furthermore, flow after t= 0.1046 is neglected due to switch-over factor.

4.1.2 1-D Radial Flow in Hele-Shaw

Same scenario applied to 1-D planar flow is now applied to 1-D radial flow. The aspect ratio of this analysis is chosen similarly for Hele-Shaw solution. Molten polymer enters from middle of the cavity as shown in Fig. 4.5. Same material properties are used for this analysis as those of 1-D planar flow analysis.

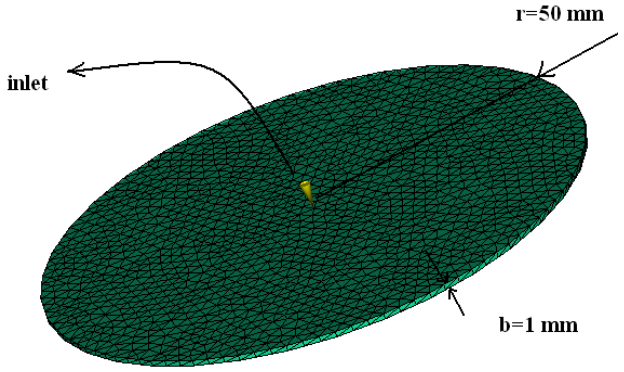

Figure 4.5 Representation of thin cylinder

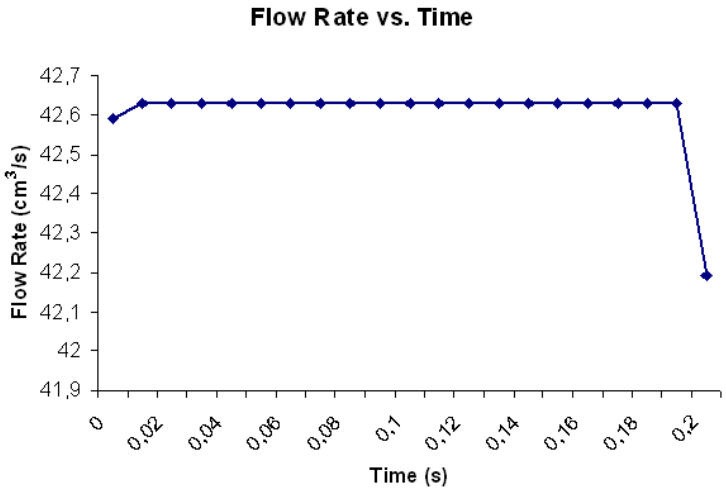

Figure 4.6 Injection flow rate during filling in thin cylinder cavity

For the numerical simulation of filling in MPI, initial molten polymer temperature is arranged $230\,°C$ and mold temperature is $40\,°C$. Injection time is arranged constant ($t_{inj} = 0.20\,s$) at the beginning of the analysis. Fig. 4.6 presents the injection flow rate during filling. As in planar flow, the injection flow rate suddenly decreases at the end of filling due to pressure/velocity switch factor. Therefore, when the numerical and analytical results are compared, this sudden drop in flow rate and the numerical results beyond t=0.1681 s (when the switch-over takes effect) will not be considered.

For the analytical solution of 1-D filling in the given disc domain, Hele-Shaw approximation eqn. (A.23) yields

$$\frac{\partial}{\partial r}\left(Sr\frac{\partial P}{\partial r}\right) = 0 \tag{4.11}$$

where the fluidity, S, is constant due to constant viscosity of the polymer

$$S = \int_0^b \frac{z^2}{\mu} dz = \frac{b^3}{3} \approx 0.04167 \ \left(mm^3.s/Pa\right)$$

Integrating pressure along the radial path twice leads to

$$P = D_1 \ln r + D_2 \tag{4.12}$$

where D_1, D_2 are integration constants. The constants D_1 and D_2 will be determined from the appropriate boundary conditions.

Injection time is given at the beginning of the analysis, also volumetric flow rate is known, therefore average velocity is found from eqn. (4.13)

$$\bar{u}_r = \frac{\dot{Q}}{4\pi rb} \tag{4.13}$$

where A (=$2\pi rb$) is the cross sectional area that the polymer flows through.

Due to 1-D, radial flow, eqn. (4.13) gives the average flow velocity throughout the flow domain.

The average flow velocity is related to the pressure gradients per eqn. (A.18.a) as

$$\bar{u} = -\frac{S}{2b}\frac{\partial P}{\partial r} \tag{4.14}$$

where b(=0.5 mm) is the half of the thickness of the cavity

Combining eqn. (4.13) and eqn. (4.14) yields the pressure gradient along the flow path as

$$\frac{\partial P}{\partial r} = -\frac{\dot{Q}}{2\pi r S} \tag{4.15}$$

Pressure gradient along flow path can be also found from eqn. (4.12) as

$$\frac{\partial P}{\partial r} = \frac{D_1}{r} \tag{4.16}$$

Then, the integration constants (D_1) can be found from eqns. (4.15) & (4.16) as

$$D_1 = -\frac{\dot{Q}}{2\pi S} \tag{4.17}$$

Using eqn. (2.25.a), coefficient C_2 in eqn. (4.12) is found as

$$P = 0 \qquad r = R_{ff}$$

where R_{ff} is flow front radial position

$$D_2 = \frac{\dot{Q}}{2\pi S} \ln R_{ff} \tag{4.18}$$

Placing eqns. (4.17) & (4.18) into eqn. (4.12) yields

$$P = \frac{\dot{Q}}{2\pi S} \ln\left(\frac{R_{ff}}{r}\right) \tag{4.19}$$

where r is the position within the flow domain. Fludity S is calculated based on the constant viscosity (1 Pa.s). The other process parameters in eqn. (4.19) are the same as those for the numerical solution

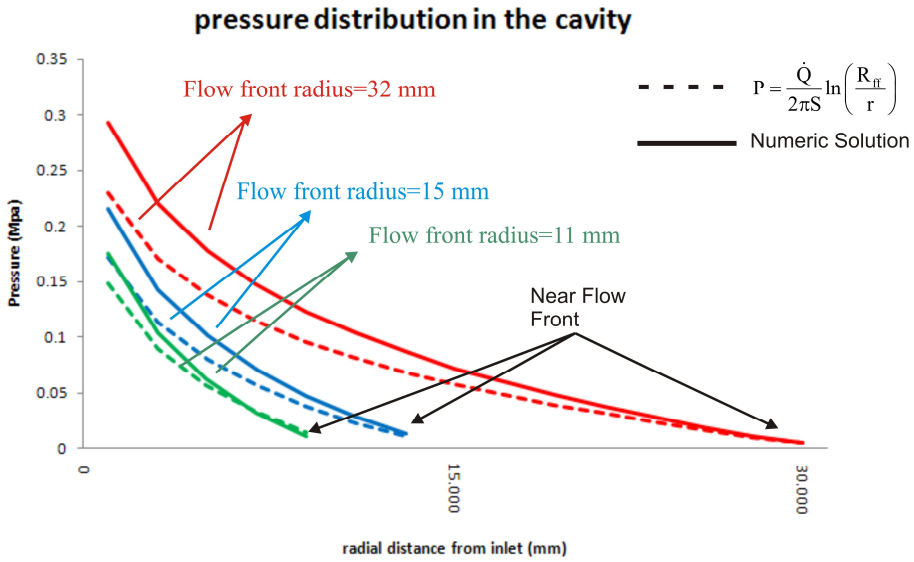

Figure 4.7 Pressure variation in 1-D flow in disc cavity

Fig. 4.7 represents the pressure distribution in the disc. In planar flow pressure distribution was found according to injection time, but in radial flow, pressure decreases exponentially with radial distance from inlet. Errors get lessen from gate to end of filling. Because, Hele-Shaw does not model precisely sudden expansions such as gate. After 1-D planar flow, assumption for radial flow is also valid. Furthermore, Hele-Shaw models the disc flow better than planar flows with less error.

4.2 Comparison of The Effects of Conventional and Conformal Cooling Channels In a Curved Part Geometry

In 1-D filling analysis, model of Moldflow was verified with given boundary conditions. In this study, a half cylinder shell part (imaginary part) will be analyzed with both conformal cooling channels and conventional ones. The purpose is to study the effects of conventional and conformal cooling channels on the process. Therefore, the half cylinder shell part cooled by conformal cooling channels will be compared with conventional ones.

Fig. 4.8 presents the half cylinder shell part geometry. Thickness is smaller than other dimensions to fit Hele-Shaw approximation.

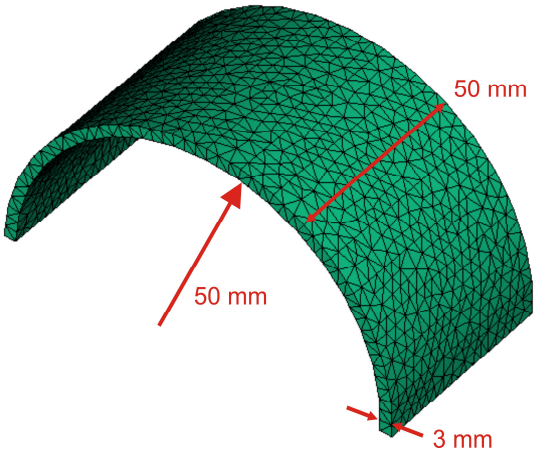

Figure 4.8 Half cylinder shell part to be molded

Fig. 4.9 presents mold layouts of the half cylinder shell part with conventional and conformal cooling channels.

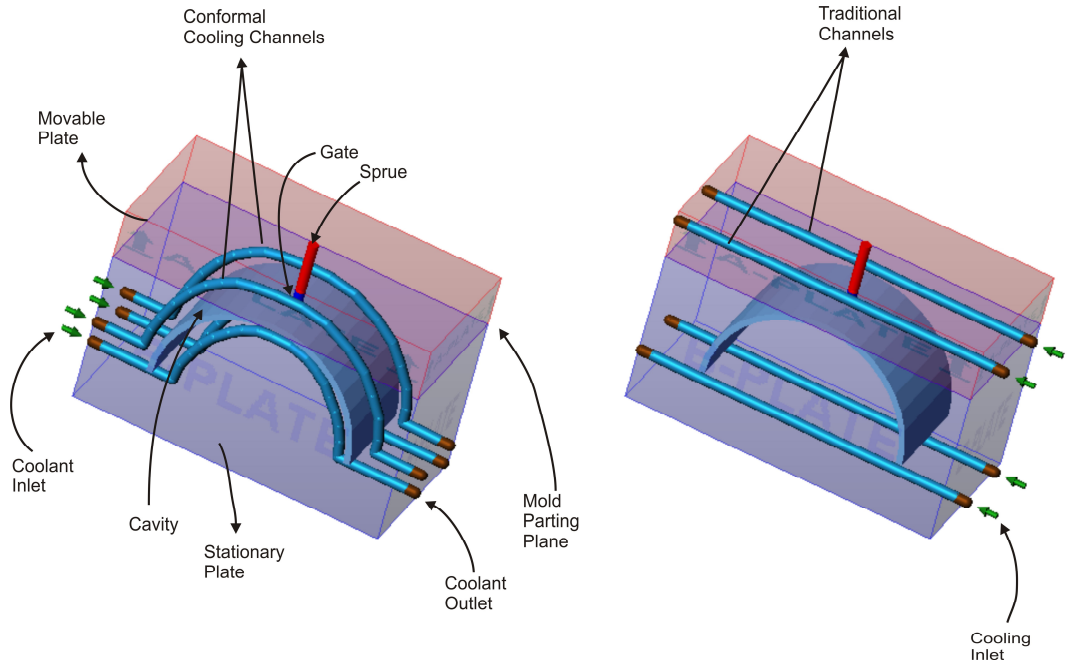

(a) **(b)**

Figure 4.9 Closed mold with conventional cooling channels, closed mold with conformal cooling channels for the half cylinder shell production

In order to make comparison between these cooling channels layouts correctly, process parameters, part and mold material are given as same for two cooling channel layouts as shown in the Table 4.1. Fig. 4.10 presents packing profile of the half cylinder shell during production. Ejection criteria is arranged according to frozen percentage of part at ejection. It is arranged as %100 for both conformal cooling channels and conventional ones.

Table 4.1 Process parameters for the half cylinder shell production

Mold Material	Thyroplast 2738 (DIN 1.2738)
Part Material	Polystyrol 165H
Flow Rate of The Coolant	7 l/min
Coolant Inlet Temperature	20 °C
Initial Mold Temperature	40 °C
Initial Melt Temperature	230 °C

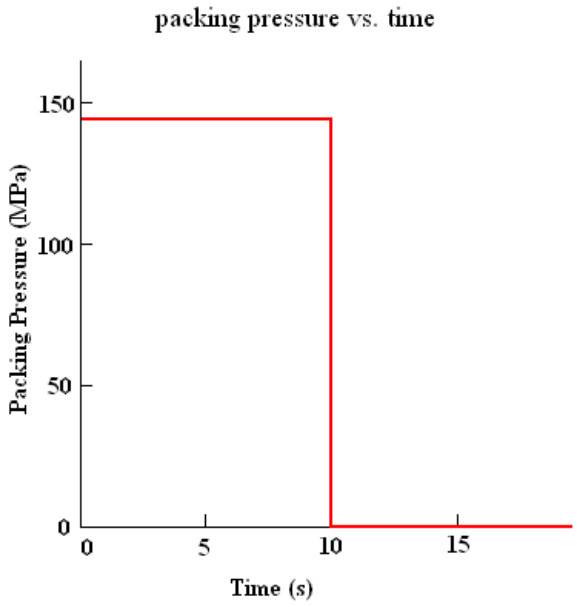

Figure 4.10 Packing profile of the half cylinder shell

Fig. 4.11 presents the cooling quality results. Cooling quality show where heat is not taken away properly from the part. Yellow area shown in Fig. 4.11.b presents that heat is not taken away evenly and as fast as other regions of the part, Fig. 4.11.a represents that conformal channels cool that area uniformly. Cooling quality results are

a combination of the “Surface Temperature Variance” and “Freeze Time Variance“ results. Fig. 4.12 represents “Surface Temperature Variance” which indicates temperature deviation from the average cycle temperature of the part. The area where cooling quality is low is the hottest area during the filling as shown in the Fig. 4.12.b and heat is not taken as much as the other regions, because that area is the hottest point and molten polymer is injected at that area. “Freeze Time Variance“ result shows the deviation of the time it takes the polymer to freeze in any region of the part, from the average time to freeze for the entire part. The area where cooling quality is low is cooled slower than the other areas by conventional cooling channels as shown in Fig. 4.13.b. Because, the area where cooling quality is low is far away from the cooling channels. Therefore, it is very hard to cool uniformly with conventional cooling channels. However, heat is taken evenly everywhere by conformal cooling channels as shown in Fig. 4.11.a. Because, distance between conformal cooling channels and part is same everywhere. Furthermore, low quality area cooled by conventional channels is cooled faster and more uniform by conformal cooling channels as shown in Fig. 4.12.a and 4.13.a. It is also shown that from Table 4.2, conformal cooling channels cool the part in less cooling time with respect to conventional cooling channels.

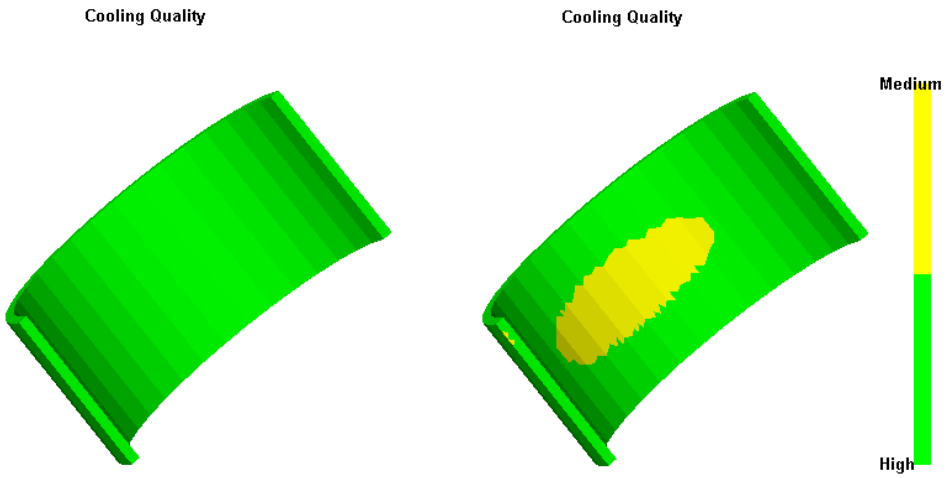

Figure 4.11 (a) Cooling quality results in conformal cooling channels (b) Cooling quality results in conventional cooling channels

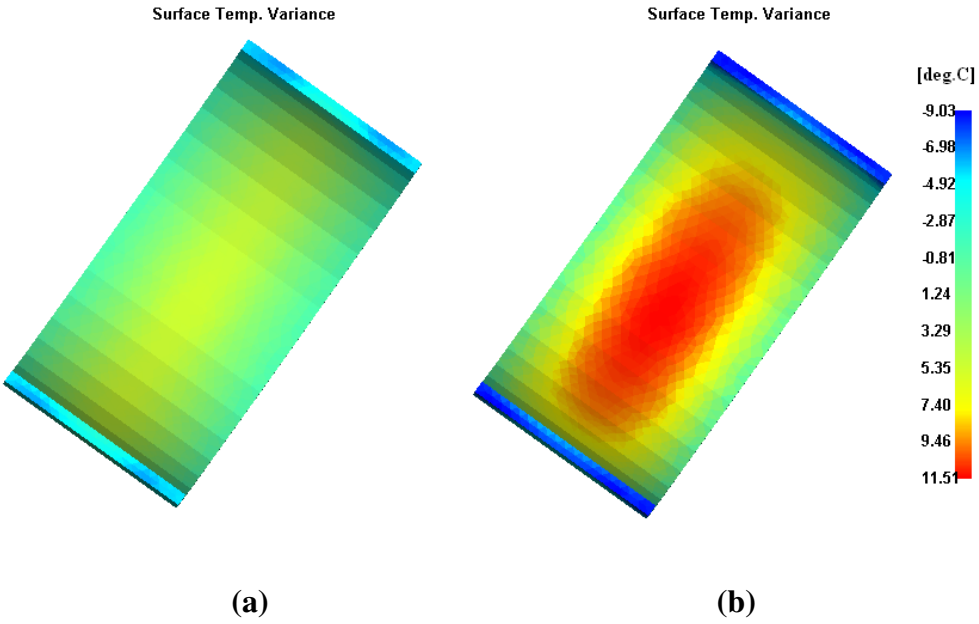

Figure 4.12 (a) Surface temperature variation with conformal cooling channels (b) Surface temperature variation with conventional cooling channels

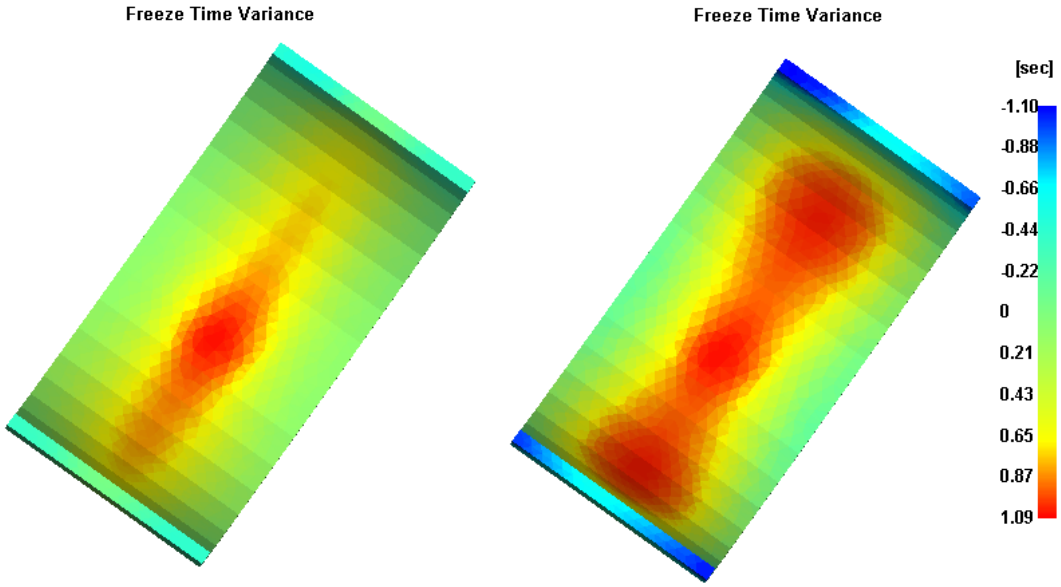

Figure 4.13 (a) Freeze time variance with conformal cooling channels (b) Freeze time variance with conventional cooling channels

Table 4.2 Results of channel configurations

	Conventional Cooling	Conformal Cooling
Cycle Time (s)	21.68	16. 42
Cooling Time (s)	9.2	3.95

Fig. 4.14 shows temperature rise of the coolant. Temperature rise in conformal cooling channels is higher than that in conventional ones. Because, it absorbs more heat from the part as it cools the mold more effectively. Therefore, part surface temperature (surface temperature of the part at the ejection stage) in conformal cooling configuration is less than that in conventional cooling configuration as shown in Fig. 4.15.

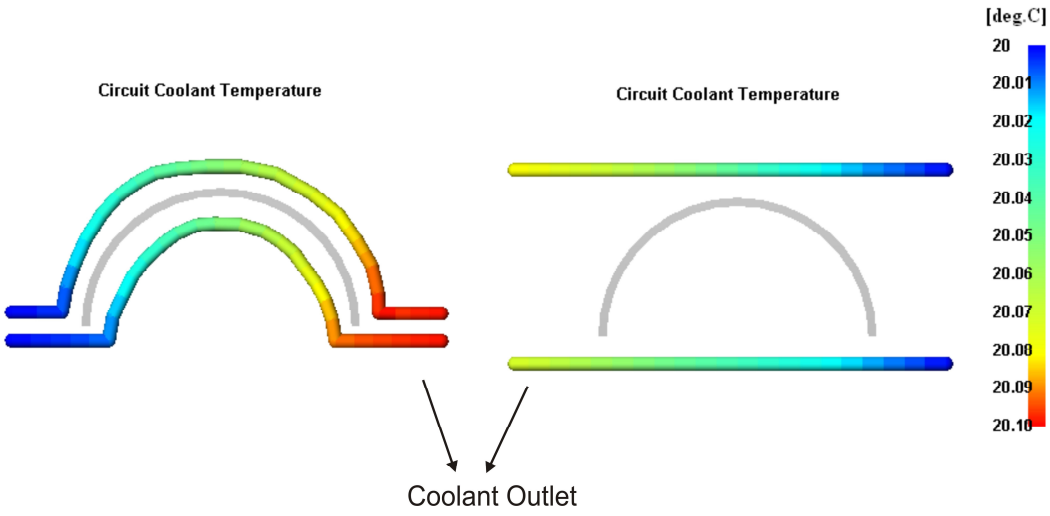

(a) **(b)**

Figure 4.14 (a) Circuit coolant temperature in conformal cooling channels (b) Circuit coolant temperature in conventional cooling channels

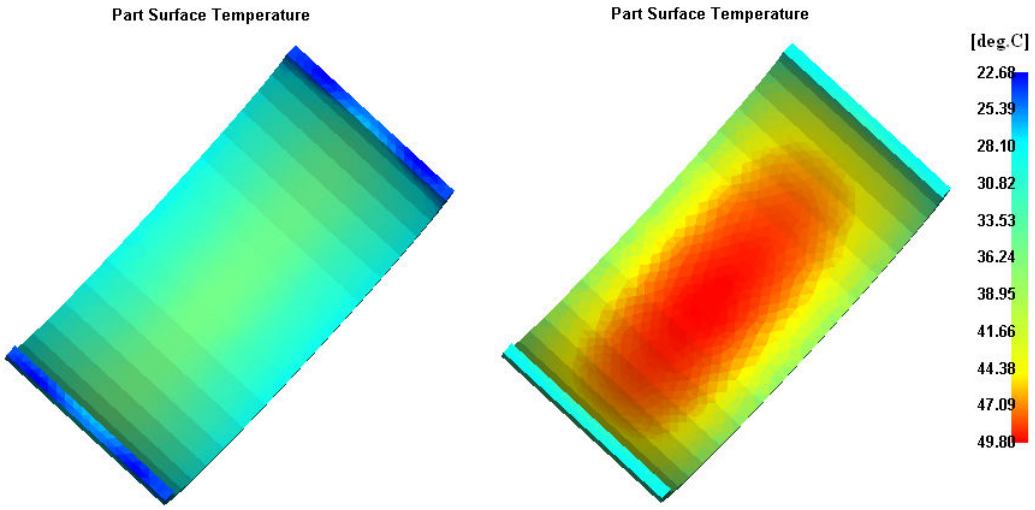

(a) **(b)**

Figure 4.15 (a) Part surface temperature in conformal configuration at $t_{cycle} = 16.42$ s (b) Part surface temperature in conventional configuration at $t_{cycle} = 21.68$ s

Circuit pressure in Fig. 4.16 presents pressure drop in the cooling channels. Circuit pressure in conformal channels is more than twice of that in the conventional one. Therefore, energy consumption spent to operate cooling pumps with conformal configuration increases more than twice of that in the conventional one.

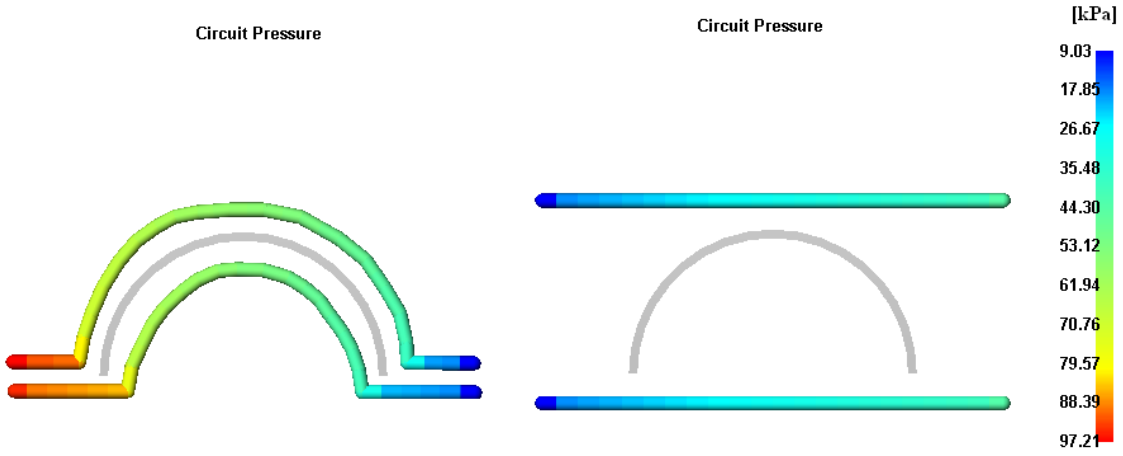

(a) **(b)**

Figure 4.16 (a) Circuit pressure in conformal cooling channels (b) Circuit pressure in conventional cooling channels

Figure 4.17 presents path of the molten polymer and how long it takes to fill. Conformal cooling channels has no significant effect on the filling stage, cavity is filled at the same time with both confomal and conventional cooling channels. However this little effect is seen from pressure drop results and frozen layer results. Pressure drop represents the drop in pressure from the injection location to that place on the model, at the moment that place was filled as shown in Fig. 4.18. Cavity with conformal channel layout needs 0.08 MPa higher pressure to drive progress of filling with respect to cavity having conventional channel layout. There are two reasons why cavity with conformal cooling channels need more injection pressure. Firstly, conformal cooling channels cools the molten polymer more than conventional one,

therefore viscosity of molten polymer is higher in conformal channel layout. Molten polymer with higher viscosity needs higher injection pressure to fill cavity. The other reason is frozen layer. Frozen layer result in Fig 4.19 shows the frozen layer as percentage at the end of filling. Frozen layer thickness has very significant effect on the flow resistance. The thickness of the flow layer is also reduced as the thickness of the frozen layer increases. Therefore, flow of the molten polymer fills harder due to thinner flow area. The frozen layer in conformal configuration is thicker than the part in conventional one during filling due to better cooling capability of the conformal cooling channels as shown in Fig. 4.16. That is why molten polymer requires more injection pressure to complete filling.

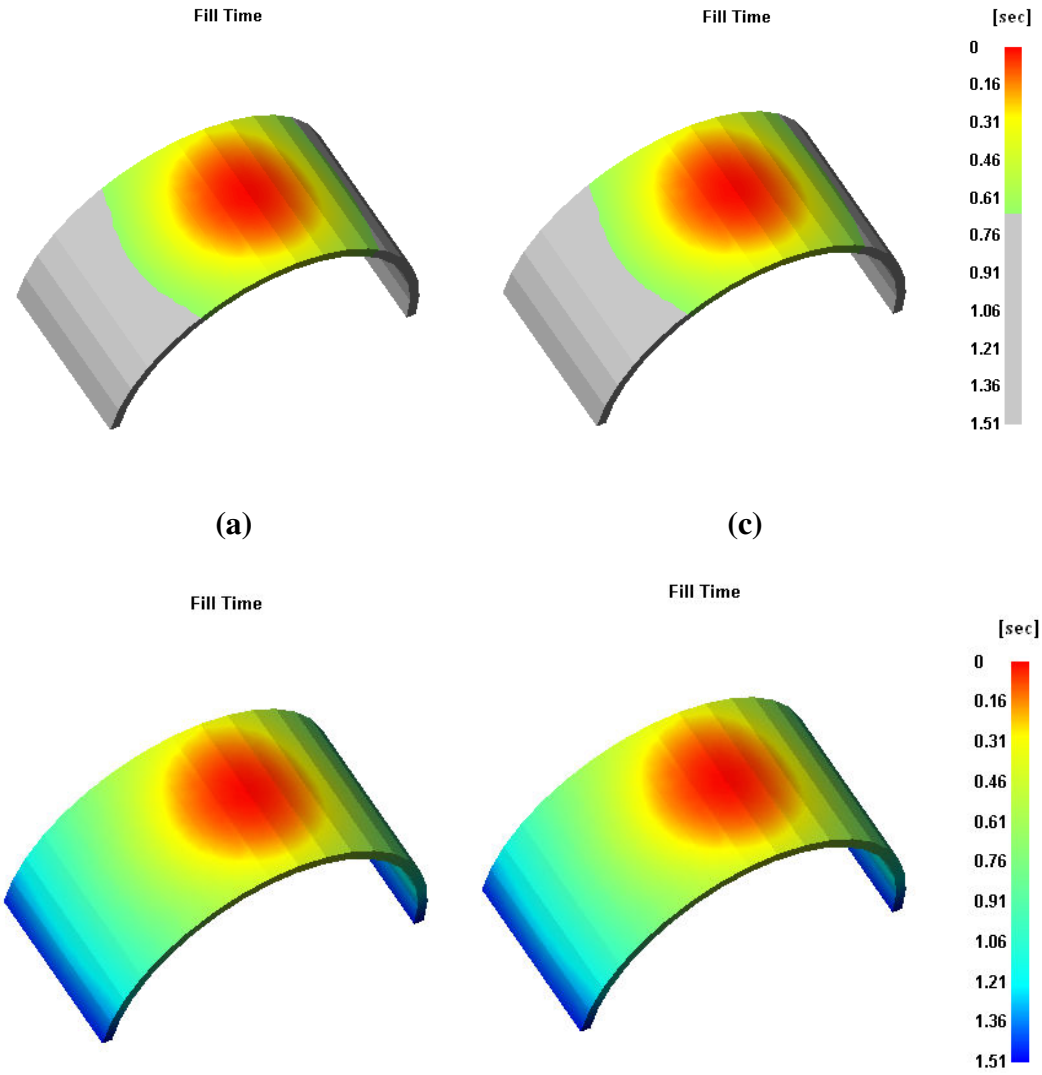

Figure 4.17 Filling time of the cavity with conformal cooling configurations (a) t = 0.69 s (b) t=1.52 s, filling time of the cavity with conventional cooling configurations (c) t=0.69 s (d) t=1.52 s

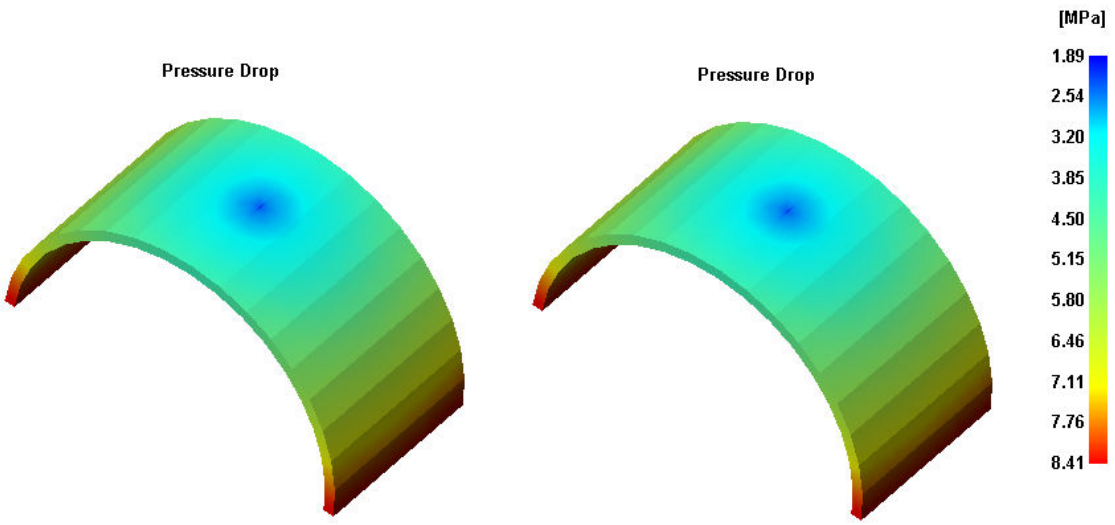

(a) **(b)**

Figure 4.18 (a) Pressure drop in conformal cooling configurations (b) Injection Pressure in conventional cooling configurations

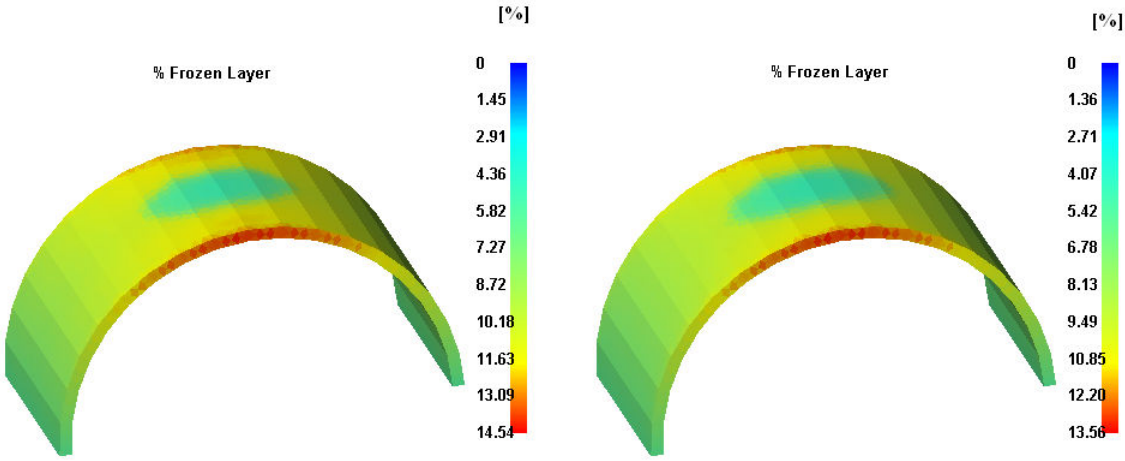

(a) **(b)**

Figure 4.19 (a) Frozen layer percentage at conformal cooling channels at the end of filling (b) Frozen layer percentage conventional cooling channels at the end of filling

Thermally induced stresses develop principally during the cooling stage of an injection molded part, mainly as a consequence of the difference in temperature between the molten resin and the mold. An uneven temperature field causes the material to cool from above to below the glass transition temperature at different times. Thus the material experiences differential shrinkage causing thermal stresses. These stresses not only cause the warpage of a molded part, but also have an effect on its appearance and properties [39]. The temperature difference between cavity and part cooled by conventional channel layouts are larger than that in the conformal cooling channel layouts as shown in Table 4.3. Therefore, after ejection stage, deflection of part cooled by conventional channels is larger than that of part cooled by conformal one as shown in Fig. 4.20.

Table 4.3 Cavity temperature results with conformal cooling and conventional cooling channels

	Conventional Cooling	Conformal Cooling
Minimum Cavity Temperature (deg)	26.7	21.24
Maximum Cavity Temperature (deg)	50.18	41.48
Average Cavity Temperature (deg)	38.2	24.55
Surface Temperature Variance Range (deg)	(-6.69) - (5.26)	(-9.03) - (11.51)

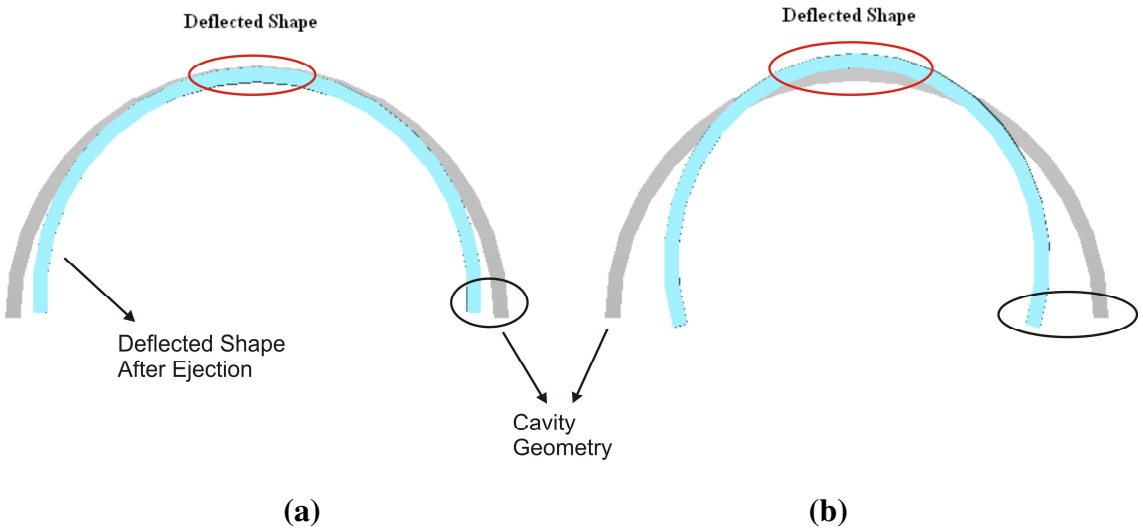

Figure 4.20 (a) Deflection after ejection in conformal configuration (b) Deflection after ejection in conventional configuration

The deflections shown in red and black circles in Fig. 4.20 are shown better by the "Warpage Indicator" result as shown in Fig. 4.22. Warpage indicator presents shrinkage variations due to non-uniform cooling. Firstly, a reference plane is determined from three points as shown in Fig. 4.21 and nominal maximum deflection value (NMD) is entered as input to define deflections with respect to that reference plane. Deflection is ranged according to colors red (high deflection), yellow (medium deflection) and green (low deflection). Green represents the out-of-plane deflection which is less than 80% of the specified NMD value. Yellow (medium) represents the out-of-plane deflection which is between 80% and 120% of the specified NMD. Red are represents the out-of-plane deflections which is greater than 120% of the specified NMD.

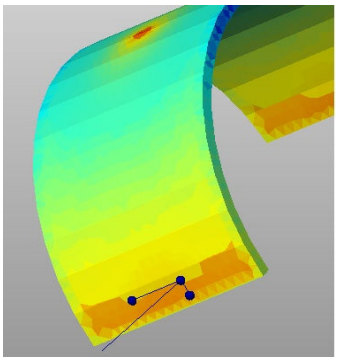

Figure 4.21 Reference plane for warpage indicator

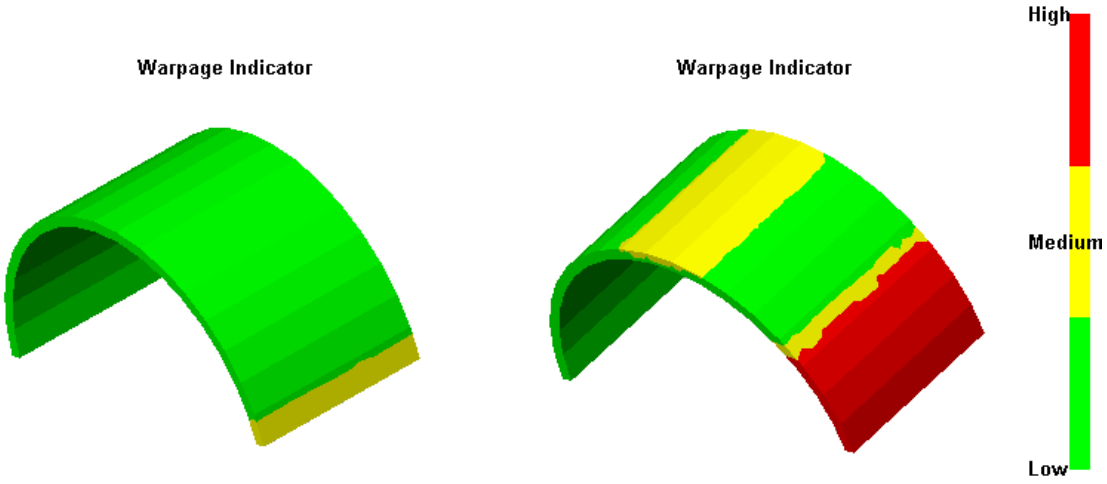

(a) **(b)**

Figure 4.22 (a) Warpage in conformal configurations (b) Warpage in conventional configurations

4.3 Real Life Case Study: IM of "Refrigerator Shelf"

The proposed benchmark study is the refrigerator shelf manufactured by Arçelik Refrigerator Factory. Geometry of the refrigerator shelf is shown in Fig. 4.23. Arçelik produced this part with mold design as shown in the Fig. 4.24. Part thickness is same everywhere (2.8 mm), no thickness variations. Part is manufactured from Polystyrol 165H, it is thermoplastic material (polystyrene).

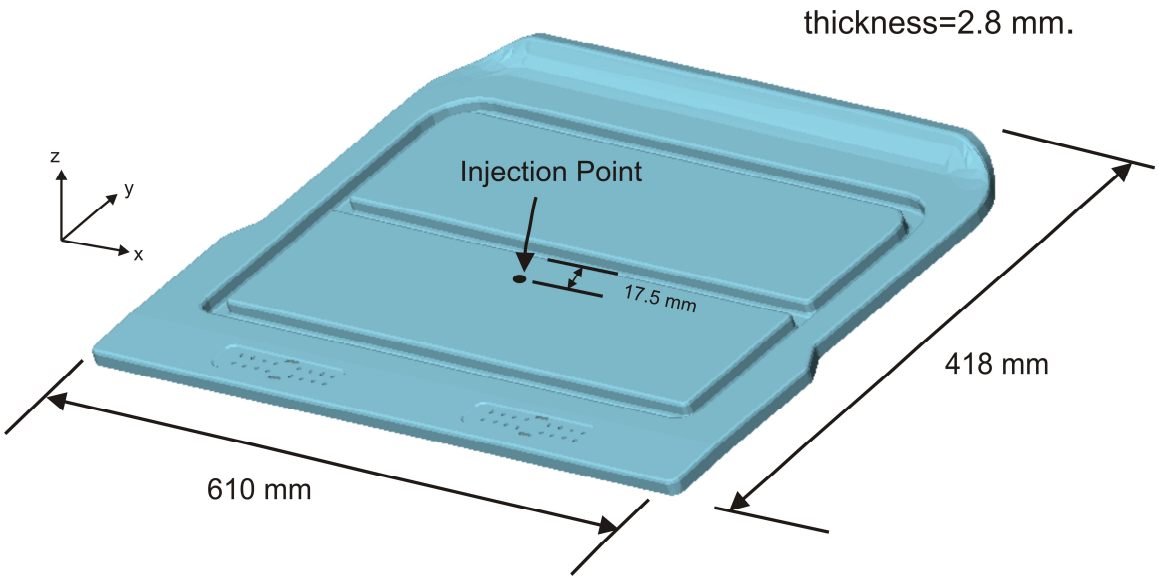

Figure.4.23 Geometry of refrigerator shelf

Mold design of the refrigerator shelf is shown in Fig. 4.24. Mold material is DIN 1.2738 steel. Feed system design is very simple. There is no runner, because it is not family mold. Diameter of gate and sprue is 10 mm. Pure water is used as coolant. Cooling channel design of the refrigerator shelf is represented in Fig. 4.24. Cooling channel design criteria of the refrigerator shelf was very simple and based on experience in Arçelik. Cooling channels of the refrigerator shelf were drilled by conventional methods. Distance between cooling channels is not below 1.5 times of the cooling channel diameter, length of the cooling channel does not exceed 1.5 m. and distance between cooling channel and cavity surface is 3 times of the cooling channel diameter.

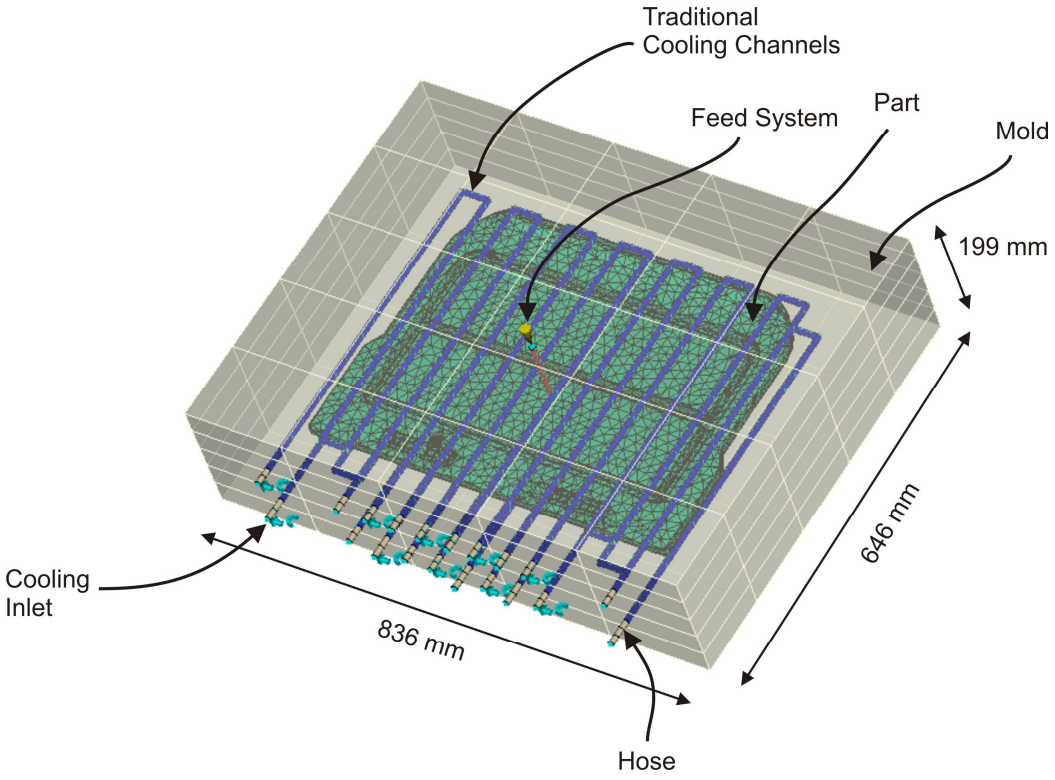

Figure 4.24 Representation of mold layout of the refrigerator shelf

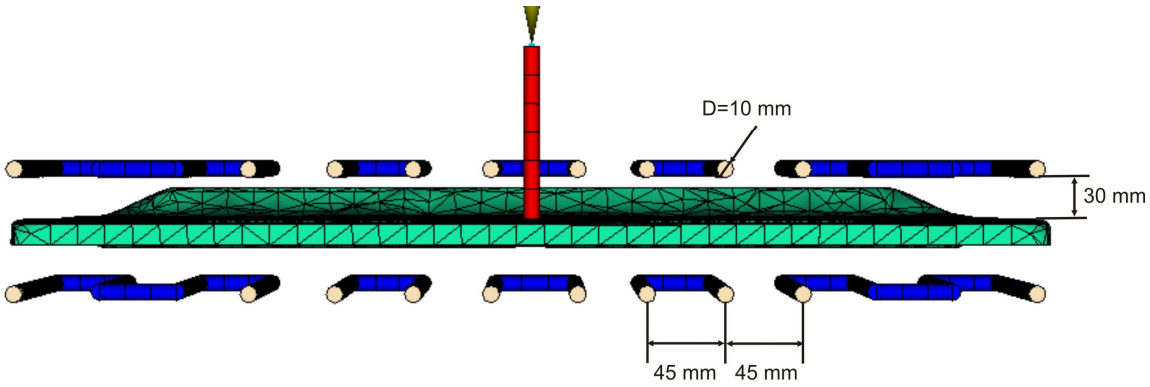

Figure 4.25 Representation of refrigerator shelf modeling in Moldflow

Arçelik has manufactured refrigerator shelf based on process parameters as shown in Table 4.4 and packing phase digram is shown in Fig. 4.26. Arçelik found these process parameters in real life experiment by trial-error methods after many

attemps. Before production of the refrigerator shelf, Arçelik did not use any simulation programs. Furthermore, coolant inlet temperature and coolant flow rate were not known before making simulations. Therefore, they were defined according to trial-error methods until ejection temperature of refrigerator shelf simulated by Moldflow coincides with that of real life experiments.

Arçelik has manufactured the refrigerator shelf 500000 times per year. Even small savings in mass production make enourmos profits for Arçelik. Therefore, Arçelik decided to decrease cycle time of the refrigerator shelf. Therefore, cycle time (58 s.) was tried to be decreased by re-arranging process parameters without deteriorating the surface quality appearance of the refrigerator shelf in Arçelik. The target cycle time was to reach 50 s.

Table 4.4 Process paramaters of the refrigerator shelf

Mold Material	Thyroplast 2738 (DIN 1.2738)
Part Material	Polystyrol 165H
Flow Rate of The Coolant	5 l/min
Coolant Inlet Temperature	22 °C
Injection Pressure	80 MPa
Initial Mold Temperature	40 °C
Initial Melt Temperature	230 °C
Coolant (water)Inlet Temperature	22 °C
Injection Time	3.05 s
Packing Time	10 s.
Cooling Time	41 s.
CycleTime	58 s.

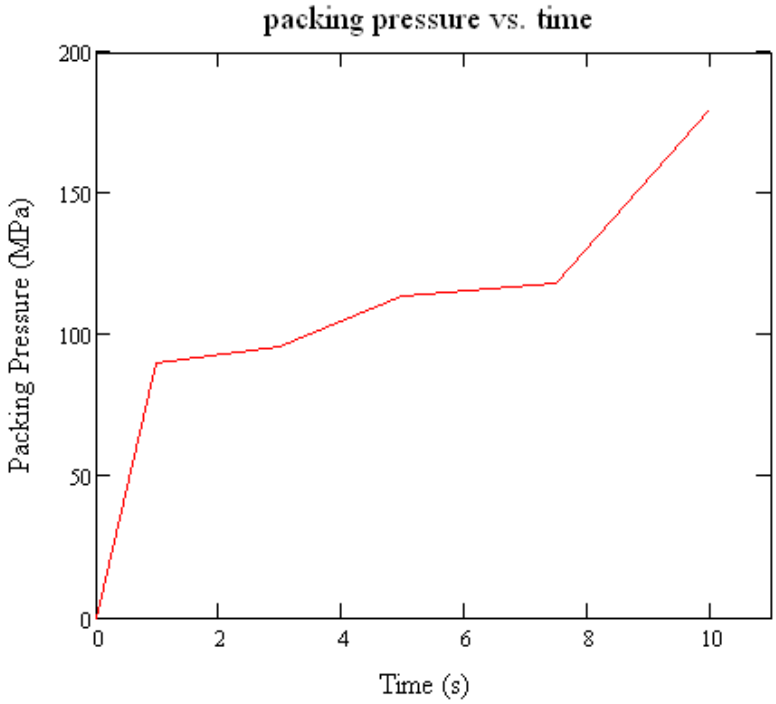

Figure 4.26 Packing pressure profile vs. time of refrigerator shelf

Before re-arranging the process parameters, process of the refrigerator shelf is modelled in Moldflow according to process parameters of real experiment as shown in Table 4.4. Then it is compared with experimental results. After ejection stage, part surface temperature is taken from five points including injection point at real life experiments and five data were collected by a laser gun and recorded at Table 4.5. Fig. 4.27 presents part surface temperature of refrigerator shelf simulated by Moldflow. Table 4.5 presents the surface temperature errors between the experimental results and simulation results. The largest error in Table 4.5 is point 5 (%12). Because, Hele-Shaw does not model locations suddenly expanded such as injection point (gate).

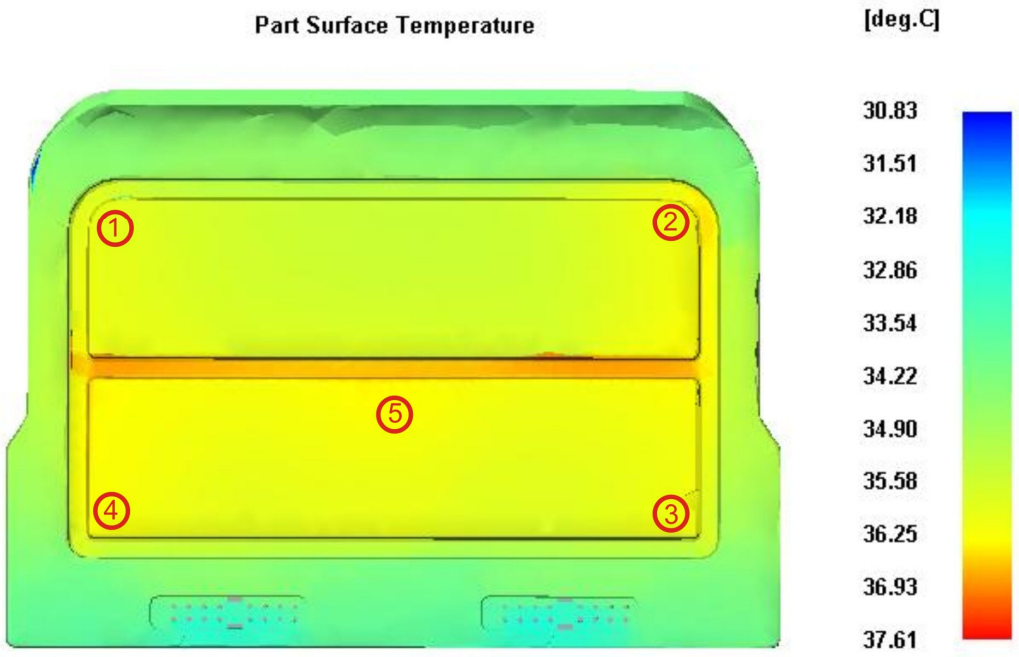

Figure 4.27 Part surface temperature results of refrigerator shelf simulation with Moldflow

Table 4.5 Ejection temperature comparison between experimental results and Moldflow results

Points	1	2	3	4	5
Part Temperature at Ejection in Experiment (°C)	35.5	34.2	34.8	35	41
Part Temperature at Ejection in Moldflow (°C)	35	36	35.2	35.7	36
Error %	1.4	5.2	1.5	1.4	12

Arçelik firstly tried to decrease cycle by decreasing cooling time. This time, Arçelik used the process parameters same as Table 4.4 except the cooling time. Arçelik directly decrease the cooling time from 41 s to 33 s to reach target cycle time. However, part was not cooled enough and it was too hot. Therefore, it was stuck to the

mold and ejected to hard. After the part dropped, it was observed that roughness of the surface was too much at the curved area of the part. Furthermore, sometimes refrigerator shelf was broken due to excessively adhered to the mold cavity during experiments. Refrigerator shelf was also simulated by Moldflow same as process parameters in Table 4.4 except cooling time. Cooling time was taken as 33 s. Fig. 4.28 presents the "Quality Prediction" of refrigerator shelf. Definition of "Quality Prediction" is given at the Appendix B. Then same failure at the curved area is also shown in Fig. 4.27.

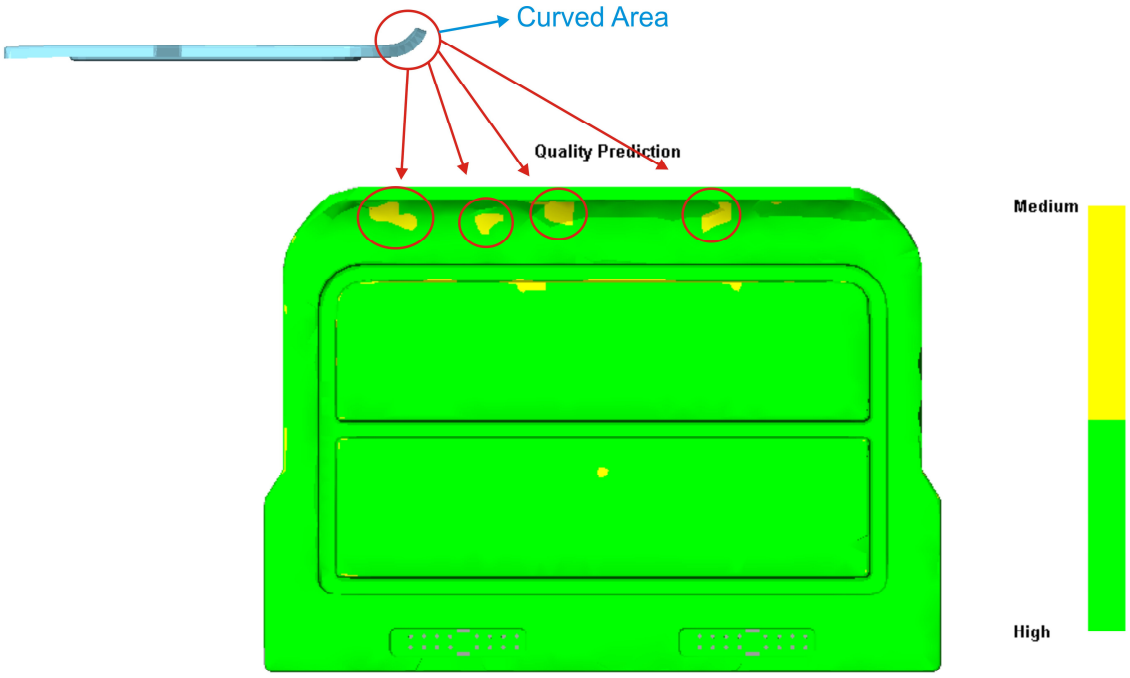

Figure 4.28 Part surface quality of the part after decreasing cooling time

Decreasing cooling time decreased the cycle time, but also surface quality of the part decreased. Therefore, cycle time was tried to be decreased by re-arranged another process parameters. Same process parameters in Table 4.4 were also used in this experiment again, except two parameters. At the second experiment, initial melt temperature of the part in Table 4.4 was decreased from 230 °C to 200 °C to decrease

cooling time, but viscosity of molten polymer gets higher due to lower temperature and it gets harder to inject molten polymer into the mold. Therefore, injection pressure is increased 10 % (from 80 MPa to 88 MPa) to drive molten polymer flow progression. However, parts were ejected as short shot at edge of the curvature area in Arçelik. Also, same experiment with re-arranged process parameters was modeled with Moldflow. Same result was found at the edge of the curved area and shown in Fig. 4.29.

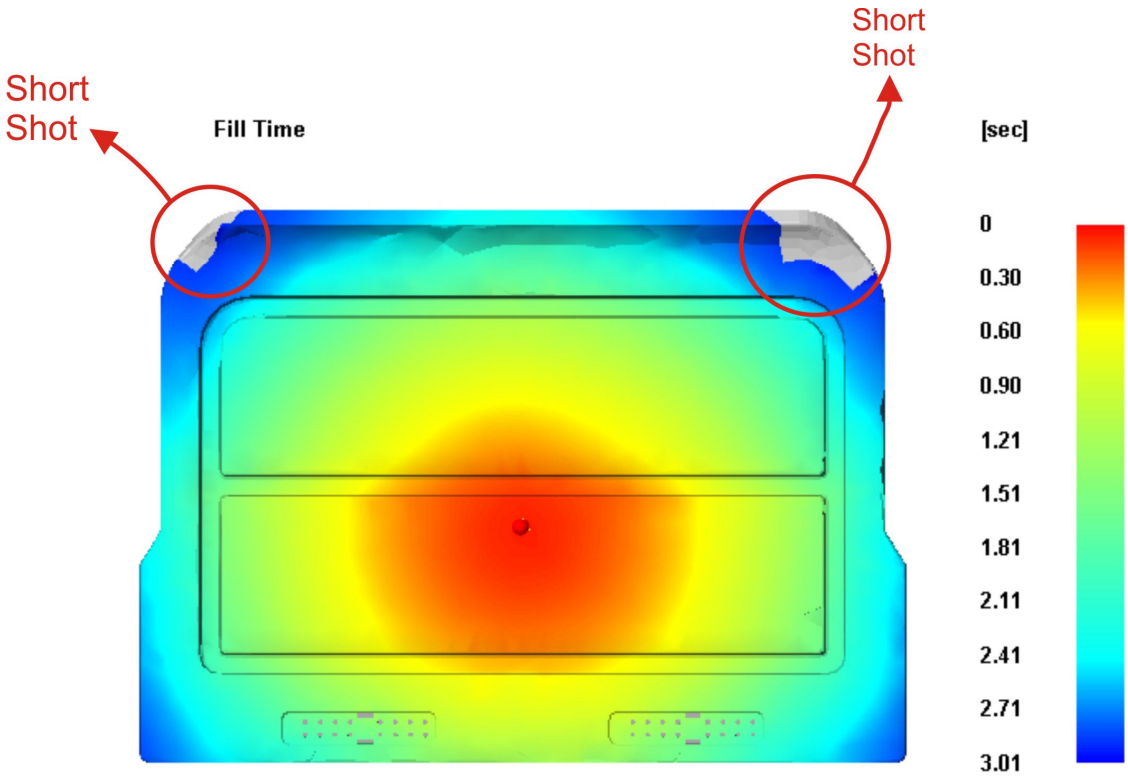

Figure 4.29 Short shot part after decreasing initial temperature of molten polymer

Attempting to decrease cycle time by re-rearranging process parameters was failed. Therefore, cooling channel layout of the mold could be revised to cool refrigerator shelf more uniformly. However that kind of mold was not manufactured by Arçelik, it was only designed, modeled with Moldflow. Then, they were compared

with process made by real process parameters in Table 4.4 to observe improvements of conformal cooling channels. That kind of cooling channel configuration decrease cooling time with preserving the surface quality of the parts due to uniform cooling. Fig. 4.30 presents conformal cooling channels layouts. The major difference between straight and conformal is that conformal channels cover the curved area at the same distance everywhere. Therefore, cycle time of the refrigerator shelf can be decreased by preserving the quality appearance at curved area.

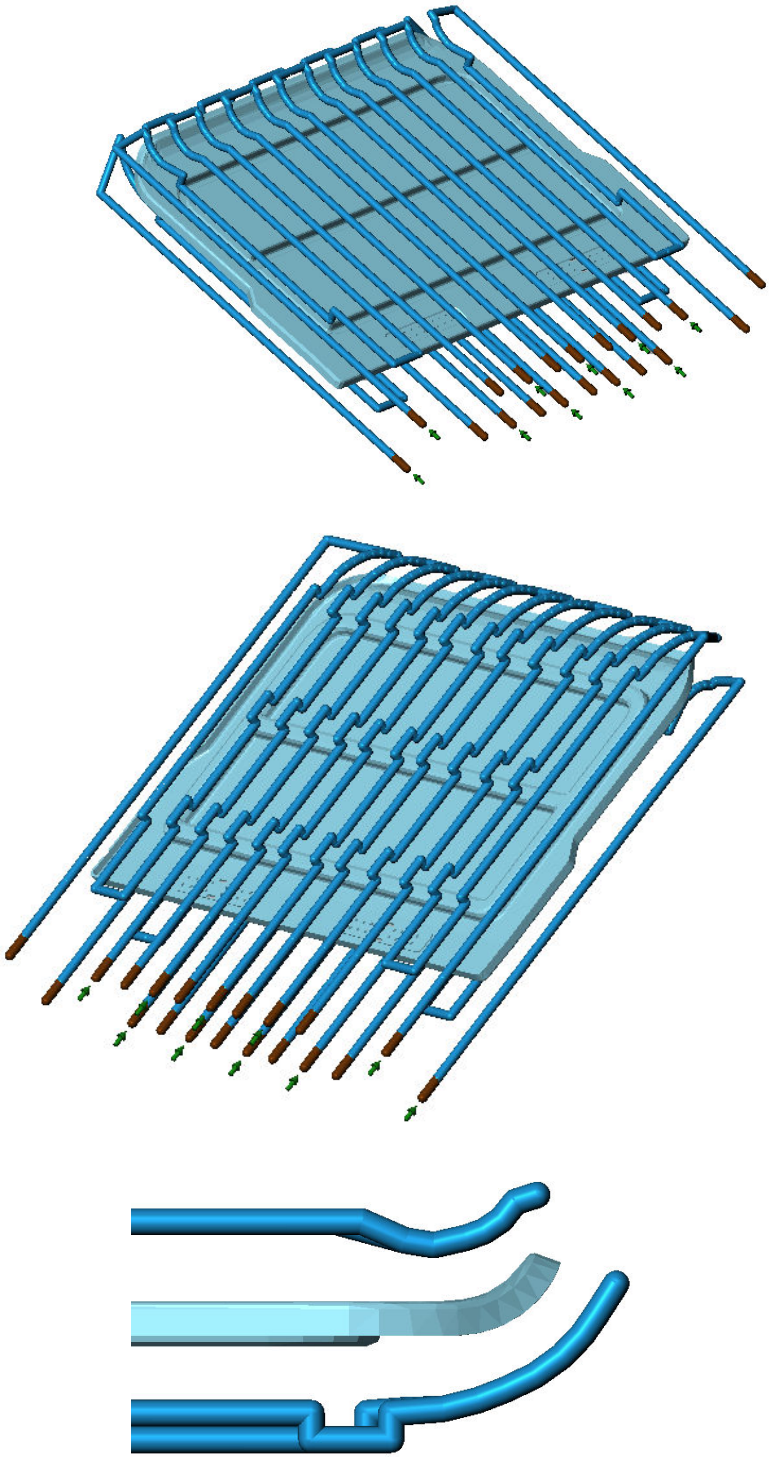

Figure 4.30 Different isometric views of the conformal cooling channels

Process conditions for conformal cooling channels are same as that for the traditional cooling channels as shown in Table 4.4 except cooling time. Simulations of conformal cooling channels were made by an order. Firstly, cooling time is arranged as 27 s, and then results of conformal cooling configuration (surface quality, freeze time variance and surface temperature variance) were compared with that of straight cooling channels. Then, it was seen that surface and cooling quality of part cooled by conformal cooling channels were not as good as that of part cooled by straight cooling channels. Then, same simulations were repeated by adding one second to cooling time and "Quality Prediction" results of conformal cooling channels were compared with that of straight channels until "Quality Prediction" results of conformal cooling channels were almost same as that of straight one. Finally, expected results were found when cooling time was increased to 33 s. Cooling time is decreased from 41 s to 33 s without any corruption in surface quality as shown in the Fig. 4.33. Furthermore, conformal cooling channels cools the refrigerator shelf as uniform as traditional cooling channels in less cooling time as shown in surface temperature variance result (Fig. 4.31) and freeze time variance result (Fig. 4.32). The only disadvantage of the conformal cooling channels with respect to the straight ones is the requirement of high coolant pump capacity as shown in Fig. 4.34.

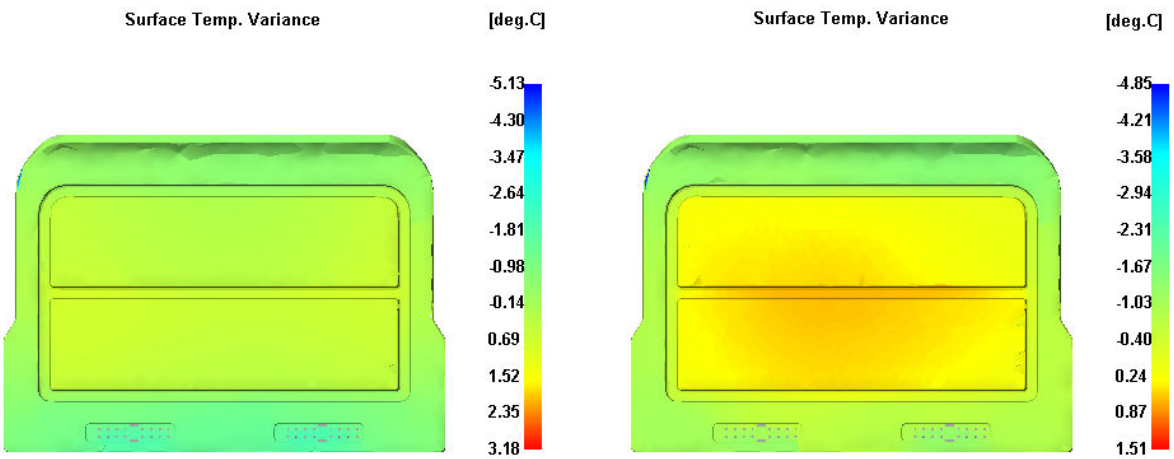

(a) **(b)**

Figure 4.31 (a) Surface temperature variance of refrigerator shelf cooled by traditional cooling channels (b) Surface temperature variance of refrigerator shelf cooled by conformal cooling channels

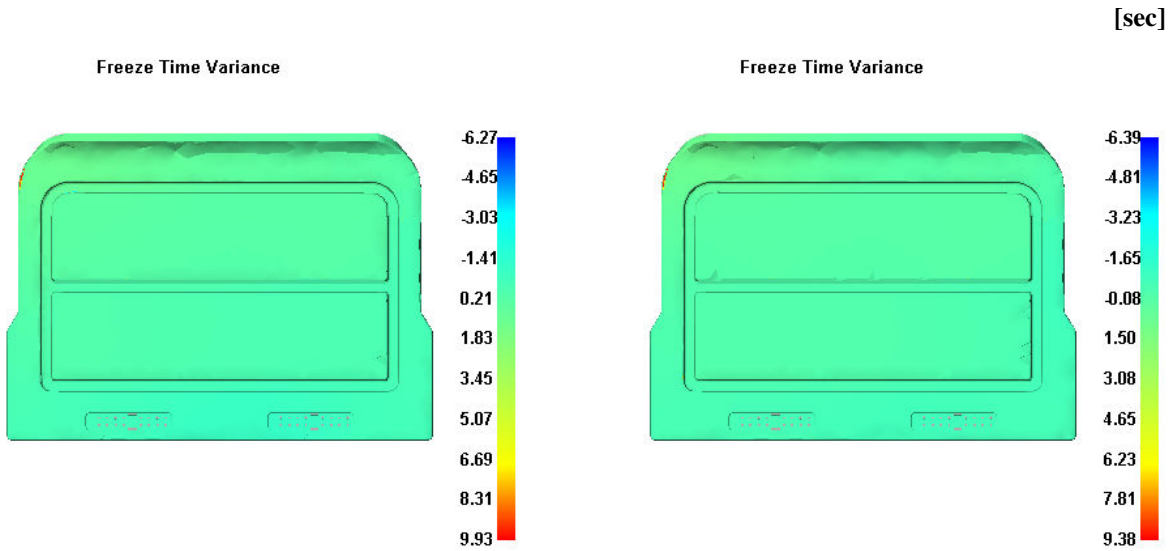

(b) **(b)**

Figure 4.32 (a) Freeze time variance of refrigerator shelf cooled by traditional cooling channels (b) Freeze time variance of refrigerator shelf cooled by conformal cooling channels

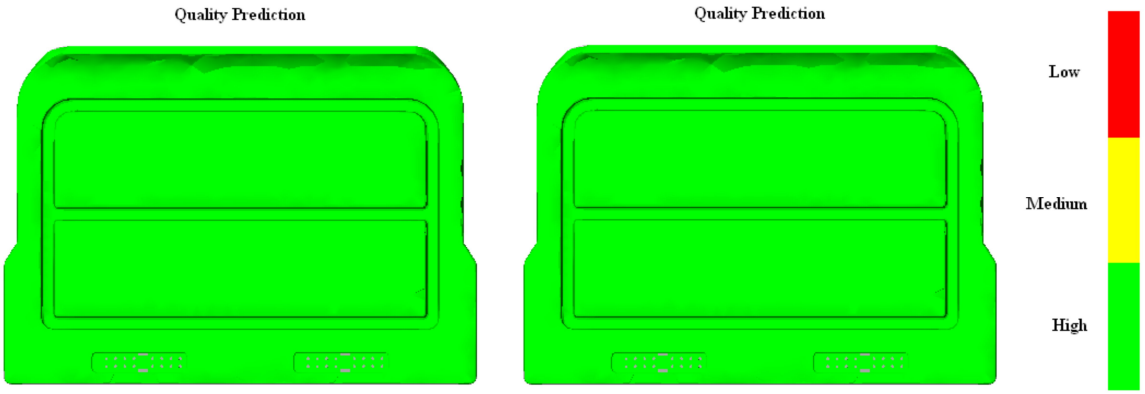

Figure 4.33 (a) Surface quality of refrigerator shelf cooled by conventional cooling channels (b) Surface quality of refrigerator shelf cooled by conformal cooling channels

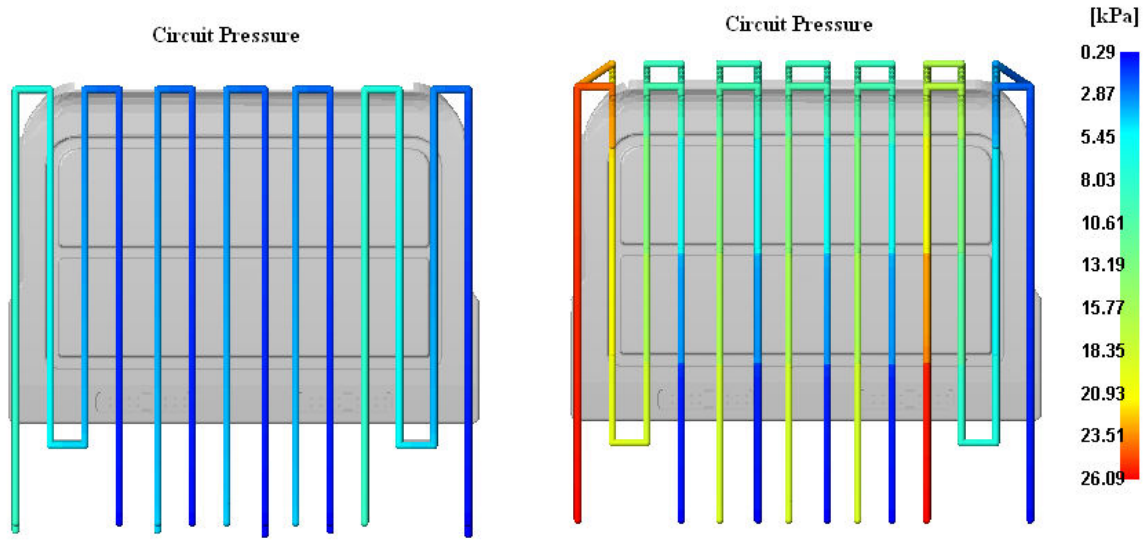

(a) **(b)**

Figure 4.34 (a) Circuit pressure in conventional cooling channels (b) Circuit pressure in conformal cooling channels

CHAPTER 5

CONCLUSIONS AND RECOMMENDATIONS

Injection molds must take heat away from the parts as fast and as uniformly to produce high quality parts economically. Therefore, cooling channels design has important effects on economic of the process and quality of the parts. Especially economic effect is more important in products manufactured by mass production. Even, a little savings on parts or process make enormous profits to the companies.

- Firstly, on two different simple geometries (rectangular prism and thin cylinder), filling analyzes have been done by MPI software filling module. Analytical solution is found from 1-D Hele-Shaw equations. For planar flow, 1-D Hele Shaw equation is derived from eqn. (2.24). Hele-Shaw derivation for 1-D radial flow is shown in Appendix-A. Pressure distribution comparison for planar flow was shown in Fig. 4.4 and it is observed that assumptions for 1-D planar flow are correct with acceptable errors. Simulation result on thin cylinder is nearly same as the analytical solution as shown in the Fig. 4.7. Results of planar flow are not as good as that of radial flow as shown in the Fig. 4.4, because filling is not planar at the beginning of the filling at the planar flow analysis.

- Secondly, before modeling of the real example, an imaginary part was modeled by both conformal cooling and traditional cooling channels. Conformal cooling channel configuration in thin shell cylinder is compared with the traditional one in the same benchmark study with same process parameters. From filling results, it has been observed that conformal cooling channels have no important impact on the filling, but it only effects the cooling phase of the part. From results, it was indicated that conformal cooling channels decrease cooling time from 9.2 s to 3.95

s. From surface temperature variance results, it was observed that conformal channel configuration cools the part more uniform than the conventional cooling channel configuration without corruption of the surface quality. The only disadvantages of the conformal cooling channels, pressure drop across the conformal cooling channels is higher than the straight channels due to complexity of conformal channels layouts.

- Finally, as a real life example, injection molding simulation of a refrigerator shelf produced by Arçelik company was presented. The company aimed to decrease the cycle time from 58 s to 50 s to reduce processing cost. To do this, the process parameters were varied in order to decrease the cycle time at the factory, but part was short shot or appearance quality of the part was not enough. In this thesis, conformal cooling channels were offered as an alternative solution to decreasing cycle time. The original processing conditions with straight channels were simulated using Moldflow and remaining unknown process parameters (such as coolant temperature, coolant flow rate) were determined on a trial-and-error basis, until the results of the simulation matched with actual production results. Then, the same processing conditions were retained while conformal cooling channels were introduced into the simulation. From the surface temperature and freeze time variance results, conformal cooling channels were seen to cool the part more uniformly with good surface quality, compared to straight channels. Furthermore, conformal cooling channels cool the part faster than straight channels, because cooling time decreases from 41 s to 33 s. The only disadvantage of conformal cooling channels was found to be the requirement of the high coolant pump capacity.

5.1 Recommendations for Future Study

For the future study, injection molding simulation software packages can be developed and disadvantages of production methods of conformal cooling channels (such as rapid tooling methods) can be lessened.

- At the beginning of the thesis, there are lots of problems faced off software package. Firstly, refrigerator shelf was tried to be modeled with Fluent and Fidap software package programs. However, it was understood that Fluent is not appropriate to simulate injection molding process, because it does not precisely model highly viscous material. Fidap is more general purpose software program including to model injection molding process. However, Fidap needs enormous computational CPU to model injection molding even part has simple geometry. Furthermore, Fidap does not import properly CAD/CAM models (.stl files), especially parts having complex geometry such as refrigerator shelf are corrupted in importing stage. Moldflow has no problems such as deformations in geometry when the part is imported. Furthermore, designing structure of the mold is very easy such as sprue, gate and runners. Moldflow also mesh the part automatically, so waste of time is prevented. However, user must spend great effort and time to correct the mesh quality of the part. Therefore, a preprocessor must be developed to control the mesh quality of the part by user. In addition to this, Moldflow use only triangular elements to model the part. For the future research, the simulations program can be developed in order to remove these weakness mentioned above.

- In chapter 1, design issues of conformal cooling channels were mentioned. Today, thermal conductivity of mold resin manufactured by rapid tooling methods is increased by putting some additives. However, mechanical strength of mold is not enough to manufacture the part in mass production. Also, cavity surface of the molds manufactured by rapid tooling methods is worse than molds manufactured by conventional methods. Even rapid tooling molds uniformly cools the part, the surface appearance of the part does not satisfies the manufacturer due to excessive roughness on the cavity surface. For future studies, mechanical strength of rapid tooling molds can be improved by working on the mold resin and surface roughness of mold cavity will be tried to be smoother based on these future studies.

REFERENCES

[1] A. Brent Strong, Plastics Materials and Processing, Second Edition Prentice-Hall Inc., pg 419-474, 1996

[2] Moldflow Introduction Brochure, Plastic Overview, prepared by Moldflow Inc, July 2007

[3] Introduction to injection molding machines, www.ab.com/appsys/pset/pset200/download/injintro.rtf, Rockwell Automation, last accessed September 2007

[4] Plastic Part Manufacture, Injection Molding, http://www.ielm.ust.hk/dfaculty/ajay/courses/ieem215/lecs/6_plastics.pdf, The Hong Kong University of Science and Technology, last accessed March 2007

[5] K. M. Au and K. M. Yu, A scaffolding architecture for conformal cooling design in rapid plastic injection molding, Int. J. Adv. Manufacturing Technology 34:496–515, 2007

[6] Ji-Zhao Liang, An Optimal Design of Cooling System For Injection Mold, Polymer Plastic Technology Engineering, 41(2), 261–271, 2002

[7] Natti S. Rao, Guenter Schumacher, Nick R. Schott, Keith T. O'Brien,Optimization of Cooling Systems in Injection Molds by an Easily Applicable Analytical Model, Journal of Reinforced Plastics and Composites, Vol. 21, No. 5, 2002

[8] E. Mathey, L. Penazzi, F.M. Schmidt and F. Rondé-Oustau, Automatic optimization of the cooling of injection mold based on the boundary element

method, Material Processing and Design: Modeling, Simulation and Applications, NUMIFORM, 2004

[9] Y. F. Sun, K. S. Lee and A. Y. C. Nee, The application of U-shape milled grooves for cooling of injection molds, Proc Instn Mech Engrs Vol 216 Part B: J Engineering Manufacture, 2002

[10] Emanuel Sachs, Edward Wylqms, Samuel Allev, Michael Cima and Honglin Guo, Production of Injection Molding Tooling With Conformal Cooling Channels Using the Three Dimensional Printing Process, Polymer Engineering and Science, Vol. 40, No. 5, 2000

[11] Hilton, Peter D., Rapid Tooling: Technologies and Industrial Applications, NY, USA: Marcel Dekker Incorporated, p 72, 2002

[12] C. H. Ahrens; A. S. Ribeiro Jr.; V. E. Beal, Heat flux canals (HFC) technique: an alternative to cool down stereolithography molds, J. Braz. Soc. Mech. Sci.& Eng. vol.25 no.3, 2003

[13] Giang T. Pham and Jonathan S. Colton, Ejection Force Modeling for Stereolithography Injection Molding Tools, Polymer Engineering and Science, Vol. 42, No. 4, 2002

[14] R. S. Spencer and G. D. Gilmore, Mod. Plastics, 28, 97, 1950

[15] E. Broyer,C. Gutfinger and Z. Tadmor , A theoretical model for the cavity filling Process in injection molding , Transactions Of The Society Of Rheology 19:3,423-444, 1975

[16] G. Menges and D. Liebfried, Plasverarbeiten, 31, 5951, 1970

[17] J.L. White and H. B. Dee, Polymer Engineering Science, 14 (9), 212, 1974

[18] J. L. Berger and C. G. Gogos, SPE The Papers, pg. 17, 1971

[19] M. R. Kamal and S. Kenig, Polymer Engineering Science, 12 (4), 294, 1972

[20] P. C. Wu, C. F. Huang, C. G. Gogos, Simulation of Mold Filling Process, Polymer Engineering Science, 14 (14), 223-230, 1980

[21] C.A. Hieber and S.F. Shen, A finite-element/finite-difference simulation of the injection molding filling process, Journal of Non-Newtonian Fluid Mechanics, 1980

[22] Huamin Zhou,Tie Geng and Dequn Li , Numerical filling simulation of injection molding based on 3-D finite element model , Journal of reinforced plastics and composites, Vol. 24, No. 8, 2005

[23] J.F. Hetu, D.M. Gao, A. Garcia Rejon,G Salloum, 3D Finite Element Method for the Simulation of the Filling Stage in Injection Molding, Polymer engineering and science, Vol. 3B, No. 2, 1998

[24] Frank M. White, Viscous Fluid Flow, Second Edition McGraw-Hill, 1991

[25] Guy Courbebaisse, David Garcia, Shape analysis and injection molding optimization, Computational Materials Science, pg 547–553, 2002

[26] David Garcia, Guy Courbebaisse and Michel Jourlin , Image Analysis Dedicated To Polymer Injection Molding , Image Anal Stereol, pg 143-148, 2001

[27] Bing-yan Jiang, Jue Zhong, Bai-yun Huang, Xuan-hui Qu, Yi-min Li ,Element modeling of FEM on the pressure field in the powder injection mold filling process, Journal of Materials Processing Technology, 74-77, 2003

[28] X. Chen, Y. C. Lam, K.C. Tam, S.C.M. Yu, Particle migration of quasi-steady flow in concentrated suspension for powder injection molding, School of Mechanical & Production Engineering, Nanyang Technological University, Nanyang Avenue, Singapore, 1998

[29] Moldflow Introduction Brochure, MPI Theory, prepared by Moldflow Inc., July 2007

[30] How Moldflow Works, http://www.mechse.uiuc.edu/content/about/academics/course.php?course_id=17, Mechanical Science and Enginnering University of Illinois at Urban Champaign, last accessed September 2007

[31] J. Koszkul, J. Nabialek, Viscosity models in simulation of the filling stage of the injection molding process, Journal of Materials Processing Technology, 157–158,183–187, 2004

[32] Abdulmecit Güldaş, Onuralp Uluer, Ahmet Özdemir, The determination of viscosity and density variations of molten thermoplastics, TECHNOLOGY, Volume 9, Issue 2, 127-135, 2006

[33] Li Q. Tang, Kishore Pochiraju, Constantin Chassapis and Souran Manoochehri, Three dimensional transient mold cooling analysis based on Galerkin Finite Element Gradient Technique Formulation with a matrixfree conjugate, International journal for numerical methods in engineering, vol.39, 3049-3064, 1996

[34] N. Narazaki and A. Mizukami, Simulation of polymeric flows in the injection molding process, Convex Users Conf., Texas, 1990

[35] C.W. Fox, A. J. Poslinski, and R. M. Shay, Jr., A Simplified Flow Analysis for Predicting Molding Pressure and Flow Length of Polymer Melts, http://www.crd.ge.com/cooltechnologies/pdf/1998crd098.pdf, GE Research & Development Center, last accessed September 2007

[36] Fluent, Solution Methods, http://www.fluent.com/software/fidap/index.htm, last accessed September 2007

[37] Moldex, Moldex3D Overview, http://www.moldex3d.com/en/products/download/Moldex3D-DM.pdf, last accessed September 2007

[38] J. A. Henz, K. Himasekhar, Design Sensitivities of Mold-Cooling CAE Software: An Experimental Verification, Advances in Polymer Technology, Vol. 15, No. 1, 1-16, 1996

[39] X. Chen, Y.C. Lam and D.Q. Li, Analysis of thermal residual stress in plastic injection molding, Journal of Materials Processing Technology, 101, 275-280, 2000

APPENDIX A

1-D HELE SHAW IN RADIAL FLOW

One-dimensional radial flow needs to be modeled for the radial flow analysis. Using the assumptions that have been previously stated, Navier - Stokes continuity equation in cylindrical coordinates

$$\frac{\partial \rho}{\partial t}+\frac{1}{r}\frac{\partial\left(\rho r u_r\right)}{\partial r}+\frac{1}{r}\frac{\partial\left(\rho u_\theta\right)}{\partial \theta}+\frac{\partial\left(\rho u_z\right)}{\partial z}=0 \tag{A.1}$$

Applying the Hele-Shaw approximation to the continuity eqn. (A.1) yields. Since, the z-component of the velocity is neglected and the fluid is incompressible, eqn. (A.1) becomes

$$\frac{\partial\left(r u_r\right)}{\partial r}+\frac{\partial u_\theta}{\partial \theta}=0 \tag{A.2}$$

Navier - Stokes momentum equation in r-direction

$$\rho\left(\frac{\partial u_r}{\partial t}+u_r\frac{\partial u_r}{\partial r}+\frac{u_\theta}{r}\frac{\partial u_r}{\partial \theta}-\frac{u_\theta^2}{r}+u_z\frac{\partial u_z}{\partial z}\right)=-\frac{\partial P}{\partial r}$$

$$+\mu\left[\frac{\partial}{\partial r}\left(\frac{1}{r}\frac{\partial}{\partial r}\left(r u_r\right)\right)+\frac{1}{r^2}\frac{\partial^2 u_r}{\partial \theta^2}-\frac{2}{r^2}\frac{\partial u_\theta}{\partial \theta}+\frac{\partial^2 u_r}{\partial z^2}\right]+\rho g_r \tag{A.3.a}$$

Navier - Stokes momentum equation in θ-direction

$$\rho\left(\frac{\partial u_\theta}{\partial t}+u_r\frac{\partial u_\theta}{\partial r}+\frac{u_\theta}{r}\frac{\partial u_\theta}{\partial \theta}-\frac{u_r u_\theta}{r}+u_z\frac{\partial u_\theta}{\partial z}\right)=-\frac{1}{r}\frac{\partial P}{\partial \theta}$$

$$+\mu\left[\frac{\partial}{\partial r}\left(\frac{1}{r}\frac{\partial}{\partial r}\left(ru_\theta\right)\right)+\frac{1}{r^2}\frac{\partial^2 u_\theta}{\partial \theta^2}+\frac{2}{r^2}\frac{\partial u_r}{\partial \theta}+\frac{\partial^2 u_\theta}{\partial z^2}\right]+\rho g_\theta \qquad \text{(A.3.b)}$$

For the r- and θ- momentum equation eqns. (A.3.a) & (A.3.b), neglecting the velocity component in z-direction and body forces yields

$$\rho\left(\frac{\partial u_r}{\partial t}+u_r\frac{\partial u_r}{\partial r}+\frac{u_\theta}{r}\frac{\partial u_r}{\partial \theta}-\frac{u_\theta^2}{r}+u_z\frac{\partial u_z}{\partial z}\right)=-\frac{\partial P}{\partial r}+\mu\left[\frac{\partial}{\partial r}\left(\frac{1}{r}\frac{\partial}{\partial r}\left(ru_r\right)\right)\right.$$

$$\left.+\frac{1}{r^2}\frac{\partial^2 u_r}{\partial \theta^2}-\frac{2}{r^2}\frac{\partial u_\theta}{\partial \theta}+\frac{\partial^2 u_r}{\partial z^2}\right] \qquad \text{(A.4.a)}$$

$$\rho\left(\frac{\partial u_\theta}{\partial t}+u_r\frac{\partial u_\theta}{\partial r}+\frac{u_\theta}{r}\frac{\partial u_\theta}{\partial \theta}-\frac{u_r u_\theta}{r}+u_z\frac{\partial u_\theta}{\partial z}\right)=-\frac{1}{r}\frac{\partial P}{\partial \theta}+\mu\left[\frac{\partial}{\partial r}\left(\frac{1}{r}\frac{\partial}{\partial r}\left(ru_\theta\right)\right)\right.$$

$$\left.+\frac{1}{r^2}\frac{\partial^2 u_\theta}{\partial \theta^2}+\frac{2}{r^2}\frac{\partial u_r}{\partial \theta}+\frac{\partial^2 u_\theta}{\partial z^2}\right] \qquad \text{(A.4.b)}$$

The left hand side of the momentum equations denotes inertial forces. Since, in the Hele-Shaw approximation, the viscous forces dominate the inertial forces, then the r- and θ- momentum equation becomes

$$0=-\frac{\partial P}{\partial r}+\mu\left[\frac{\partial}{\partial r}\left(\frac{1}{r}\frac{\partial}{\partial r}\left(ru_r\right)\right)+\frac{1}{r^2}\frac{\partial^2 u_r}{\partial \theta^2}-\frac{2}{r^2}\frac{\partial u_\theta}{\partial \theta}+\frac{\partial^2 u_r}{\partial z^2}\right] \qquad \text{(A.5.a)}$$

$$0=-\frac{1}{r}\frac{\partial P}{\partial \theta}+\mu\left[\frac{\partial}{\partial r}\left(\frac{1}{r}\frac{\partial}{\partial r}\left(ru_\theta\right)\right)+\frac{1}{r^2}\frac{\partial^2 u_\theta}{\partial \theta^2}+\frac{2}{r^2}\frac{\partial u_r}{\partial \theta}+\frac{\partial^2 u_\theta}{\partial z^2}\right] \qquad \text{(A.5.b)}$$

Due to small gap presence, the velocity gradient along z-direction dominates other velocity gradients, i.e

$$\frac{\partial u_\theta}{\partial z}, \frac{\partial u_r}{\partial z} >> \frac{\partial u_r}{\partial \theta}, \frac{\partial u_\theta}{\partial \theta}, \frac{\partial u_r}{\partial r}, \frac{\partial u_\theta}{\partial r} \tag{A.6}$$

$$0 = -\frac{\partial P}{\partial r} + \mu \frac{\partial^2 u_r}{\partial z^2} \tag{A.7.a}$$

$$0 = -\frac{1}{r}\frac{\partial P}{\partial \theta} + \mu \frac{\partial^2 u_\theta}{\partial z^2} \tag{A.7.b}$$

Integrating equation with respect to z

$$\frac{\partial u_r}{\partial z} = \frac{\partial P}{\partial r}\frac{z}{\mu} + f(r,\theta) \tag{A.8.a}$$

$$\frac{\partial u_\theta}{\partial z} = \frac{\partial P}{\partial \theta}\frac{rz}{\mu} + g(r,\theta) \tag{A.8.b}$$

f and g are integration functions ; $\frac{\partial P}{\partial r}$ can only be functions of r and $\frac{\partial P}{\partial \theta}$ can only be function of θ. Flow is symmetric which means $\frac{\partial u_r}{\partial z} = \frac{\partial u_\theta}{\partial z} = 0$ at z = 0.Thus

$$\left(\frac{\partial u_r}{\partial z}\right)_{z=0} = \frac{\partial P}{\partial r}\frac{0}{\mu} + f(r,\theta) = 0 \tag{A.9.a}$$

then $f(r, \theta) = 0$

$$\left(\frac{\partial u_\theta}{\partial z}\right)_{z=0} = \frac{\partial P}{\partial \theta}\frac{0r}{\mu} + g(r,\theta) = 0 \tag{A.9.b}$$

then $g(r, \theta) = 0$

Then (A.9.a) and (A.9.b) becomes

$$\frac{\partial u_r}{\partial z} = \frac{\partial P}{\partial r}\frac{z}{\mu} \tag{A.10.a}$$

$$\frac{\partial u_\theta}{\partial z} = \frac{\partial P}{\partial \theta}\frac{rz}{\mu} \tag{A.10.b}$$

Integrating with respect to z from $z^* = z \quad z^* = b$

$$\int_{u_r(r,\theta,z)}^{u_r(r,\theta,b)} du_r = \int_{z^*=z}^{z^*=b} \frac{\partial P}{\partial r}\frac{z^*}{\mu} dz^* \tag{A.11.a}$$

$$\int_{u_\theta(r,\theta,z)}^{u_\theta(r,\theta,b)} du_\theta = \int_{z^*=z}^{z^*=b} \frac{\partial P}{\partial \theta}\frac{rz^*}{\mu} dz^* \tag{A.11.b}$$

z is dummy variable then

$$u_r(r,\theta,b) - u_r(r,\theta,z) = \frac{\partial P}{\partial r}\int_z^b \frac{z^*}{\mu} dz^* \tag{A.12.a}$$

$$u_\theta(r,\theta,b) - u_\theta(r,\theta,z) = \frac{\partial P}{\partial \theta}\int_z^b \frac{rz^*}{\mu} dz^* \tag{A.12.b}$$

No slip condition at z=b, therefore $u_r(r,\theta,b) = u_\theta(r,\theta,b) = 0$, thus

$$u_r(r,\theta,z) = -\frac{\partial P}{\partial r}\int_z^b \frac{z^*}{\mu} dz^* \tag{A.13.a}$$

$$u_\theta(r,\theta,z) = -\frac{\partial P}{\partial \theta}\int_z^b \frac{rz^*}{\mu} dz^* \tag{A.13.b}$$

Average velocities is found from across the gap

$$\bar{u}_r = \frac{1}{b}\int_0^b \left[-\frac{\partial P}{\partial r}\int_z^b \frac{z^*}{\mu} dz^* \right] dz \tag{A.14.a}$$

$$\bar{u}_\theta = \frac{r}{b}\int_0^b \left[-\frac{\partial P}{\partial \theta}\int_z^b \frac{z^*}{\mu} dz^* \right] dz \tag{A.14.b}$$

which leads

$$\bar{u}_r = -\frac{1}{b}\frac{\partial P}{\partial r}\int_0^b \int_z^b \frac{z^*}{\mu} dz^* dz \tag{A.15.a}$$

$$\bar{u}_\theta = -\frac{r}{b}\frac{\partial P}{\partial \theta}\int_0^b \int_z^b \frac{z^*}{\mu} dz^* dz \tag{A.15.b}$$

Equations are double integrals in the $z = z^*$ domain. The integration region is shown above planar flow

Change the order of integration and adjust integration limits accordingly

$$\bar{u}_r = -\frac{1}{b}\frac{\partial P}{\partial r}\int_0^b \int_z^b \frac{z^*}{\mu} dz^* dz = -\frac{1}{b}\frac{\partial P}{\partial r}\int_0^b \int_0^{z^*} \frac{z}{\mu} dz dz^* \tag{A.16.a}$$

$$\bar{u}_\theta = -\frac{r}{b}\frac{\partial P}{\partial \theta}\int_0^b \int_z^b \frac{z^*}{\mu} dz^* dz = -\frac{r}{b}\frac{\partial P}{\partial \theta}\int_0^b \int_0^{z^*} \frac{z}{\mu} dz dz^* \tag{A.16.b}$$

$$S = \int_0^b \frac{z^2}{\mu} dz \tag{A.17}$$

Then replacing equation (A.17) into equations (A.16.a) and (A.16.b), last form of average velocities become

$$\bar{u}_r = -\frac{1}{2b}\frac{\partial P}{\partial r}\int_0^b \frac{z^2}{\mu}dz = -\frac{S}{2b}\frac{\partial P}{\partial r} \tag{A.18.a}$$

$$\bar{u}_\theta = -\frac{r}{2b}\frac{\partial P}{\partial \theta}\int_0^b \frac{z^2}{\mu}dz = -\frac{Sr}{2b}\frac{\partial P}{\partial \theta} \tag{A.18.b}$$

From equation take gapwise integral over the continuity equation (A.2)

Then put (A.18.a) and (A.18.b) in equation (A.2)

$$\int_0^b \frac{\partial}{\partial r}\left(-r\frac{\partial P}{\partial r}\int_z^b \frac{z^*}{\mu}dz^*\right)dz + \int_0^b \frac{\partial}{\partial \theta}\left(-r\frac{\partial P}{\partial \theta}\int_z^b \frac{z^*}{\mu}dz^*\right)dz = 0 \tag{A.19}$$

Multiplying by 1/b

$$\frac{1}{b}\int_0^b \frac{\partial}{\partial r}\left(-r\frac{\partial P}{\partial r}\int_z^b \frac{z^*}{\mu}dz^*\right)dz + \frac{1}{b}\int_0^b \frac{\partial}{\partial \theta}\left(-r\frac{\partial P}{\partial \theta}\int_z^b \frac{z^*}{\mu}dz^*\right)dz = 0 \tag{A.20}$$

Taking constants outside of the integral

$$\frac{\partial}{\partial r}\left[-\frac{r}{b}\frac{\partial P}{\partial r}\int_0^b\int_z^b \frac{z^*}{\mu}dz^*dz\right] + \frac{\partial}{\partial \theta}\left[-\frac{r}{b}\frac{\partial P}{\partial \theta}\int_0^b\int_z^b \frac{z^*}{\mu}dz^*dz\right] = 0 \tag{A.21}$$

Final pressure distribution equation becomes

$$\frac{\partial}{\partial r}\left(\frac{\partial P}{\partial r}Sr\right) + \frac{\partial}{\partial \theta}\left(\frac{\partial P}{\partial \theta}Sr\right) = 0 \tag{A.22}$$

Derivative of r with respect to θ is zero, then the last form

$$\frac{\partial}{\partial r}\left(\frac{\partial P}{\partial r}Sr\right) + \frac{\partial}{\partial \theta}\left(\frac{\partial P}{\partial \theta}S\right) = 0 \tag{A.23}$$

Energy equation in cylindirical coordinates [46]

$$\rho C_P\left(\frac{\partial T}{\partial t}+u_r\frac{\partial T}{\partial r}+\frac{u_\theta}{r}\frac{\partial T}{\partial \theta}+u_z\frac{\partial T}{\partial z}\right)=k\left[\frac{1}{r}\frac{\partial}{\partial r}\left(r\frac{\partial T}{\partial r}\right)+\frac{1}{r^2}\frac{\partial^2 T}{\partial \theta^2}+\frac{\partial^2 T}{\partial z^2}\right]+\Phi \qquad (A.24)$$

In order to find final form the energy equation, apply Hele-Shaw assumptions

Neglecting velocity component in the thickness direction $(u_z=0)$, then the energy equation becomes

$$\rho C_P\left(\frac{\partial T}{\partial t}+u_r\frac{\partial T}{\partial r}+\frac{u_\theta}{r}\frac{\partial T}{\partial \theta}\right)=k\left[\frac{1}{r}\frac{\partial}{\partial r}\left(r\frac{\partial T}{\partial r}\right)+\frac{1}{r^2}\frac{\partial^2 T}{\partial \theta^2}+\frac{\partial^2 T}{\partial z^2}\right]+\Phi \qquad (A.25)$$

Heat conduction in the flow direction is neglected,

$$\frac{\partial^2 T}{\partial z^2}>>\frac{\partial^2 T}{\partial \theta^2},\frac{\partial^2 T}{\partial r^2} \qquad (A.26)$$

$$\rho C_P\left(\frac{\partial T}{\partial t}+u_r\frac{\partial T}{\partial r}+\frac{u_\theta}{r}\frac{\partial T}{\partial \theta}\right)=k\frac{\partial^2 T}{\partial z^2}+\Phi \qquad (A.27)$$

The shear rate is given by in cylindrical coordinates

$$\Phi=2\mu\left[\left(\frac{\partial u_r}{\partial r}\right)^2+\left(\frac{1}{r}\frac{\partial u_\theta}{\partial \theta}+\frac{u_r}{r}\right)^2+\left(\frac{\partial u_z}{\partial z}\right)^2+\frac{1}{2}\left(\frac{\partial u_\theta}{\partial z}+\frac{1}{r}\frac{\partial u_z}{\partial \theta}\right)^2+\frac{1}{2}\left(\frac{\partial u_z}{\partial r}+\frac{\partial u_r}{\partial z}\right)^2\right.$$

$$\left.+\frac{1}{2}\left(\frac{1}{r}\frac{\partial u_r}{\partial \theta}+r\frac{\partial}{\partial r}\left(\frac{u_\theta}{r}\right)\right)^2-\frac{1}{3}(\nabla.v)\right] \qquad (A.28)$$

From continuity equation, then

$$\Phi = 2\mu\left[\left(\frac{\partial u_r}{\partial r}\right)^2 + \left(\frac{1}{r}\frac{\partial u_\theta}{\partial \theta} + \frac{u_r}{r}\right)^2 + \left(\frac{\partial u_z}{\partial z}\right)^2 + \frac{1}{2}\left(\frac{\partial u_\theta}{\partial z} + \frac{1}{r}\frac{\partial u_z}{\partial \theta}\right)^2 + \frac{1}{2}\left(\frac{\partial u_z}{\partial r} + \frac{\partial u_r}{\partial z}\right)^2 + \frac{1}{2}\left(\frac{1}{r}\frac{\partial u_r}{\partial \theta} + r\frac{\partial}{\partial r}\left(\frac{u_\theta}{r}\right)\right)^2\right] \quad \text{(A.29)}$$

Neglect velocity component in the thickness direction, then

$$\Phi = 2\mu\left[\left(\frac{\partial u_r}{\partial r}\right)^2 + \left(\frac{1}{r}\frac{\partial u_\theta}{\partial \theta} + \frac{u_r}{r}\right)^2 + \frac{1}{2}\left(\frac{\partial u_\theta}{\partial z}\right)^2 + \frac{1}{2}\left(\frac{\partial u_r}{\partial z}\right)^2 + \frac{1}{2}\left(\frac{1}{r}\frac{\partial u_r}{\partial \theta} + r\frac{\partial}{\partial r}\left(\frac{u_\theta}{r}\right)\right)^2\right] \quad \text{(A.30)}$$

The velocity gradient in the r- and θ - directions is negligible with respect to z direction

$$\frac{\partial u_r}{\partial z}, \frac{\partial u_\theta}{\partial z} >> \frac{\partial u_r}{\partial r}, \frac{\partial u_r}{\partial \theta}, \frac{\partial u_\theta}{\partial r}, \frac{\partial u_\theta}{\partial \theta} \quad \text{(A.31)}$$

$$\dot{\gamma} = \left[\left(\frac{\partial u_\theta}{\partial z}\right)^2 + \left(\frac{\partial u_r}{\partial z}\right)^2\right]^{\frac{1}{2}} \quad \text{(A.32)}$$

Final form of the energy equation becomes

$$\rho C_P\left(\frac{\partial T}{\partial t} + u_r\frac{\partial T}{\partial r} + \frac{u_\theta}{r}\frac{\partial T}{\partial \theta}\right) = k\frac{\partial^2 T}{\partial z^2} + \mu\left[\left(\frac{\partial u_\theta}{\partial z}\right)^2 + \left(\frac{\partial u_r}{\partial z}\right)^2\right] \quad \text{(A.33)}$$

APPENDIX B

QUALITY PREDICTION

"Quality Prediction" result estimates the expected quality of the part's appearance and ranks according to colors as shown in Fig. B.1. This result is derived from flow front temperature, pressure drop, cooling time, shear rate and shear stress.

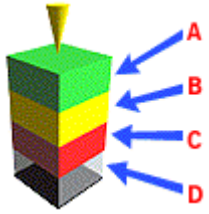

Figure B.1. Quality Prediction Result, A will have high quality, B may have quality problems, C will definitely have quality problems, D will not fill (short shot)

Green means the preffered surface quality appearance, and following conditions are achived.

1) The flow front temperature is between the minimum (T_{min}) and maximum (T_{max}) recommended temperatures for the material in the material database

$T_{min} < T < T_{max}$

2) Pressure drop is less than 80% of the maximum injection pressure (P_{max})

$P_{drop} < (0.8P_{max})$

3) The cooling time (t) is less than 1.5 times the average cooling time for the part (t_{av})

$t < 1.5t_{av}$

4) The shear rate ($\dot{\gamma}$) is less than the maximum recommended shear rate in the material record ($\dot{\gamma}_{max}$)

$\dot{\gamma} < \dot{\gamma}_{max}$

5) The shear stress (τ) is less than the maximum recommended shear stress in the material record (τ_{max}).

$\tau < \tau_{max}$

Yellow means surface quality is acceptable but not good.

1) The flow front temperature (T) is between the minimum (T_{min}), recommended temperature for the material and a value 5°C above the maximum (T_{max}), recommended temperature for the material.

$T_{min} < T < (T_{max} + 5°C)$

2) The pressure drop (P_{drop}) lies in the range between 80% and 100% of the maximum injection pressure (P_{max})

$(0.8P_{max}) < P_{drop} < P_{max}$

3) The cooling time (t) is between 1.5 and 5 times the average cooling time for the part

$1.5t_{av} < t < 5t_{av}$

4) The shear rate ($\dot{\gamma}$) is between 1 and 2 times the maximum shear rate ($\dot{\gamma}_{max}$).

$\dot{\gamma}_{max} < \dot{\gamma} < 2\dot{\gamma}_{max}$

5) The shear stress (τ) is between 1 and 2 times the maximum shear stress rate (τ_{max}).

$\tau_{max} < \tau < 2\tau_{max}$

Red means surface quality is unacceptable

1) The flow front temperature (T) is more than 5°C above the maximum recommended temperature for the material (T_{max})

$T > (T_{max} + 5°C)$

2) The pressure drop (P_{drop}) is greater than or equal to the maximum injection pressure (P_{max})

$P_{drop} \geq P_{max}$

3) The cooling time (t) is more than 5 times above the average cooling time for the part (t_{av})

$t > 5t_{av}$

4) The shear rate ($\dot{\gamma}$) is more than double the maximum recommended in the material record ($\dot{\gamma}_{max}$)

$\dot{\gamma} > 2\dot{\gamma}_{max}$

5) The shear stress (τ) is more than double the maximum recommended in the material record (τ_{max})

$\tau > 2\tau_{max}$